Anomalies of hypersound velocity and attenuation in ferroelectric tris-sarcosine calcium chloride (TSCC) for Brillouin small angle, right angle and backscattering

by Jin Tong Wang

A thesis submitted in partial fulfillment of the requirements for the degree of Doctor of Philosophy i n Physics

Montana State University

Abstract:

The Brillouin spectra of the ferroelectric Tris-Sarcosine Calcium Chloride crystal have been observed in small angle, right angle and backsattering. The smallest angle we have achieved is 7. 48°. The frequency range we were working on is about 2 GHz to 32 GHz. Brillouin investigation in such large frequency range is significantly important. The anomalies of hypersound velocity and attenuation were obtained.

We are the first to calculate the polarization of the scattered light in a orthorhombic crystal like TSCC. We are quite successful in interpreting the anomalies of sound velocities and attenuation for the phonon along [001] by piezoelectric coupling and we are the first to interpret the anomalies of sound velocities and attenuation for phonons along the polar axis [010] by the small depolarization effect.

We are the first experimentally to prove the relation Tc-Tm∞ω for [001] phonons and Tc-Tm =Constant for [010] phonons.

We estimated the elementary relaxation time To=5. 25*10-14 sec for [001] phonons and To =8. 24*10-12 sec for [010] phonons.

ANOMALIES OF HYPERSOUND VELOCITY AND ATTENUATION IN FERROELECTRIC TRIS-SARCOSINE CALCIUM CHLORIDE (TSCC) FOR BRILLOUIN SMALL ANGLE, RIGHT ANGLE AND BACKSCATTERING

by

Jin Tong Wang

A thesis submitted in partial fulfillment
of the requirements for the degree

of

Doctor of Philosophy

in

Physics

MONTANA STATE UNIVERSITY
Bozeman, Montana

July, 1986

APPROVAL

of a thesis submitted by

Jin Tong Wang

This thesis has been read by each member of the thesis committee and has been found to be satisfactory regarding content, English usage, format, citations, bibiographic style, and consistency, and is ready for submission to the College of Graduate Studies.

July 25, 1986
Date

V. Hugo Schmidt
Chairperson,
Graduate committee

Approved for the Major Department

July 25, 1986
Date

Head, Major Department

Approved for the College of Graduate Studies

July 28, 1986
Date

Henry L. Parsons
Graduate Dean

STATEMENT OF PERMISSION TO USE

In presenting this thesis in partial fulfillment of the requirements for a doctoral degree at Montana State University, I agree that the Library shall make it available to borrowers under rules of the Library. I further agree that copying of this thesis is allowable only for scholarly purposes, consistent with "fair use" as prescribed in the U.S. Copyright Law. Requests for extensive copying or reproduction of the thesis should be referred to University Microfilms International, 300 North Zeeb Road, Ann Arbor, Michigan 48106, to whom I have granted "the exclusive right to reproduce and distribute copies of the dissertation in and from microfilm and the right to reproduce and distribute by abstract in any format."

Signature_____

Date____July 25, 1986_____

ACKNOWLEDGEMENTS

The author wishes to thank the National Science Foundation, MONTS and the Physics Department of Montana State University for financial assistance and for providing the material and equipment used in this research. To his advisor, Dr. V. Hugo Schmidt, he is especially grateful for his very helpful discussion, instruction and for his help in personal things that bothered the author and his family very much. He especially thanks Dr. Tomi HIKITA for the fact that the author's experimental skills and elementary theoretical knowledge about Brillouin Scattering were learned from him. Dr. HIKITA taught unselfishly and useful suggestions for this research were given by him. It should be said Dr. HIKITA is the second advisor for Mr. Jin Tong Wang. He thanks Paul Schnackenberg and Paul Schuele for their experimental assistance. He thanks Professor Robert Gammon and Professor Herman Z. Cummins for their valuable discussion, Alfred Beldring for his efforts in repairing the laser options and some other instruments and Professor George F. Tuthill and Professor Wm. M. Kinnersley for their help with the computer work.

TABLE OF CONTENTS

LIST OF TABLES

LIST OF FIGURES

LIST OF FIGURES-CONTINUED

LIST OF FIGURES-CONTINUED

ABSTRACT

The Brillouin spectra of the ferroelectric Tris-Sarcosine Calcium Chloride crystal have been observed in small angle, right angle and backscattering. The smallest angle we have achieved is 7.48°. The frequency range we were working on is about 2 GHz to 32 GHz. Brillouin investigation in such large frequency range is significantly important. The anomalies of hypersound velocity and attenuation were obtained.

We are the first to calculate the polarization of the scattered light in a orthorhombic crystal like TSCC. We are quite successful in interpreting the anomalies of sound velocities and attenuation for the phonon along [001] by piezoelectric coupling and we are the first to interpret the anomalies of sound velocities and attenuation for phonons along the polar axis [010] by the small depolarization effect.

We are the first experimentally to prove the relation $T_c - T_m \propto \Omega$ for [001] phonons and $T_c - T_m$=constant for [010] phonons.

We estimated the elementary relaxation time $\tau_0 = 5.25 * 10^{-14}$ sec for [001] phonons and $\tau_0 = 8.24 * 10^{-12}$ sec for [010] phonons.

CHAPTER I

INTRODUCTION

The study of phase transitions both theoretically and experimentally has found widespread interest during the past few years. Two main aspects make this subject so attractive: the many-particle or cooperative nature of these phenomena and the hypothesis of universality. It stands to reason that the field of phase transitions and critical phenomena has experienced a period of extremely rapid growth during the last two decades, both in the application of new experimental techniques and in the development of new theoretical approaches.[1]

A given assembly of atoms and molecules may be homogeneous or inhomogeneous. The homogeneous parts of such a assembly, called phases, are characterized by thermodynamic properties like volume, pressure, temperature, and energy. An isolated phase is stable only when its free energy is a minimum for the specified thermodynamic conditions.

As to thermodynamic considerations, the classical

Clapeyron equation satisfactorily predicts the features of first-order phase transitions involving discontinuous changes in the first derivatives of the Gibbs free energy such as entropy and volume shown in Fig. 1. Unlike the case of first-order transition, where the free energy surfaces, G(p, T), of the two phases intersect sharply at the transition temperature, it is difficult to visualize the nature of the free energy surfaces in second or higher-order transitions. In second-order transitions, where changes in heat capacity as well as compressibility and thermal expansivity are noticed at the transition, Landau made a momentous contribution to our understanding of phase transitions by expanding the free energy in terms of long-range order parameters Q; Q decreases with an increase of temperature and goes to zero at the transition temperature. The concept of an order parameter today provides a very general way of examining phase transitions.[2]

The idea of phase transitions and spontaneous symmetry breaking has been widely used in physics since the 1930's (Landau 1937). Its application has been significant in both elementary particle physics, and for structural transitions, where it is described (Cochran, 1960, 1961) by the collapse of the energy of an optical phonon, i.e., "soft mode". The diagram in Fig. 2 is now familiar in a

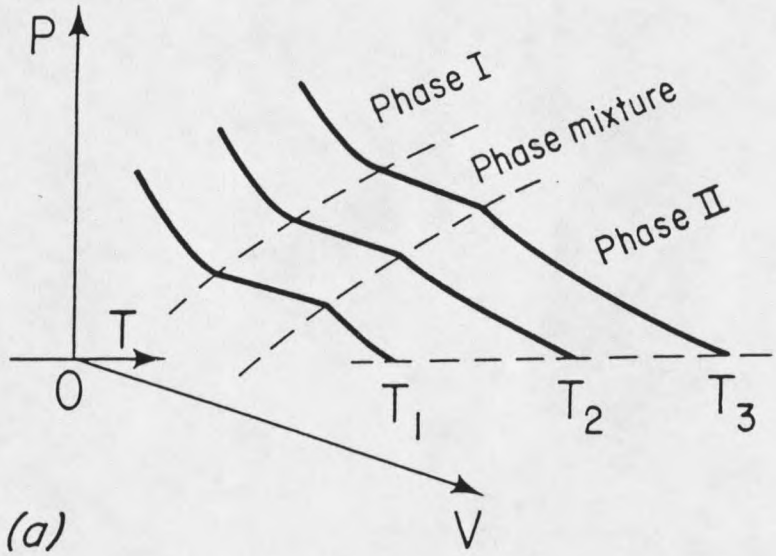

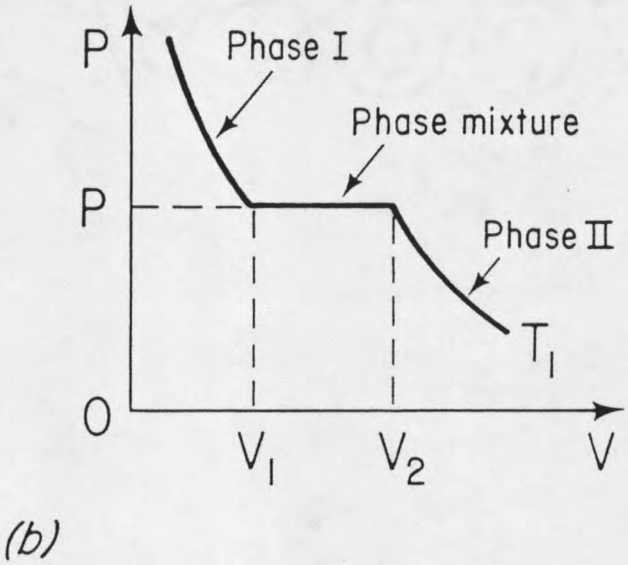

Fig. 1. Phase surface

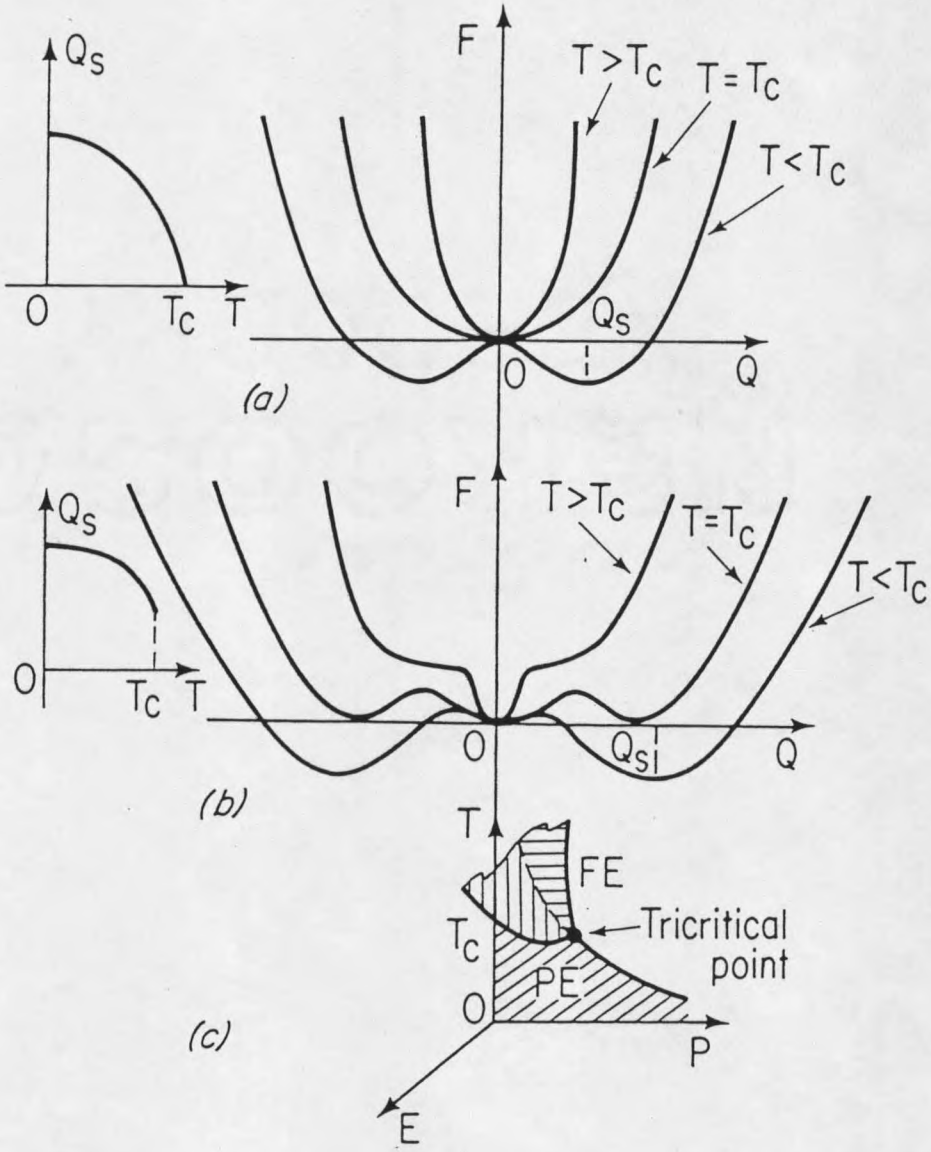

Fig. 2. Free energy and phase transition

variety of contexts. The free energy of a system is plotted versus a general displacement coordinate (order parameter) Q. Below a certain critical temperature T_c the lowest free energy state is obtained at nonzero values of Q. Depending on the sign of the quartic coefficient B in the free energy, the transition may be either continuous (second order) or discontinuous (first-order)[2]. The value of Q which minimizes the free energy at a given temperature T is called the spontaneous value of the order parameter and is usually denoted $Q_s(T)$. Fig. 2(a) shows the dependence of the free energy on Q and T for a continuous transition (in which the quartic coefficient B in Eq. (I-1) is positive); the insert plots $Q_s(T)$ versus T for this case. Fig. 2(b) shows the dependence of free energy on Q and T for a discontinuous transition (in which the quartic coefficient B in Eq. (I-1) is negative); the insert plots $Q_s(T)$ versus T for this case. Fig. 2(c) shows second-order transitions as solid lines; first-order as dashed lines. The black dot is the tricritical point.[3]

The free energy used in this application is phenomenologically written as

$$F(Q,T)=A_0(T-T_0)Q^2+BQ^4+CQ^6 \qquad \text{----------} \qquad (I-1)$$

where $A_0(T-T_0)$ is a linear approximation for the quadratic coefficient which results from the mean field assumption

that all particles interact equally in the system; this is equivalent (Stanley 1971) to the assumption of interaction forces of infinite range, and is expected to be a good approximation for systems where Coulomb forces are dominant. The coefficient B is an explicit function of other variables, such as pressure p, applied electrical field E (for a ferroelectric), or stress S (for a ferroelastic). If B(p) changes sign, a point(T_c, p_c) where the transition changes from second-order to first-order exists in (p, T) space. This is called a tricritical point, because in the three-dimensional T, p, E parameter space for a ferroelectric there are three lines of second-order phase transition boundaries which intersect at (T_c, p_c). This is diagrammed in Fig. 2(c)(Scott, 1976). Such situation are well-known in ferroelectrics such as KH_2PO_4 and SbSI, and they have been studied in detail by light scattering by Peercy (1976).[3] Gammon et al. found that at pressure near and above the tricritical pressure the Brillouin spectrum becomes strongly overdamped and narrower than 50 MHz, the width of the elastic peak in the best crystal.[4] In the free energy expansion, there may be logarithmic terms which result from dipole-dipole interactions in a system, that is so-called logarithmic corrections.[5] Free energy descriptions have been applied successfully in some steady-state systems. From the

point of view of statistical mechanics, a grand partition function, Z_G is given by

$$Z_G(z, V, T) = \sum_{N=0}^{\infty} z^N Z_N(V, T) \quad \text{----------} \quad (I-2)$$

where N is number of a system, V is the volume, T is temperature, z is equal to $\exp(\mu/kT)$, where μ is its chemical potential, Z_N is the classical canonical partition function given by

$$Z_N(V, T) = (1/N\lambda^{3N}) \int \exp[-\Omega(\bar{r}_1, \bar{r}_2, \cdots\cdots \bar{r}_N)/kT]\, d^{3N}\bar{r} \quad (I-3)$$

where λ, the thermal wavelength, is given by $\sqrt{h^2/(2\pi mkT)}$, and $\Omega(\bar{r}_1, \bar{r}_2, \cdots\cdots \bar{r}_N)$ is the potential energy of the system, which indicates all interactions among the particles. Obviously, the partition function

$$Z_G(z, V, T) \approx \sum_{N=0}^{B} z^N Z_N(V, T) \quad \text{----------} \quad (I-4)$$

if B is large enough, and then

$$Z_G(z, V, T) \approx \prod_{N=0}^{B} (1 - z/z_k) \quad \text{----------} \quad (I-5)$$

where z_k are the roots of the polynomial $\sum_{N=0}^{B} z^N Z_N(V, T)$.
Let z_0 be the value on the real axis corresponding to a

zero of $Z_G(z, V, T)$. At this point some thermodynamic variables or their derivatives may show discontinuities, when the volume V goes to infinity. This point is the phase transition point[2].

While the thermodynamic treatment of phase transitions is very fundamental and useful, it does not provide a geometrical picture of the microscopic changes accompanying a transition. The transitions accompanied by microscopic structural change are called structural phase transitions (SPT). The ferroelectric (FE) phase transitions are structural phase transitions. However, two categories, the displacive transition and order-disorder transition are generally classified[6]. Two limiting cases are known:

1) The crystal symmetry is lowered by a spontaneous displacement of sublattices against each other (displacive transition) or

2) Certain atoms or atomic groups have several positions (spatial or directional). In the disordered phase these positions are occupied at random, while in the ordered phase spontaneous ordering in one position takes place (order-disorder transition)[7].

During the phase transition the physical properties of the material such as the dielectric constant or stiffness constant will change. For structural phase transitions we

must study not only the static but also the dynamic properties of the material such as the soft mode, frequency shift of the phonon, attenuation anomalies along with the dielectric constant for a ferroelectric material.

According to the well-known Lyddane-Sachs-Teller (LST) relation

$$\Omega_{L0}/\Omega_{T0}=\sqrt{\epsilon_s/\epsilon_\infty} \qquad \text{(I-6)}$$

where Ω_{L0} is the frequency of the longitudinal optical mode, Ω_{T0} is the frequency of the transverse optical mode. ϵ_s is the static dielectric constant while ϵ_∞ the infinite frequency dielectric constant corresponding to frequencies much higher than phonon frequencies, at which only the electrons contribute to the dielectric response[8].

For some dielectric crystals, when $T=T_c$, ϵ_s goes to infinity and then Ω_{T0} goes to zero.

Practically all experimental investigations deal with the order parameter, either measuring it directly or a generalized susceptibility, which describes its response in space and time. The pertinent experimental methods can be classified into two groups:

1) The system to be studied is exposed to an external influence and the response of the whole system is measured.

2) The variation of local properties is probed locally

within the system.

To the first group belong all the scattering experiments, where the external influence is, for example, a laser beam, x-rays or thermal neutrons and also measurement of material properties, such as the dielectric constant, refractive index, specific heat, etc.. By the method in the first category one determines a correlation of physical quantities.[9]

Examples for the second group are electron and nuclear magnetic resonance experiments.

With the introduction of lasers in the 1960's, light scattering spectroscopy was immediately transformed into a straightforward experimental technique. Raman scattering studies of the soft modes in $KTaO_3$ and $SrTiO_3$ were first reported by Fleury and Worlock (1967). Subsequently, Kaminow and Damen(1968) observed an overdamped soft mode in the Raman spectrum of KH_2PO_4. Fleury et al.(1968) first demonstrated the utility of the soft mode concept for cell-multiplying phase transitions in their study of the cubic-tetragonal transition in $SrTiO_3$. Similarly, Brillouin scattering (Mandelstam-Brillouin scattering in the Russian literature) was applied to the investigation of acoustic modes near phase transitions, complementing the earlier techniques of acoustic resonance and ultrasonic propagation. A soft acoustic mode in KH_2PO_4[1]

was observed by Brillouin scattering by Brody and Cummins (1968).

Since 1970 the emphasis in light scattering of phase transitions has gradually shifted from simple soft mode analysis to aspects of spectra associated with mode coupling, central peaks, polarization coupling with the phonons, modification of the classical soft mode behavior due to critical fluctuations, etc..

The main activity in light scattering investigations of phase transitions concerns the spectrum of scattered light. The starting point of the theory of spectral anomalies is also the idea of the loss of stability, i.e., vanishing of restoring forces for a lattice distortion at the phase transition temperature. This leads to the condition that one of the lattice frequencies is expected to become zero at the phase transition, i.e., to the famous "soft mode" concept. This concept was developed primarily by Ginzburg (1949a,b), Cochran (1960, 1961) and Anderson (1960). There are several types of fluctuation responsible for the scattering. These different sources of scattering can be distinguished on the basis of their temporal behavior in the spectrum of the scattering light. In an insulating crystal the main source of scattering is dielectric constant modulation by acoustic lattice vibrations. Another source in crystals containing certain

atom groups (such as sarcosine) is the internal vibration modes of the molecular group. The optical vibrations of the lattice and the molecular vibrations are the source of what is called the vibrational Raman effect. The optical vibrations of the lattice and the molecular vibrations are of higher frequency. These vibrations result in spectral lines that are displaced from the incident light frequency by from about 50 to over 3500 cm^{-1}. The acoustic lattice vibrations which are much lower frequency for the small wavevectors involved in light scattering are the sources of the Brillouin spectrum, which usually is within 1 cm^{-1} from the incident light frequency. For acoustic modes each primitive cell acts as one mass point, so there are three acoustic modes or branches corresponding to the three degrees of freedom per particle. Thus the Brillouin spectrum will contain three sets of doublets symmetrically placed about the Rayleigh line. But often, the degeneracies in the acoustic branches and selection rules governing the scattered intensity reduce the number of observed Brillouin components. The longitudinal acoustic vibration mode alters the density of the sample and thus the dielectric constant. One predicts the intensity of the longitudinal Brillouin components to be stronger than the intensity of the transverse Brillouin components.

Now we can relate the observed Brillouin splitting, $\delta\Omega$,

to the incident light frequency, Ω_0, and the scattering angle θ, via the Brillouin relation

$$\delta\Omega/\Omega_0 = 2n(v/c)\sin(\theta/2) \qquad \text{(I-7)}$$

where n is the refractive index of the scattering medium and c is the velocity of light in vacuum. Obviously, ~~the~~ Ω_0 is given (the laser frequency is known), and the refractive index n is given or can be measured and the scattering angle θ is determined by the experimental geometry. Thus we need only measure the Brillouin shift of the spectrum to determine the sound velocity of thermally excited acoustic lattice vibrations. This is the essence of the principle of Brillouin scattering.

We can consider the Brillouin scattering process as Bragg diffraction of the incident beam by the wave corresponding to some fluctuation. Even more simply, Brillouin scattering can be viewed as diffraction of incident light by gratings created by sound waves. For example, sound waves cause fluctuations of density, and thus of dielectric constant. These fluctuations act like a grating moving along the wavevector at the speed of sound, so the diffracted light suffers the Doppler shift.

Brillouin scattering was first observed by Gross[10] in liquids and has been used to investigate the elastic properties of alkali halide crystals, quartz,

ferroelectric transitions and other crystals exhibiting other transitions.

For a given scattering wavevector (i.e. for a given scattering angle) there is also scattering produced by non-propagating diffusive fluctuations. The frequency of this scattering light is the same as the frequency of incident light. Fluctuations of the temperature and non-propagating density fluctuations are the sources of this elastic scattering.

For a liquid-gas or liquid-solid transition in the vicinity of the critical point there is a scattering peak produced by density fluctuation. These fluctuations cause critical opalescence, which was first explained by Von Smoluchowski and Einstein. The scattering intensity is related to density-density correlations. We can picture this scattering as caused by a lot of "islands" of liquid in the gas or "islands" of solid in the liquid, resulting from big fluctuations in the vicinity of the critical point,

Recent studies of this critical opalescence using laser light sources and light-beating spectroscopy have greatly increased our knowledge of such transitions.

Ginzburg suggests[11] that an enhanced scattering, similar to critical opalescence, should be observed in the vicinity of an order-disorder transition. This scattering

would be produced by large fluctuations in the degree of order. An enhanced scattering at the α-ß transition in quartz was observed,[12] but it was shown to be due to a static twinning of the crystal.[13]

Because the ferroelectric-paraelectric transition is a structural phase transition, the measurement stated above may provide an indication of the presence of such a "critical opalescence" in the vicinity of the structural phase transition in Tris-Sarcosine Calcium Chloride (TSCC). Such an enhanced quasi-elastic scattering may be performed in the future.

The second reason for the present measurement is to investigate the high frequency sound velocities, the elastic constants, and the attenuation in both the paraelectric and ferroelectric phases. The criterion for deciding what is a high or lower frequency is the inverse of the response time of the order parameter, which is called the relaxation time.

Brillouin scattering measures phonon frequencies in the microwave region. These frequencies are higher than the inverse of the relaxation time for the order parameter. Thus, Brillouin scattering measurements can provide data on the magnitude of the dispersion in the longitudinal sound velocities in TSCC.

We have measured a temperature dependent dispersion in

the velocities of the longitudinal modes propagating along b and c crystal directions. We have done right angle scattering, small angle scattering and backscattering. The smallest angle we have achieved is 7.48°. The large frequency range that we worked on is about 2 GHz to 32 GHz. We have measured the natural line width of the longitudinal Brillouin components for temperatures from 300 K to 110 K. From these widths we determined the lifetime of the microwave frequency of sound waves in the 300 K-110 K temperature region. We also got the temperature dependence of the phonon life times.

From the temperature dependence of the velocities investigated in this work, we can also determine the temperature dependence of the three elastic constants of TSCC via the relation of the velocity to the elastic constant and density.

In Chapter II we present the theory of Brillouin scattering for crystals of orthorhombic structure such as TSCC. Chapter III presents the experimental technique and apparatus used in our experiment. Chapter IV presents the experimental results of our measurements of Brillouin spectra. Chapter V gives a discussion of these results in terms of the relaxation theory of sound absorption due to phonon-polarization coupling theory in TSCC. We interpret the anomalies of sound velocities and attenuations for

[001] phonons by pure piezoelectric coupling and for [010] phonons by piezoelectric coupling with small depolarization effect.

CHAPTER II

THEORY OF BRILLOUIN SCATTERING IN ORTHORHOMBIC CRYSTAL

Introduction

In this chapter we will calculate the Brillouin spectrum from orthorhombic crystals in terms of the sound velocities, polarization, and the wavevector of the acoustic modes with respect to elastic constants and then calculate the intensity, polarization and frequency splitting of the Brillouin components for the scattering from acoustic modes propagating in the a, b, and b, c planes of an orthorhombic crystal. The complete theory of Brillouin scattering in cubic crystals has been given by Benedek and Fritsch.[14] The general equations of their calculation are specialized to the case of scattering from acoustic modes propagating in the [110] planes. Nobody has yet provided the theory of Brillouin scattering in orthorhombic crystals. In this case the calculation will be more complicated than for a cubic crystal. Principal axes of the dielectric tensor are the crystal axes,

and the three elements are equal for cubic crystals, while for orthorhombic crystals the principal axes of the dielectric tensor are the crystal axes also, but the three elements are not equal. The stiffness tensor for orthorhombic crystals has more elements than for cubic crystals.

The Spectrum of the Scattering Field

Basically, the Brillouin scattering is a sort of radiation by the current and charge systems which are functions of time. We can expand these function in Fourier series. Thus we only need to deal with each Fourier component. We only consider the potential, field and radiation produced by finite systems of current and charge without losing generality.[15]

We assume

$$\rho(\bar{r}, t) = \rho(\bar{r})\, e^{-i\Omega t}$$

$$\bar{J}(\bar{r}, t) = \bar{J}(\bar{r})\, e^{-i\Omega t} \qquad \text{(II-1)}$$

As usual the real parts of these functions are the physical quantities.

In the Lorentz gauge the vector potential is

$$\bar{A}(\bar{R},t)=(1/c)\int d^3\bar{r}\int dt'(\bar{J}(\bar{r},t')/|\bar{R}-\bar{r}|)\delta[t'+(|\bar{R}-\bar{r}|/c)-t] \qquad \text{(II-2)}$$

Substituting (II-1) into (II-2), we get

$$\bar{A}(\bar{R})=(1/c)\int \bar{J}(\bar{r})(e^{ik|\bar{R}-\bar{r}|}/|\bar{R}-\bar{r}|)d^3\bar{r} \qquad \text{(II-3)}$$

where $k=\Omega/c$ and

$$\bar{A}(\bar{R},t)=\bar{A}(\bar{R})e^{-i\Omega t} \qquad \text{(II-4)}$$

Then the magnetic field is

$$\bar{B}=\bar{\nabla}\times\bar{A} \qquad \text{(II-5)}$$

and the electric field outside the source is

$$\bar{E}=(i/k)\bar{\nabla}\times\bar{B}=(i/k)\bar{\nabla}\times(\bar{\nabla}\times\bar{A}) \qquad \text{(II-6)}$$

In principle, if the current distribution $\bar{J}(\bar{r})$ is given, we can calculate the field via the integral (II-3). There are three regions. Let the size of the source be d, the wave length λ, the distance from the origin to the position of observation R. The three regions are

near (static) region	$d \ll R \ll \lambda$
middle (induction) region	$d \ll R \approx \lambda$
far (radiation) region	$R \gg \lambda \gg d$

Here, we are only interested in the radiation region.

In this region as shown in Fig. 3, $kr >> 1$ and e^{ikr} oscillates very fast. Then we can make the sufficiently accurate approximation

$$|\bar{R}-\bar{r}| \approx R-\bar{I}\cdot\bar{r} \qquad \text{(II-7)}$$

where $\bar{I}$ is the unit vector in the direction of $\bar{R}$ and $\bar{r}$ is the distance to the radiating point. Then the integral (II-3) becomes

$$\lim_{R\to\infty} \bar{A}(\bar{R}) = (e^{ikR}/cR)\int \bar{J}(\bar{r})\, e^{-ik\bar{I}\cdot\bar{r}}\, d^3\bar{r} \qquad \text{(II-8)}$$

This means that in the far region, the vector potential is that of a expanding spherical wave with a factor which is a function of the solid angle. It is easy to show that the fields calculated from (II-5) and (II-6) are transverse to the radius vector and decrease as R^{-1}. They thus correspond to the radiation field. If the source dimensions are small compared to a wavelength it is appropriate to expand the integral in (II-8) in powers of k.

$$\lim_{kR\to\infty} \bar{A}(\bar{R}) = (e^{ikR}/cR)\,\Sigma[(-ik)^n/n!]\int \bar{J}(\bar{r})(\bar{I}\cdot\bar{r})^n\, d^3\bar{r} \qquad \text{(II-9)}$$

If only the first term in (II-9) is kept, then the vector

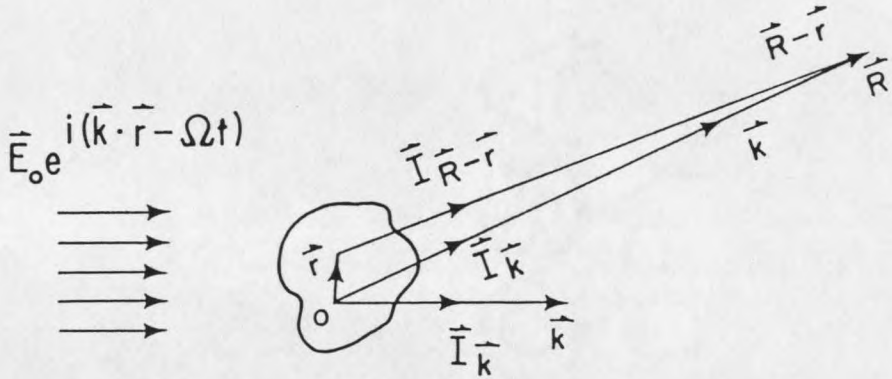

Fig. 3. Light scattering diagram

potential will be

$$\bar{A}(\bar{R}) = (e^{ikR}/cR)\int \bar{J}(\bar{r})\, d^3\bar{r} \quad \text{----------} \quad (II\text{-}10)$$

The integral can be put in more familiar terms by an integration by parts

$$\int \bar{J}(\bar{r})\, d^3\bar{r} = -\int \bar{r}(\bar{\nabla}' \cdot \bar{J})\, d^3\bar{r} + \bar{r}\cdot\bar{J}\Big|_{-\infty}^{\infty} \quad \text{--------} \quad (II\text{-}11)$$

In the limit of large $\bar{r}$, $\bar{r}\cdot\bar{J}=0$, so

$$\int \bar{J}\, d^3\bar{r} = -i\Omega\int \bar{r}\rho(\bar{r})\, d^3\bar{r} \quad \text{----------} \quad (II\text{-}12)$$

since from the continuity equation

$$i\Omega\rho(\bar{r}) = \bar{\nabla}\cdot\bar{J} \quad \text{----------} \quad (II\text{-}13)$$

Thus the vector potential is

$$\bar{A}(\bar{R}) = (-ike^{ikR}/R)\int \bar{P}(\bar{r})\, d^3\bar{r} \quad \text{---------} \quad (II\text{-}14)$$

where $\bar{P} = \rho(\bar{r})\cdot\bar{r}$, the polarization.

Now we calculate the intensity and spectrum of light scattered from thermal fluctuations in liquids and solids. Since the media contain about 10^9 atoms in a region as small as the cube of the light wavelength, for a dimension of this order a liquid or solid may be regarded as a

continuum. A light wave passing through the medium produces an oscillating dipole moment per unit volume of polarization $\bar{P}(\bar{r},t)$ at each point $\bar{r}$ and at time t. The oscillating moments in turn radiate or scatter electromagnetic waves in all directions. From Equations (II-6) and (II-14), the electric field $d\bar{E}'$ at the field point $\bar{R}$ caused by the oscillating dipole moments within a volume $|d^3\bar{r}| << \lambda^3$ is[14]

$$d\bar{E}'(\bar{R},t)=[\bar{I}_{R-r}x(\bar{I}_{R-r}xd^2\bar{p}(\bar{r},t')/dt^2)/c^2|\bar{R}-\bar{r}|]d^3\bar{r} \qquad \text{(II-15)}$$

where the vectors $\bar{R}$, $\bar{r}$ are the observation point outside the medium and the radiating point inside the medium. The unit vector $\bar{I}$ is shown in Fig. 3.

If the radiation has low intensity, the local polarization is linearly proportional to the electric field. The proportional factor is a tensor α. It is convenient to decompose α into its time-average part $\langle\alpha\rangle$ and the time-space fluctuations $\delta\alpha(\bar{r},t)$ produced by thermal fluctuations in the medium. In liquids and in cubic crystals the time-average polarizability $\langle\alpha\rangle$ is a scalar times the unity tensor and the index of refraction n is independent of the direction of propagation. However, the thermal fluctuation in a crystal causes off-diagonal components in the polarizability tensor, so we

should regard $\delta\alpha$ as a tensor whose elements fluctuate in time. Writing the electric field of the incident wave within the medium as

$$\bar{E}(\bar{r},t)=\bar{E}_0 e^{i(\bar{k}\cdot\bar{r}-\Omega t)} \qquad \text{----------} \qquad (II\text{-}16)$$

where $k=n\Omega/c$ is the wave vector of the light wave in the medium, we find that the polarization at each point in the medium is

$$\bar{p}(\bar{r},t)=(\langle\alpha\rangle+\delta\alpha(\bar{r},t))\cdot\bar{E}_0 e^{i(\bar{k}\cdot\bar{r}-\Omega t)}$$

To calculate the second derivative of $\bar{p}$ as required by Eq.(II-1), we have

$$d\bar{p}/dt=-i\Omega_0\langle\alpha\rangle\bar{E}_0 e^{i(\bar{k}\cdot\bar{r}-\Omega t)}-i\Omega_0\delta\alpha\bar{E}_0 e^{i(\bar{k}\cdot\bar{r}-\Omega t)}$$

$$+[d(\delta\alpha)/dt]\bar{E}_0 e^{i(\bar{k}\cdot\bar{r}-\Omega t)} \qquad \text{---------} \qquad (II\text{-}17)$$

$$d^2\bar{p}/dt^2=-\Omega_0{}^2\langle\alpha\rangle\bar{E}_0 e^{i(\bar{k}\cdot\bar{r}-\Omega t)}-\Omega_0{}^2\bar{E}_0\delta\alpha e^{i(\bar{k}\cdot\bar{r}-\Omega t)}$$

$$-2i\Omega_0\bar{E}_0 e^{i(\bar{k}\cdot\bar{r}-\Omega t)}d(\delta\alpha)/dt$$

$$+[d^2(\delta\alpha)/dt]^2\bar{E}_0 e^{i(\bar{k}\cdot\bar{r}-\Omega t)} \qquad \text{-----} \qquad (II\text{-}18)$$

We can see that the characteristic frequencies for

thermal fluctuations are small ($\leq 10^{12}$ Hz) compared to the light frequency in the optical region ($\approx 5*10^{12}$ Hz). We may therefore keep just the first two terms in Eq.(2-18) and write

$$d^2\bar{p}(\bar{r},t)/dt^2 \approx -\Omega^2(\langle\alpha\rangle+\delta\alpha)\bar{E}_0 e^{i(\bar{k}\cdot\bar{r}-\Omega t)}$$

$$= -\Omega^2\bar{p}(\bar{r},t) \qquad \text{----------} \qquad \text{(II-19)}$$

On substituting Eqs.(II-19) and (II-18) into (II-15), (II-1) and carrying out the integration over the illuminated volume V at the retarded time t', we find that if $\bar{R}>>\bar{r}$

$$\bar{E}'(\bar{R},t) = [-(\Omega/c)^2 e^{i(\bar{k}\cdot\bar{R}-\Omega t)}/R]\cdot\bar{I}_K x[\bar{I}_K$$

$$x\int(\langle\alpha\rangle+\delta\alpha(\bar{r},t))\bar{E}_0 e^{i(\bar{k}-\bar{k}')\cdot\bar{r}}]d^3\bar{r} \qquad \text{(II-20)}$$

where we have made use of the fact that if $\bar{R}>>\bar{r}$,

$$\bar{I}_{R-r} \approx \bar{I}_k$$

and

$$n\Omega/c|\bar{R}-\bar{r}| \approx n\Omega/c\bar{I}_k\cdot(\bar{R}-\bar{r})$$

and

$$\bar{k}' = n\Omega\bar{I}_k/c$$

and

$$|\bar{R}-\bar{r}| \approx R$$

The integral (II-20) indicates the superposition of phases of waves scattered from each illuminated point in the crystal volume. If the fluctuation $\delta\alpha$ is absent, this superposition leads to a complete cancellation of the scattered waves. The contribution to the integral from the $\langle\alpha\rangle$ term is zero except in the forward direction. Scattering out of the incident direction results entirely from fluctuations in the polarizability.

By decomposing the fluctuations into their spatial Fourier components

$$\delta\alpha(\bar{r}, t') = (2\pi)^{-3/2} \sum_{\mu} \int |dq| \, \delta\alpha(\bar{q}) \, e^{i[\bar{q}\cdot\bar{r} \pm \Omega_\mu(\bar{q})t']} \qquad \text{(II-21)}$$

where $\bar{q}$ is the wavevector of the fluctuation and $\Omega_\mu(\bar{q})$ is the frequency of the fluctuation corresponding to this wavevector (wavelength). The superscript μ denotes the branch in the dispersion relation connecting $\bar{q}$ and Ω. In general, $\Omega_\mu(\bar{q})$ can be complex to include a description of the damping of the fluctuations. $\Omega_\mu(\bar{q})$ is double valued

with ± to account for the degeneracy in the dispersion relation for positive and negative running waves. We now can put Equation (II-21) into (II-20), being careful to include the effect of time retardation in $\delta\alpha$. We obtain

$$\bar{E}'(\bar{R},t)=-(\Omega/c)^2\sum_{\mu}[e^{i(\bar{k}'\cdot\bar{R}-t)}/R]\bar{I}_k x[\bar{I}_k x\int\int(2\pi)^{-3/2}$$

$$|dq|\delta\alpha_\mu(\bar{q})e^{i(\bar{q}\cdot\bar{r}\pm\Omega_\mu(\bar{q})t)}\bar{E}_0 e^{i(\bar{k}-\bar{k}')\cdot\bar{r}}|d\bar{r}|$$

$$=-(\Omega/c)^2\sum_{\mu}e^{i(\bar{k}'\cdot\bar{R}-\Omega_\mu(\bar{q})t)}/R\bar{I}_k x\{\bar{I}_k$$

$$x\int|dq|\delta\alpha_\mu(\bar{q})e^{i[\bar{q}\cdot\bar{r}\pm\Omega_\mu(\bar{q})(t-\bar{I}_k\cdot(\bar{R}-\bar{r})/c_m)]}$$

$$\bar{E}_0\int e^{i(\bar{k}-\bar{k}')\cdot\bar{r}}d^3\bar{r} \qquad \text{----------} \qquad \text{(II-22)}$$

$$e^{i\bar{k}'\cdot\bar{R}}\cdot e^{-i\Omega_\mu/c_m\bar{I}_k\cdot\bar{R}}=e^{i(\bar{k}'-\Omega_\mu/c_m\bar{I}_k)\cdot\bar{R}}$$

$$=e^{i(\Omega/c\pm\Omega_\mu/c_m)\bar{I}_k\cdot\bar{R}}$$

$$=e^{i((\Omega\pm\Omega_\mu)/c_m)\bar{I}_k\cdot\bar{R}}$$

$$=e^{i\bar{k}\cdot\bar{R}}$$

where $\bar{k}=(\Omega\pm\Omega_\mu(\bar{q}))/c_m$

$$e^{i(\bar{q}\cdot\bar{r}\pm\Omega_\mu/c_m\bar{I}_k\cdot\bar{r})}e^{i(\bar{k}-\Omega/c_m\bar{I}_k\cdot\bar{r})}$$

$$=e^{i(\bar{q}-(\Omega\pm\Omega_\mu)/c_m\bar{I}_k-\bar{k})\cdot\bar{r}}$$

$$=e^{i(\bar{q}-\bar{k}'+\bar{k})\cdot\bar{r}}$$

Hence

$$\bar{E}'(\bar{R},t)=-(\Omega/c)^2\sum_{\mu}\bar{I}_k x[\bar{I}_k x\int|dq|\delta\alpha_\mu(\bar{q})\cdot\bar{E}_0$$

$$\cdot(e^{i[\bar{k}\cdot\bar{R}-[\Omega\pm\Omega_\mu(\bar{q})]t]}/R)$$

$$\cdot(2\pi)^{-3/2}\int|d\bar{r}|e^{i(\bar{k}-\bar{k}'+\bar{q})\cdot\bar{r}} \qquad \text{(II-23)}$$

The final integral in Equation (II-23) is a delta function provided that the illuminated region is very large compared to the wavelength of light. In this case

$$\int e^{i(\bar{k}-\bar{k}'+\bar{q})\cdot\bar{r}}|d\bar{r}|=(2\pi)^3\delta[\bar{q}-(\bar{k}'(\bar{q})-\bar{k})] \qquad \text{(II-24)}$$

Thus the wavevector of the fluctuation which produces the scattering in the direction $\bar{k}'$ is that which satisfies the implicit equation

$$\bar{q}=\bar{k}'(\bar{q})-\bar{k}=\bar{K} \quad \text{----------} \qquad \text{(II-25)}$$

We replace vector $\bar{q}$ in Equation (II-25) by $\bar{K}$ and call it the scattering vector. The vector $\bar{K}$ in this Equation can be interpreted physically in two equivalent ways. In photon terminology, it implies the conservation of momentum among the incident photon $\bar{k}$, the scattered photon $\bar{k}'$ and the scattering fluctuation $\bar{K}$. We notice the relation $\bar{k}'=(\Omega\pm\Omega_\mu(\bar{q}))/c$. The wavelength of the scattered light is different from that of the incident

light because the scattering fluctuation can add or subtract a quantum of energy $\pm h\Omega_\mu(\bar{K})$ to the incident photon. In classical terms, Equation (II-5) indicates that a spatially periodic fluctuation can modulate the polarizability and hence the phase of waves scattered from each point in such away as to exactly cancel out the phase factor $e^{i(\bar{k}'-\bar{k})\cdot\bar{r}}$ produced by the combined effect of the spatial variation of the incident wave and the time retardation. As a result of this cancellation the radiation from each point in the medium adds coherently at the field point, or we can regard this phenomena as a Doppler effect. In this classical description, Equation (II-25) corresponds to a Bragg reflection of the light waves off the wave front of the fluctuation. We substitute Equations (II-25) and (II-24) into (2-23) and replace $\delta\alpha$ by $\delta\epsilon/4\pi$, where $\delta\epsilon$ is the fluctuation in the dielectric constant tensor. Obviously, $\bar{I}_R=\bar{I}_k$, so we relabel $\bar{E}'(\bar{R},t)=\bar{E}(\bar{k}',t)$, (i.e. we emphasize the dependence of the scattered field on the direction of scattering)

$$\bar{E}'(\bar{R},t)=\bar{E}(\bar{k}',t)=[-(\Omega/c)^2(2\pi)^{3/2}/4\pi R]\sum_\mu e^{i[\bar{k}\cdot\bar{R}-(\Omega\pm\Omega_\mu)t]}$$

$$\cdot\bar{I}_k x[\bar{I}_k x(\delta\epsilon(\bar{K})\cdot\bar{E}_0] \quad \text{------} \quad \text{(II-26)}$$

We can see from this equation there are three $\Omega_\mu(\bar{K})$ for the same wavevector $\bar{K}$. Thus in the spectrum there would

be three Brillouin scattering peaks.

The fluctuation of the dielectric constant is caused by the fluctuation of the lattice strain. The optical properties of crystals historically have been specified in terms of the indicatrix, and ellipsoid of resolution, the principal axes of which have length given by the inverse dieletric constants in the principal directions of the crystal. In more modern terms we may say that diagonalizes the dielectric tensor.

Equation (II-25) states that the scattering results from a particular Fourier component of the fluctuations in the dielectric constant. In the scattering process, momentum and enegry are conserved. Momentum conservation relates the wavevectors of the incident wave $\bar{k}$, the scattered wave $\bar{k}'$ and the scattering fluctuation $\bar{K}$

$$h\bar{k}' = h\bar{k} + h\bar{K} \qquad \text{(II-27)}$$

Energy conservation is indicated in the relationship between the incident light frequency Ω, the scattered light frequency Ω' and the frequency of the Fourier component of the fluctuation responsible for the scattering $\Omega_\mu(\bar{K})$

$$h\Omega' = h\Omega \pm h\Omega_\mu(\bar{K}) \qquad \text{(II-28)}$$

where the ± sign allows for scattering accompanied by

creation or annihilation of a phonon. These equations state that we are dealing with Bragg reflection of the incident light wave off the wavefront of the fluctuations for a particular wavevector $\bar{K}$. We can regard this scattering as the incident light being scattered by a moving one-dimensional periodic lattice. But since these fluctuations are propagating, the light frequency suffers a Doppler shift $\Omega \pm \Omega_\mu$.

We now calculate the magnitude of the wavevector of the fluctuation wave $\bar{K}$

$$|\bar{k}| = (n/c)(\Omega \pm \Omega_\mu)$$

$$\approx (n/c)\Omega. \qquad \text{----------} \qquad \text{(II-29)}$$

because

$$\Omega_\mu << \Omega$$

and

$$|\bar{k}'| = n\Omega/c$$

$$|\bar{K}|^2 = k'^2 + k^2 - 2k'k\cos\theta$$

$$= (n_0\Omega/c)^2 + (n^k\Omega/c)^2 - 2n^k n_0 \Omega^2/c^2 \cos\theta$$

$$= (\Omega/c)^2 (n_0^2 + n^{k\,2} - 2n_0 n^k \cos\theta \qquad \text{--} \qquad \text{(II-30)}$$

$$|\bar{K}| = (\Omega/c)\sqrt{n_0^2 + n^{k\,2} - 2n_0 n^k \cos\theta} \qquad \text{---} \qquad \text{(II-30')}$$

If $n_0 = n^k = n$

$$|\bar{K}| = (2\Omega n/c)\sin\theta \quad \text{----------} \quad (II\text{-}31)$$

For small angle scattering $\theta \approx 0$ whether $n_0 = n^k$ or not

$$|\bar{K}| = (\Omega/c)\sqrt{n_0^2 + n_0^2 + 2n_0(dn/d\theta)\theta - 2n_0(n_0 + (dn/d\theta)\theta)\cos\theta}$$

$$= (\Omega/c)\sqrt{2n_0^2 - 2n_0^2\cos\theta + (1-\cos\theta)2n_0(dn/d\theta)\theta}$$

$$= (\Omega/c)\sqrt{2n_0^2(1-\cos\theta) + 2n_0(dn/d\theta)\theta(1-\cos\theta)}$$

$$= (2\Omega/c)\sqrt{n_0^2 + n_0(dn/d\theta)\theta\sin^2(\theta/2)}$$

$$\approx (2\Omega/cn_0)\sin(\theta/2) \quad \text{----------} \quad (II\text{-}32)$$

For anisotropic homogeneous meterial, the indicatrix has the following important properties. Draw through the origin a straight line OP in an arbitrary direction. Draw the central section of the indicatrix perpendicular to the line OP. This will be an ellipse. If the displacement $\bar{D}$ of the wave propagating along OP is polarized in the direction of the semi-axis OA of the ellipse (i.e. $\bar{D}$ vibrates parallel to OA), this has refractive index OA. If $\bar{D}$ is parallel to OB (another semi-axis of the ellipse), then the wave has refractive index OB. Thus, only if the polarization of the light is along either OA

or OB, does the wave has a single refractive index shown in Fig. 4.

Assume the direction of the incident light is $\bar{k}$ and polarization for $\bar{E}$ inside the crystal is perpendicular to $\bar{k}$. The central section of the indicatrix perpendicular to $\bar{k}$ must be an ellipse. If the semi-axes are OA and OB, the component of $\bar{E}$ along OA and OB have refractive indices n_1 and n_2 respectively. The same relation holds for the scattered light. Each component of the incident light beam creates scattered light in the $\bar{k}'$ direction. The scattered light itself has two components, with refractive indices, say, n_1' and n_2'. We may observe four phonons following the relations

$$k_1 = \Omega / c\sqrt{n_1^2 + n_1'^2}$$

$$k_2 = \Omega / c\sqrt{n_1^2 + n_2'^2}$$

$$k_3 = \ / c\sqrt{n_2^2 + n_1'^2}$$

$$k_4 = \Omega / c\sqrt{n_2^2 + n_2'^2} \qquad \text{----------} \qquad \text{(II-33)}$$

If we do not distinguish the four waves, we can never measure the peak and particularly the lifetime of a given phonon. To obviate this problem, we have to find the optical axes and be very careful with the scattering geometry. Fortunately, TSCC is an orthorhombic structure

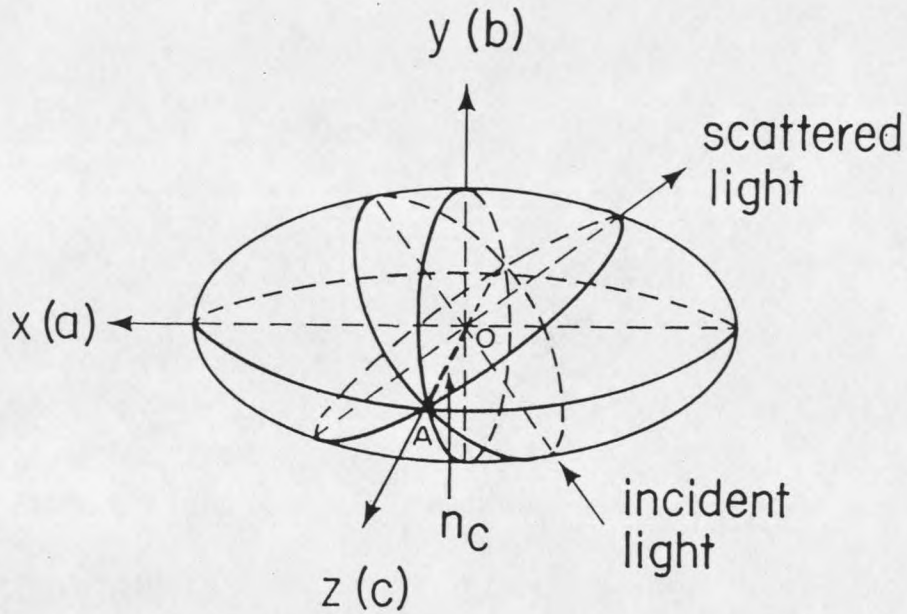

Fig. 4. Refractive indicatrix

for which the optical tensor axes lie along the crystal axes, and we are only interested in the longitudinal phonons. In this case the polarization of both the incident and scattered light is vertical, so that we don't worry about this problem.

The Fluctuation $\delta\bar{\bar{\epsilon}}$ of the Dielectric Constant

The refractive index of a crystal is specified by the indicatrix, which, as we have seen in section B, is an ellipsoid whose coefficients are the components of the refractive dielectric impermeability tensor B_{ij} for the optical axes, namely,

$$B_{ij}x_i x_j=1 \qquad \text{(II-34)}$$

and by the definition, $B_{ij}=k_0 dE_i/dD_j$, and $\epsilon_{ij}=dD_i/dE_j$, we have

$$\bar{\bar{\epsilon}}=1/B$$

In general, a small change of refractive index, more precisely, a small change in the shape, size and orientation of the indicatrix, is produced by electric field and stresses. This change is most conveniently specified by giving the small change in the coefficients B_{ij}. If we neglect higher-order terms than the first in the fields and stresses, the changes of B_{ij} in the

coefficients under an applied field E_K and an applied strain ϵ_{rs} are given by

$$\delta B_{ij} = Z_{ijk} E_k + p_{ijrs} \epsilon_{rs} \quad \text{----------} \quad (II\text{-}36)$$

In the Brillouin scattering, we only consider the second term, namely

$$\delta B_{ij} = p_{ijrs} \epsilon_{rs} \quad \text{----------} \quad (II\text{-}37)$$

or in another way

$$\delta B_m = p_{mn} \epsilon_n \quad (m, n = 1, 2, 3, 4, 5, 6) \quad \text{---} \quad (II\text{-}38)$$

Using the following conversion scheme

tensor notation	11	22	33	23, 32	31, 13	12, 21
matrix notation	1	2	3	4	5	6

The source of the fluctuation in $\bar{\bar{\epsilon}}$ that interest us is the acoustic lattice vibrations or phonons. There are three such acoustic modes for each $\bar{K}$. These thermally excited lattice vibrations modulate the dielectric properties of the medium. This modulation occurs because the optical dielectric constant or refractive index is a function of the state of strain of the lattice. The optical properties of the crystal have been specified in terms of dielectric tensor ϵ_{ij}. In general, the fluctuation of the dielectric tensor can be expressed as

$$\delta\epsilon_{ij}=\Sigma p_{ijrs}e_{rs} \qquad \text{----------} \qquad (II\text{-}39)$$

where the ϵ_{rs} are the strain components which are defined in terms of the particle displacement u_i as

$$\epsilon_{rs}(\bar{r},t)=(1/2)[du_r(\bar{r},t)/dx_s+du_s/dx_r]$$

The indices r, s range over the values 1 to 3.

From Equation (II-20) we see that $\bar{E}_0$ can be taken outside the integral only if it does not change its direction. We assume the polarization of the incident light is along the optical axis. Thus for the outgoing light beam, we have two components in the direction of the two optical axes. The result for the intensity scattered into a unit solid angle in the direction $\bar{K}$ is

$$dP_\perp/d\Omega=P_0 n_\perp(\Omega/c)^4[(2\pi)^3/(4\pi)^2]\sum_{\mu=1}^{3}[V/(2\pi)^3$$

$$\cdot kT/2\Omega_\mu(\bar{K})^2]\,|\bar{A}_\perp|^2K^2$$

$$=P_0(\Omega/c)^4[V/(4\pi)^2]n_\perp\sum_{\mu=1}^{3}|\bar{A}_\perp|^2/(\rho v(\bar{K},\Omega_\mu)^2)$$

$$\text{----------} \qquad (II\text{-}40)$$

$$dP_\parallel/d\Omega=P_0 n_\parallel(\Omega/c)^4[V/(4\pi)^2]\sum_{\mu=1}^{3}|\bar{A}_\parallel|^2/(\rho v(\bar{K},\Omega_\mu)^2)$$

$$\text{----------} \qquad (II\text{-}41)$$

The temperature dependence comes from the kinetic energy of the phonon.

$$\langle E\rangle = 2\langle m|\dot{u}|^2\rangle/2$$

$$= 1/[1-e^{h\nu/(kT)}]$$

$$\approx kT/h$$

The first form of (II-40) shows essential features of the intensity. The Ω^4 term is just the Rayleigh law, the parentheses include terms which are just the mean squared amplitude of the acoustic mode of frequency Ω propagating in the direction $\bar{K}$. The quantity $|\bar{A}_\mu|^2$ is the coupling constant that includes the selection rules and strength of the photoelastic coupling between the acoustic vibration and the dielectric constant. The K^2 term arises from the fact that the number of modes per unit frequency interval increases with K^2.

We know that

$$\int \delta(\Omega)\, dK_x\, dK_y\, dK_z = \int \delta(\Omega)\, 2\pi K^2\, dK$$

$$= \int \delta(\Omega)\,(2\pi K^2/v)\, d\Omega$$

$$= (2\pi/v^3)\int \delta(\Omega_\mu' - \Omega_\mu)\,\Omega_\mu'^{\,2}\, d\Omega_\mu'$$

$$= (2\pi/v^3)(\Omega_\mu)^2 \qquad \text{----} \qquad \text{(II-42)}$$

Substituting expression $\Omega_\mu = v(\bar{I}_k).K$, we get the second form of Equation (II-40). The summation over μ is a sum over the three acoustic branches, each of which has a polarization orthogonal to the other two branches.

We may thus expect the intensity

$$dP_\perp/d\Omega = P_0 n_\perp (\Omega/c)^4 (V/(4\pi)^2) \sum_{\mu=1}^{3} |\bar{A}_\perp|^2 / [\rho\, v(\bar{K}, \Omega_\mu)^2]$$

$$\cdot \int (1/\pi) \{\Gamma_\mu / [(\Omega' - \Omega \pm \Omega_\mu)^2 + \Gamma_\mu^2]\} d\Omega'$$

---------- (II-40')

$$dP_\parallel/d\Omega = P_0 n_\parallel (\Omega/c)^4 (V/(4\pi)^2) \sum_{\mu=1}^{3} |\bar{A}_\parallel|^2 / [\rho\, v(\bar{K}, \Omega_\mu)^2]$$

$$\cdot \int (1/\pi) \Gamma_\mu / [(\Omega' - \Omega \pm \Omega_\mu)^2 + \Gamma_\mu^2]$$

---------- (II-41')

Here, we have included the fact that each Brillouin component has a width Γ_μ that arises from the finite lifetime of the phonons responsible for the scattering. The Lorentzian shape is a result of the assumption that phonons decay in time as $e^{-\Gamma t}$.

The $\bar{A}$ determine the intensities of the Brillouin components and include the effects arising from the geometrical relationship of incident field polarization,

sound wave polarization and sound wave propagation direction. Explicitly

$$\bar{A} = \bar{I}_k \times [\bar{I}_k \times \delta\bar{D}] \quad \text{----------} \quad (II\text{-}43)$$

where

$$\delta\bar{D} = \delta\epsilon \cdot \bar{E}_0 = \delta\bar{\bar{\epsilon}} \cdot E_0 \bar{I}_E \quad \text{----------} \quad (II\text{-}44)$$

Acoustic Modes in a Monoclinic Crystal

To calculate the acoustic velocities and their dependence on propagation direction in the lattice we must solve the dynamical equation of motion

$$\rho d^2 u_i / dt^2 = \sum_j d\sigma_{ij} / dx_j \quad \text{----------} \quad (II\text{-}45)$$

where u_i is the displacement in the ith direction, ρ is the density and σ_{ij} are elements of the stress tensor.

Now we choose coordinates for an orthorhombic crystal such as TSCC, such that x_1 is along a axis, x_2 along b and x_3 along c.

We treat the crystal in the long wavelength limit. We use the generalized Hooke's law to form the relation between the stresses and the strains.

$$\sigma_{ij} = \sum_{k,l} C_{ijkl} e_{kl} \quad \text{----------} \quad (II\text{-}46)$$

Where the C_{ijkl} are the elastic constants of the crystal and e_{kl} are the elastic strain components defined before. Substituting ϵ_{kl} into Equations (II-45) and (II-46) yields the wave equations

$$\rho d^2 u_i / dt^2 = \sum_{jkl} C_{ijkl} d^2 u_k / dx_j dx_l \quad ----- \quad (II-47)$$

We have used the symmetry property

$$C_{ijkl} = C_{ijlk}$$

and

$$C_{jikl} = C_{ijkl}$$

We seek plane wave solutions of Equation (II-47), having

$$u_i = u_{i0} e^{i(\bar{K} \cdot \bar{r} - \Omega t)}$$

$$= u_{i0} e^{i(\Sigma K_\kappa - \Omega t)} \quad ---------- \quad (II-48)$$

Substituting Equation (II-48) into Equation (II-47), we obtain

$$\rho \Omega^2 u_i = \sum_{kj} C_{ikjl} u_k K_j K_l \quad ---------- \quad (II-49)$$

Then

$$\rho \Omega^2 u_i = \sum_{kj} C_{1kj1} u_k K_j K_1 + \sum_{kj} C_{1kj2} u_k K_j K_2 + \sum_{kj} C_{1kj3} u_k K_j K_3$$

$$= \sum_k C_{1k11} u_k K_1 K_1 + \sum_k C_{1k21} u_k K_2 K_1 + \sum_k C_{1k31} u_k K_3 K_1$$

$$+\sum_k C_{1k12}u_k K_1 K_2 + \sum_k C_{1k22}u_k K_2 K_2 + \sum_k C_{1k32}u_k K_3 K_2$$

$$+\sum_k C_{1k13}u_k K_1 K_3 + \sum_k C_{1k23}u_k K_2 K_3 + \sum_k C_{1k33}u_k K_3 K_3$$

$$=\sum_k (C_{1k11}K_1 K_1 + C_{1k21}K_2 K_1 + C_{1k31}K_3 K_1 + C_{1k12}K_1 K_2$$

$$+C_{1k22}K_2 K_2 + C_{1k32}K_3 K_2 + C_{1k13}K_1 K_3 + C_{1k23}K_2 K_3$$

$$+C_{1k33}K_3 K_3)u_k \quad \text{----------} \quad (II\text{-}50)$$

Here K_j, K_l $(j, l=1, 2, 3)$ are the components of $\bar{K}$ along the crystal axes. Equation (II-50) becomes

$$\rho\Omega^2 u_1 = (C_{1111}K_1 K_1 + C_{1121}K_2 K_1 + C_{1131}K_3 K_1 + C_{1112}K_1 K_2$$

$$+C_{1122}K_2 K_2 + C_{1132}K_3 K_2 + C_{1113}K_1 K_3 + C_{1123}K_2 K_3$$

$$+C_{1133}K_3 K_3)u_1 + (C_{1211}K_1 K_1 + C_{1221}K_2 K_1$$

$$+C_{1231}K_3 K_1 + C_{1212}K_1 K_2 + C_{1222}K_2 K_2 + C_{1232}K_3 K_2$$

$$+C_{1213}K_1 K_3 + C_{1223}K_2 K_3 + C_{1233}K_3 K_3)u_2$$

$$+(C_{1311}K_1 K_1 + C_{1321}K_2 K_1 + C_{1331}K_3 K_1 + C_{1312}K_1 K_2$$

$$C_{1322}K_2 K_2 + C_{1332}K_3 K_2 + C_{1313}K_1 K_3 + C_{1323}K_2 K_3$$

$$C_{1333}K_3 K_3)u_3 \quad \text{----------} \quad (II\text{-}51)$$

We change from tensor to matrix notation, and obtain

$$\rho\Omega^2 u_1 = (C_{11}K_1K_1 + C_{16}K_2K_1 + C_{15}K_3K_1 + C_{16}K_1K_2 + C_{12}K_2K_2$$

$$+ C_{14}K_3K_2 + C_{15}K_2K_3 + C_{13}K_3K_3)\,u_1 + (C_{61}K_1K_2$$

$$+ C_{66}K_2K_1 + C_{65}K_3K_1 + C_{66}K_1K_2 + C_{62}K_2K_2 + C_{64}K_3K_2$$

$$+ C_{65}K_1K_3 + C_{64}K_2K_3 + C_{63}K_3K_3)\,u_2 + (C_{51}K_1K_1$$

$$+ C_{56}K_2K_1 + C_{55}K_3K_1 + C_{56}K_1K_2 + C_{52}K_2K_2 + C_{54}K_3K_2$$

$$+ C_{55}K_1K_3 + C_{54}K_2K_3 + C_{53}K_3K_3)\,u_3 \quad - \quad \text{(II-51')}$$

$$\rho\Omega^2 u_2 = (C_{2111}K_1K_1 + C_{2121}K_2K_1 + C_{2131}K_3K_1 + C_{2112}K_1K_2$$

$$+ C_{2122}K_2K_2 + C_{2132}K_3K_2 + C_{2113}K_1K_3 + C_{2123}K_2K_3$$

$$+ C_{2133}K_3K_3)\,u_1 + (C_{2211}K_1K_1 + C_{2221}K_2K_1$$

$$+ C_{2231}K_3K_1 + C_{2212}K_1K_2 + C_{2222}K_2K_2 + C_{2232}K_3K_2$$

$$+ C_{213}K_1K_3 + C_{2223}K_2K_3 + C_{2233}K_3K_3)\,u_2$$

$$+ (C_{2311}K_1K_1 + C_{2321}K_2K_1 + C_{2331}K_3K_1 + C_{2312}K_1K_2$$

$$+ C_{2322}K_2K_2 + C_{2332}K_3K_2 + C_{2313}K_1K_3 + C_{2323}K_2K_3$$

$$+ C_{2333}K_3K_3)\,u_3 \quad \text{----------} \quad \text{(II-52)}$$

Again changing from tensor to matrix notation,

$$\rho\Omega^2 u_2 = (C_{61}K_1K_1 + C_{66}K_2K_1 + C_{65}K_3K_1 + C_{66}K_1K_2 + C_{62}K_2K$$

$$+ C_{64}K_3K_2 + C_{65}K_1K_3 + C_{64}K_2K_3 + C_{65}K_3K_3)\,u_1$$

$$+C_{21}K_1K_1+C_{26}K_2K_1+C_{25}K_1K_3+C_{24}K_2K_3+C_{23}K_3K_3$$

$$+C_{26}K_1K_2+C_{22}K_2K_2+C_{24}K_3K_2+C_{25}K_1K_2)\,u_2$$

$$+(C_{41}K_1K_1+C_{46}K_2K_1+C_{45}K_3K_1+C_{46}K_2K_1+C_{42}K_2K_2$$

$$+C_{44}K_3K_2+C_{45}K_1K_3+C_{44}K_2K_3+C_{43}K_3K_3)\,u_3$$

---------- (II-52')

$$\rho\Omega^2 u_3=(C_{3111}K_1K_1+C_{3121}K_2K_1+C_{3131}K_3K_1+C_{3112}K_1K_2$$

$$+C_{3122}K_2K_2+C_{3132}K_3K_2+C_{3113}K_1K_3+C_{3123}K_2K_3$$

$$+C_{3133}K_3K_3)\,u_1+(C_{3211}K_1K_1+C_{3221}K_2K_1$$

$$+C_{3231}K_3K_1+C_{3232}K_3K_2{}_{312}K_1K_2+C_{3222}K_2K_2$$

$$+C_{3213}K_1K_3+C_{3223}K_2K_3+C_{3233}K_3K_3)\,u_2$$

$$+C_{3311}K_1K_1+C_{3321}K_2K_1+C_{3331}K_3K_1+C_{3312}K_1K_2$$

$$+C_{3322}K_2K_2+C_{3332}K_3K_2+C_{3313}K_1K_3+C_{3323}K_2K_3$$

$$+C_{3333}K_3K_3)\,u_3$$ ---------- (II-53)

Again changing the notation,

$$\rho\Omega^2 u_3=(C_{51}K_1K_1+C_{56}K_2K_1+C_{55}K_3K_1+C_{56}K_1K_2+C_{5K2}K_2$$

$$+C_{54}K_3K_2+C_{55}K_1K_3+C_{54}K_2K_3+C_{53}K_3K_3)\,u_1$$

$$+C_{41}K_1K_1+C_{46}K_2K_1+C_{45}K_3K_1+C_{46}K_1K_2+C_{42}K_2K_2$$

$$+C_{44}K_3K_2+C_{45}K^1K_3+C_{44}K_2K_3+C_{43}K_3K_3)u_2$$

$$+C_{31}K_1K_1+C_{36}K_2K_1+C_{35}K_3K_1+C_{36}K_1K_2+C_{32}K_2K_2$$

$$+C_{34}K_3K_2+C_{35}K_1K_3+C_{34}K_2K_3+C_{33}K_3K_3)u_3$$

---------- (II-53')

The stiffness constants depend on the crystal symmetry. For orthorhombic the stiffness tensor is

$$\begin{bmatrix} C_{11} & C_{12} & C_{13} & 0 & 0 & 0 \\ C_{21} & C_{22} & C_{23} & 0 & 0 & 0 \\ C_{31} & C_{32} & C_{33} & 0 & 0 & 0 \\ 0 & 0 & 0 & C_{44} & 0 & 0 \\ 0 & 0 & 0 & 0 & C_{55} & 0 \\ 0 & 0 & 0 & 0 & 0 & C_{66} \end{bmatrix}$$

Then Equation (II-51) becomes

$$[\rho\Omega^2-(C_{11}K_1K_1+C_{12}K_2K_2+C_{13}K_3K_3)]u_1-(2C_{66}K_2K_1)u_2$$

$$-2C_{55}K_3K_1u_3=0 \quad \text{----------} \quad (II-51'')$$

Equation (II-52) becomes

$$2C_{66}K_1K_2u_1-[\rho\Omega^2-(C_{21}K_1K_1+C_{22}K_2K_2+C_{23}K_3K_3)]u_2$$

$$+C_{33}K_3K_3)]u_3=0 \qquad \text{(II-53")}$$

For there to be non-trivial solutions of this set of equations the determinant of the coefficient matrix must vanish. This condition yields the eigenvalues of the problem, which in our case are the sound velocities. For $\bar{K}$ in an arbitary direction in the crystal.

$$\begin{vmatrix} \rho\Omega^2-(C_{11}K_1K_1+C_{12}K_2K_2+C_{13}K_3K_3) & -2C_{66}K_2K_1 & -2C_{55}K_3K_1 \\ 0 & \rho\Omega^2-(C_{21}K_1K_1+C_{23}K_3K_3+C_{22}K_2K_2) & 0 \\ 0 & 0 & \rho\Omega^2-(C_{31}K_1K_1+C_{32}K_2{}^2+C_{33}K_3K_3) \end{vmatrix}$$

$$=0 \qquad \text{(II-54)}$$

For $\bar{K}$ in the x_2(b) direction $K_1=K_3=0$, $K=K_2$, and then the determinant vanishes:

$$\begin{vmatrix} \rho\Omega^2-C_{12}K_2{}^2 & 0 & 0 \\ 0 & -\rho\Omega^2+C_{22}K_2{}^2 & 0 \\ 0 & 0 & -\rho\Omega^2+C_3K_2{}^2 \end{vmatrix}$$

$$=0 \qquad \text{(II-55)}$$

The roots of this equation and the corresponding

eigenvectors are

$$\rho\Omega^2=C_{12}K_2^2,\quad \Omega_{T2}=\sqrt{C_{12}/\rho}\,K_2,\quad v_{T2}=\sqrt{C_{12}/\rho},\quad \pi_{T2}=[100]$$

$$\rho\Omega^2=C_{22}K_2^2,\quad \Omega_{L2}=\sqrt{C_{22}/\rho}\,K_2,\quad v_{L2}=\sqrt{C_{22}/\rho},\quad \pi_{L2}=[010]$$

$$\rho\Omega^2=C_{32}K_2^2,\quad \Omega_{M2}=\sqrt{C_{32}/\rho}\,K_2,\quad v_{M2}=\sqrt{C_{32}/\rho},\quad \pi_{M2}=[001]$$

The orientations of the wave vector and the polarizations of the sound wave are shown in Fig. 5.

For $\bar{K}$ in the x_3(c) direction $K_1=K_2=0$, $K_3=K$ and then

$$\begin{vmatrix} \rho\Omega^2-C_{13}K_3^2 & 0 & 0 \\ 0 & -\rho\Omega^2+C_{23}K_3^2 & 0 \\ 0 & 0 & -\rho\Omega^2+C_{33}K_3^2 \end{vmatrix}=0 \qquad \text{(II-56)}$$

The roots of this equation and the corresponding eigenvectors are

$$\rho\Omega^2=C_{13}K_3^2,\quad \Omega_{T3}=\sqrt{C_{13}/\rho}\,K_3,\quad v_{T3}=\sqrt{C_{13}/\rho},\quad \pi_{T3}=[100]$$

$$\rho\Omega^2=C_{23}K_3^2,\quad \Omega_{M3}=\sqrt{C_{23}/\rho}\,K_3,\quad v_{M3}=\sqrt{C_{23}/\rho},\quad \pi_{M3}=[010]$$

$$\rho\Omega^2=C_{33}K_3^2.\quad \Omega_{L3}=\sqrt{C_{33}/\rho}\,K_3,\quad v_{L3}=\sqrt{C_{33}/\rho},\quad \pi_{L3}=[001]$$

The orientations of the wave vector and the polarization of the sound wave are shown in Fig. 6.

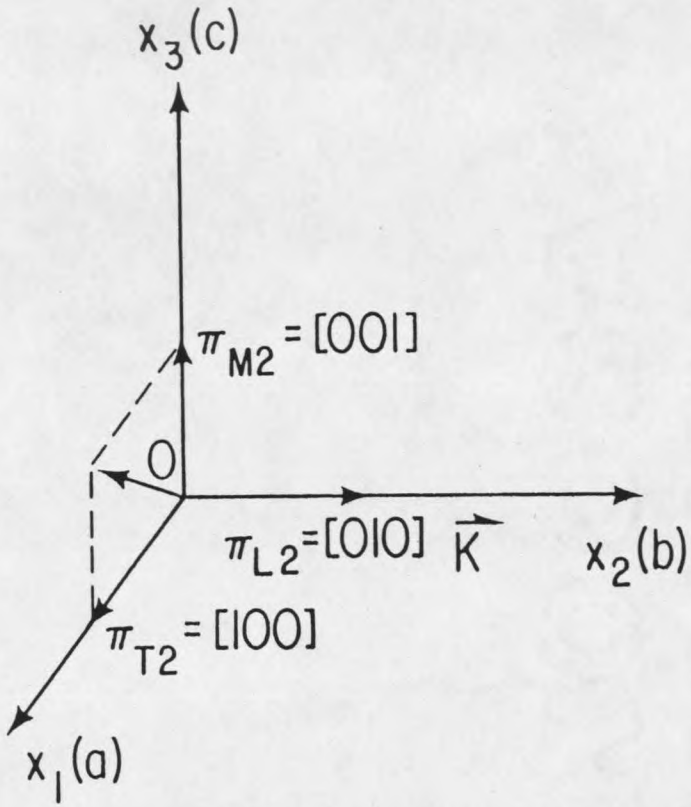

Fig. 5. Wave vector and polarization for (010) phonon

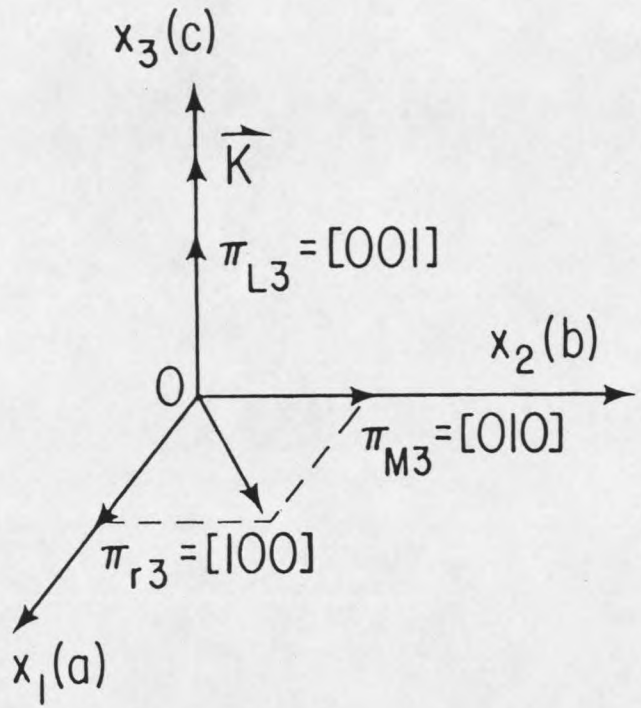

Fig. 6. Wave vector and polarization for (001) phonon

The Polarization of the Scattered Light

As stated above

$$B_{ij}=k_0\,dE_i/dD_j$$

$$=B_{ij0}+\delta B_{ij}$$

and

$$\delta B_{ij}=\Sigma p_{ijlm}\epsilon_{lm}$$

$$\epsilon_{lm}=(1/2)[du_l(\bar{x},t,\bar{K})/dx_m+du_m(\bar{x},t,\bar{K})/dx_l]$$

where p_{ijlm} are the photoelastic constants. This matrix is

$$\begin{bmatrix} p_{11} & p_{12} & p_{13} & 0 & 0 & 0 \\ p_{12} & p_{22} & p_{23} & 0 & 0 & 0 \\ p_{13} & p_{23} & p_{33} & 0 & 0 & 0 \\ 0 & 0 & 0 & p_{44} & 0 & 0 \\ 0 & 0 & 0 & 0 & p_{55} & 0 \\ 0 & 0 & 0 & 0 & 0 & p_{66} \end{bmatrix}$$

There are two cases we are going to deal with. These are:

Case 1, $\bar{K}$ is in the direction [010]

For the longitidinal phonons polarized in π_{L2}=[010]

$u_1 = u_3 = 0$, and $u_2 = u_{20} e^{-iKx}$.

Thus the strain tensor is given by

$$\epsilon_{11L} = 0 \qquad \epsilon_{12L} = 0 \qquad \epsilon_{13L} = 0$$

$$\epsilon_{21L} = 0 \qquad \epsilon_{22L} \qquad \epsilon_{23L} = 0$$

$$\epsilon_{31L} = 0 \qquad \epsilon_{32L} = 0 \qquad \epsilon_{33L} = 0$$

Then the fluctuation of the dielectric impermeability is

$$\delta B_{11} = p_{12}\epsilon_{22L} \qquad \delta B_{12} = 0 \qquad \delta B_{13} = 0$$

$$\delta B_{21} = 0 \qquad \delta B_{22} = p_{22}\epsilon_{22L} \qquad \delta B_{23} = 0$$

$$\delta B_{31} = 0 \qquad \delta B_{32} = 0 \qquad \delta B_{33} = p_{32}\epsilon_{22L}$$

For the transverse phonons polarized in $\pi_{T2} = [100]$

$u_1 \propto e^{-iKx}$, $u_2 = u_3 = 0$.

Thus

$$\epsilon_{11T} = 0 \qquad \epsilon_{12T} \qquad \epsilon_{13T} = 0$$

$$\epsilon_{12T} \qquad \epsilon_{22T} = 0 \qquad \epsilon_{23T} = 0$$

$$\epsilon_{31} = 0 \qquad \epsilon_{32T} = 0 \qquad \epsilon_{33T} = 0$$

and then

$$\delta B_{11} = 0 \qquad \delta B_{12} = p_{66}\epsilon_{12T} \qquad \delta B_{13} = 0$$

$$\delta B_{12} = p_{66}\epsilon_{12T} \qquad \delta B_{22} = 0 \qquad \delta B_{23} = 0$$

$\delta B_{31}=0$ $\delta B_{32}=0$ $\delta B_{33}=0$

For the transverse phonons polarized in $\pi_{M2}=[001]$

$u_1=0,\ u_2=0,\ u_3 \propto e^{-iKx}$.

Thus

$\epsilon_{11M}=0$ $\epsilon_{12M}=0$ $\epsilon_{13M}=0$

$\epsilon_{21M}=0$ $\epsilon_{22M}=0$ ϵ_{23M}

$\epsilon_{31M}=0$ ϵ_{32M} $\epsilon_{33M}=0$

Hence only δB_{23} exists, other elements are zero.

In the orthorhombic crystal TSCC the inverse of the dielectric tensor of a unstrained crystal B is diagonal like the following

$$B_0=\begin{bmatrix} B_{11} & 0 & 0 \\ 0 & B_{22} & 0 \\ 0 & 0 & B_{33} \end{bmatrix}$$

For the longitudinal phonon mode of wavevector [010], the fluctuation of the tensor B due to the thermal motion is

$$\delta B=\begin{bmatrix} \delta B_{11} & 0 & 0 \\ 0 & \delta B_{22} & 0 \\ 0 & 0 & \delta B_{33} \end{bmatrix}$$

The total tensor inverse dielectric permittivity tensor (dielectric impermeability) is

$$B = B_0 + \delta B$$

$$= \begin{bmatrix} B_{110} + \delta B_{11} & 0 & 0 \\ 0 & B_{220} + \delta B_{22} & 0 \\ 0 & 0 & B_{330} + \delta B_{33} \end{bmatrix}$$

The total dielectric tensor thus turns out to be

$$\bar{\epsilon} = 1/B$$

$$= \begin{bmatrix} 1/(B_{11} + \delta B_{11}) & 0 & 0 \\ 0 & 1/(B_{22} + \delta B_{22}) & 0 \\ 0 & 0 & 1/(B_{33} + \delta B_{33}) \end{bmatrix}$$

$$= \begin{bmatrix} 1/B_{11} - \delta B_{11}/B_{11}^2 & 0 & 0 \\ 0 & 1/B_{22} - \delta B_{22}/B_{22}^2 & 0 \\ 0 & 0 & 1/B_{33} - \delta B_{33}/B_{33}^2 \end{bmatrix}$$

$$= \begin{bmatrix} 1/B_{11} & 0 & 0 \\ 0 & 1/B_{22} & 0 \\ 0 & 0 & 1/B_{33} \end{bmatrix}$$

$$+ \begin{bmatrix} \delta B_{11}/B_{11}^2 & 0 & 0 \\ 0 & \delta B_{22}/B_{22}^2 & 0 \\ 0 & 0 & \delta B_{33}/B_{33}^2 \end{bmatrix}$$

$$= \bar{\bar{\epsilon}}_0 + \delta\bar{\bar{\epsilon}}$$

For our experimental situation, the polarization of the incident light is along [001]. Thus the fluctuation of the displacement is

$$\delta\bar{D} = \delta\bar{\bar{\epsilon}} \cdot \bar{E}_0$$

$$= -\delta B_{33}/B_{33}[001]$$

The polarization of the scattered light would be

$$\bar{A} = \bar{I}_k \times [\bar{I}_k \times \delta\bar{D}]$$

$$\propto [001] \qquad \text{----------} \qquad \text{(II-57)}$$

That means obviously that for the longitudinal phonon mode

the scattered light has the same polarization as the incident light.

For the transverse mode $\pi_{T2}=[100]$

$$\delta B=\begin{bmatrix} 0 & \delta B_{12} & 0 \\ \delta B_{12} & 0 & 0 \\ 0 & 0 & 0 \end{bmatrix},$$

an off-diagonal matrix. The total relative dielectric impermeability tensor is

$$B=B_0+\delta B$$

$$=\begin{bmatrix} B_{11} & \delta B_{12} & 0 \\ \delta B_{12} & B_{22} & 0 \\ 0 & 0 & B_{33} \end{bmatrix}$$

The dielectric tensor is the inverse of B, so that

$$\bar{\epsilon}=1/B$$

By the defination of the impermeability and the dielectric tensor, then

$$\bar{\epsilon}\cdot B=I$$

i.e.

$$\begin{bmatrix} \epsilon_{11} & \epsilon_{12} & \epsilon_{13} \\ \epsilon_{21} & \epsilon_{22} & \epsilon_{23} \\ \epsilon_{31} & \epsilon_{32} & \epsilon_{33} \end{bmatrix} \begin{bmatrix} B_{11} & \delta B_{12} & 0 \\ \delta B_{12} & B_{22} & 0 \\ 0 & 0 & B_{33} \end{bmatrix}$$

$$= \begin{bmatrix} 1 & 0 & 0 \\ 0 & 1 & 0 \\ 0 & 0 & 1 \end{bmatrix}$$

We have the following equations

$$\epsilon_{11} B_{11} + \epsilon_{12} \delta B_{12} = 1$$

$$\epsilon_{11} \delta B_{12} + \epsilon_{12} B_{22} = 0$$

$$\epsilon_{13} B_{33} = 0$$

$$\epsilon_{12} B_{11} + \epsilon_{22} \delta B_{12} = 0$$

$$\epsilon_{12} \delta B_{12} + \epsilon_{22} B_{22} = 1$$

$$\epsilon_{23} B_{33} = 0$$

$$\epsilon_{31} B_{11} + \epsilon_{32} \delta B_{12} = 0$$

$$\epsilon_{31} \delta B_{12} + \epsilon_{32} B_{22} = 0$$

$$\epsilon_{33} B_{33} = 0$$

Solving these equations, we obtain

$$\epsilon_{12}=\epsilon_{21}=-\delta B_{12}/(B_{11}B_{22})$$

$$\epsilon_{11}=1/B_{11}, \quad \epsilon_{22}=1/B_{22}, \quad \epsilon_{33}=1/B_{33},$$

The other elements are zero. Consequently,

$$\overset{=}{\epsilon}=\begin{bmatrix} 1/B_{11} & -\delta B_{12}/(B_{11}B_{22}) & 0 \\ -\delta B_{12}/(B_{11}B_{22}) & 1/B_{22} & 0 \\ 0 & 0 & 1/B_{33} \end{bmatrix}$$

$$=\begin{bmatrix} 1/B_{11} & 0 & 0 \\ 0 & 1/B_{22} & 0 \\ 0 & 0 & 1/B_{33} \end{bmatrix}$$

$$+\begin{bmatrix} 0 & -\delta B_{12}/(B_{11}B_{22}) & 0 \\ -\delta B_{12}/(B_{11}B_{22}) & 0 & 0 \\ 0 & 0 & 0 \end{bmatrix}$$

Obviously,

$$\delta\bar{\bar{\epsilon}}=\begin{bmatrix} 0 & -\delta B_{12}/(B_{11}B_{22}) & 0 \\ -\delta B_{12}/B_{11}B_{22} & 0 & 0 \\ 0 & 0 & 0 \end{bmatrix}$$

If the polarization of the incident light is [001] as usual, then

$$\delta\bar{D}=\delta\bar{\bar{\epsilon}}\cdot\bar{E}_0$$

$$=\begin{bmatrix} 0 & -\delta B_{12}/(B_{11}B_{22}) & 0 \\ -\delta B_{12}/(B_{11}B_{22}) & 0 & 0 \\ 0 & 0 & 0 \end{bmatrix}\begin{bmatrix} 0 \\ 0 \\ 1 \end{bmatrix}$$

$$=\begin{bmatrix} 0 \\ 0 \\ 0 \end{bmatrix}$$

There is no scattered light for this phonon mode.

For the π_{M2}=[001] phonon mode

$$\delta B = \begin{bmatrix} 0 & 0 & 0 \\ 0 & 0 & \delta B_{23} \\ 0 & \delta B_{23} & 0 \end{bmatrix}$$

In the same way we can find the fluctuation in the dielectric constant tensor

$$\delta \epsilon = \begin{bmatrix} 0 & 0 & 0 \\ 0 & 0 & -\delta B_{23}/(B_{22}B_{33}) \\ 0 & -\delta B_{23}/(B_{22}B_{33}) & 0 \end{bmatrix}$$

Then the fluctuation in electric displacement is

$$\delta \bar{D} = \delta \bar{\bar{\epsilon}} \cdot \bar{E}_0$$

If the polarization of the incident light is the same as before, then

$$\delta \bar{D} = \begin{bmatrix} 0 & 0 & 0 \\ 0 & 0 & -\delta B_{23}/(B_{22}B_{33}) \\ 0 & -\delta B_{23}/(B_{22}B_{33}) & 0 \end{bmatrix} \begin{bmatrix} 0 \\ 0 \\ 1 \end{bmatrix}$$

$$= \begin{bmatrix} 0 \\ -\delta B_{23}/(B_{22}B_{33}) \\ 0 \end{bmatrix}$$

$$= -\delta B_{23}/(B_{22}B_{33}) \begin{bmatrix} 0 \\ 1 \\ 0 \end{bmatrix}$$

The polarization of the scattered light is

$$\bar{A} = \bar{I}_K \times [\bar{I}_K \times \delta\bar{D}]$$

$$\propto [010] \qquad \text{----------} \qquad \text{(II-58)}$$

The polarization of the Brillouin-scattered light would be perpendicular to the polarization of the incident light.

This characteristic enables us to measure the Brillouin frequency shift for different modes with the same wavevector separately by using a polarizer sitting in front of the collimator lens.

Case 2: $\bar{K}$ in [001] direction

For the longitudinal mode i.e. $\pi_{L3}=[001]$, $u_1=0$,

$u_2=0$, $u_3 \propto e^{-iKx}$. Thus

$$\epsilon_{11L}=0 \qquad \epsilon_{12L}=0 \qquad \epsilon_{13L}=0$$

$$\epsilon_{21L}=0 \qquad \epsilon_{22L}=0 \qquad \epsilon_{23L}=0$$

$$\epsilon_{31L}=0 \qquad \epsilon_{32L}=0 \qquad \epsilon_{33L}$$

and then

$$\delta B_{11}=p_{13}\epsilon_{33L}$$

$$\delta B_{22}=p_{23}\epsilon_{33L}$$

$$\delta B_{33}=p_{33}\epsilon_{33L}$$

$$\delta B_{12}=\delta B_{21}=\delta B_{13}=\delta B_{31}=\delta B_{23}=\delta B_{32}=0$$

Again the whole relative dielectric impermeability tensor is

$$B=B_0+\delta B$$

$$=\begin{bmatrix} B_{11}+\delta B_{11} & 0 & 0 \\ 0 & B_{22}+\delta B_{22} & 0 \\ 0 & 0 & B_{33}+\delta B_{33} \end{bmatrix}$$

The dielectric tensor is the inverse of the relative impermeability tensor B. That is,

$$\delta\bar{\bar{\epsilon}}=1/B$$

With a little algebra work we obtain

$$\bar{\bar{\epsilon}}=\begin{bmatrix} 1/B_{11} & 0 & 0 \\ 0 & 1/B_{22} & 0 \\ 0 & 0 & 1/B_{33} \end{bmatrix}$$

$$+\begin{bmatrix} -\delta B_{11}/B_{11}^{2} & 0 & 0 \\ 0 & -\delta B_{22}/B_{22}^{2} & 0 \\ 0 & 0 & -\delta B_{33}/B_{33}^{2} \end{bmatrix}$$

$$=\bar{\bar{\epsilon}}_0+\delta\bar{\bar{\epsilon}}$$

The polarization of the incident light in this case is [010]. The fluctuation of the displacement is

$$\delta\bar{D}=\delta\bar{\bar{\epsilon}}\cdot\bar{E}_0$$

$$=\begin{bmatrix} -\delta B_{11}/B_{11}^{2} & 0 & 0 \\ 0 & -\delta B_{22}/B_{22}^{2} & 0 \\ 0 & 0 & -\delta B_{33}/B_{33}^{2} \end{bmatrix}\begin{bmatrix} 0 \\ 1 \\ 0 \end{bmatrix}$$

$$=-\delta B_{22}/B_{22}^{2}\begin{bmatrix}0\\1\\0\end{bmatrix}$$

The polarization of the scattered light is

$$\bar{A}=\bar{I}_K \times [\bar{I}_K \times \delta\bar{D}]$$

$$\propto [010] \qquad \text{----------} \qquad \text{(II-59)}$$

The direction of the polarization of the Brillouin-scattered light is the same as for the incident light.

For the transverse mode $\pi_{T2}=[100]$, $u_1=e^{-iKx}$, $u_2=0$, $u_3=0$. Thus the strain tensor will be

$\epsilon_{11T}=0$ $\quad\epsilon_{12T}=0$ $\quad\epsilon_{13T}$

$\epsilon_{21T}=0$ $\quad\epsilon_{22T}=0$ $\quad\epsilon_{23T}=0$

ϵ_{13T} $\quad\epsilon_{32T}=0$ $\quad\epsilon_{33T}=0$

And then the dielectric impermeability is

$\delta B_{11}=0$ $\quad\delta B_{12}=0$ $\quad\delta B_{13}$

$\delta B_{21}=0$ $\quad\delta B_{22}=0$ $\quad\delta B_{23}=0$

δB_{13} $\quad\delta B_{32}=0$ $\quad\delta B_{33}=0$

The whole dielectric impermeability tensor is

$$B = B_0 + \delta B$$

$$= \begin{bmatrix} B_{11} & 0 & \delta B_{13} \\ 0 & B_{22} & 0 \\ \delta B_{13} & 0 & B_{33} \end{bmatrix}$$

The dielectric tensor is the inverse of the impermeability B. That is,

$$\bar{\epsilon} = 1/B$$

$$= \begin{bmatrix} 1/B_{11} & 0 & 0 \\ 0 & 1/B_{22} & 0 \\ 0 & 0 & 1/B_{33} \end{bmatrix}$$

$$+ \begin{bmatrix} 0 & 0 & -\delta B_{31}/(B_{11}B_{33}) \\ 0 & 0 & 0 \\ -\delta B_{31}/(B_{11}B_{33}) & 0 & 0 \end{bmatrix}$$

The fluctuation of the dielectric tensor is

$$\delta\bar{\bar{\epsilon}}=\begin{bmatrix} 0 & 0 & -\delta B_{31}/(B_{11}B_{33}) \\ 0 & 0 & 0 \\ -\delta B_{31}/(B_{11}B_{33}) & 0 & 0 \end{bmatrix}$$

The fluctuation of the electric displacement is

$$\delta\bar{D}=\delta\bar{\bar{\epsilon}}\cdot\bar{E}_0$$

$$=\begin{bmatrix} 0 & 0 & -\delta B_{31}/(B_{11}B_{33}) \\ 0 & 0 & 0 \\ -\delta B_{31}/(B_{11}B_{33}) & 0 & 0 \end{bmatrix}\begin{bmatrix} 0 \\ 1 \\ 0 \end{bmatrix}$$

$$=\begin{bmatrix} 0 \\ 0 \\ 0 \end{bmatrix}$$

There is no Brillouin scattered light for this phonon mode.

For the transverse mode $\pi_{M3}=[010]$ propagating along the direction [001], $u_1=0$, $u_2 \propto e^{-iKx}$, $u_3=0$. Thus the strain tensor will be

$\epsilon_{11M}=0$ $\epsilon_{12M}=0$ $\epsilon_{13M}=0$

$\epsilon_{21M}=0$ $\epsilon_{22M}=0$ ϵ_{23M}

$\epsilon_{31M}=0$ ϵ_{23M} $\epsilon_{33M}=0$

And the fluctuation of the dielectric impermeability tensor will be

$\delta B_{11}=0$ $\delta B_{12}=0$ $\delta B_{13}=0$

$\delta B_{21}=0$ $\delta B_{22}=0$ δB_{23}

$\delta B_{31}=0$ δB_{23} $\delta B_{33}=0$

Then the total dielectric impermeability tensor will be

$$B=\begin{bmatrix} B_{11} & 0 & 0 \\ 0 & B_{22} & \delta B_{23} \\ 0 & \delta B_{23} & B_{33} \end{bmatrix}$$

The dielectric constant tensor

$$\bar{\epsilon}=1/B$$

With a little algebra we get

$$\delta\bar{\bar{\epsilon}}=-\delta B_{23}/(B_{11}B_{33})\begin{bmatrix}0&0&0\\0&0&1\\0&1&0\end{bmatrix}$$

The fluctuation of the electric displacement is

$$\delta\bar{D}=\delta\bar{\bar{\epsilon}}\cdot\bar{E}_0$$

$$=-\delta B_{23}/(B_{11}B_{33})\begin{bmatrix}0&0&0\\0&0&1\\0&1&0\end{bmatrix}\begin{bmatrix}0\\1\\0\end{bmatrix}$$

$$=-\delta B_{23}/(B_{11}B_{33})\begin{bmatrix}0\\0\\1\end{bmatrix}$$

The polarization of the scattered light

$$\bar{A}=\bar{I}_K\times[\bar{I}_K\times\delta\bar{D}]$$

$$=\begin{bmatrix}0\\0\\1\end{bmatrix} \qquad \text{(II-60)}$$

We see that the Brillouin-scattered light changes the

direction of the polarization from that of the incident light.

Summarily, we found the following selection rules:

1) The polarization of the scattered light by a longitudinal phonon in a orthorhombic crystal is the same as for the incident light.

2) The polarization of the scattered light by one of the two transverse modes with the same wavevector changes 90° from the incident light, the other transverse mode produces no scattered light.

CHAPTER III

EXPERIMENTAL EQUIPMENT AND TECHNIQUE

Introduction

This chapter, we will describe the apparatus and technique used in measurement of the scattered light spectrum. First there is a general description of the apparatus and later a discussion of certain features of the experimental technique in detail. These features are the cryostat, temperature measurement and temperature control system, light focusing and collection optics, Fabry-Perot interferometer, photomultiplier, computer and system for interfacing the computer to the equipment.

General Description of the Apparatus

The apparatus can be divided into the light system, temperature control , measurement system , computer control and record system (see Fig. 7).

The light source was a Lexel Mode 95-2 Argon Ion Laser operating at a wavelength of 5145 Å in a single mode. In order to keep the temperature difference between the

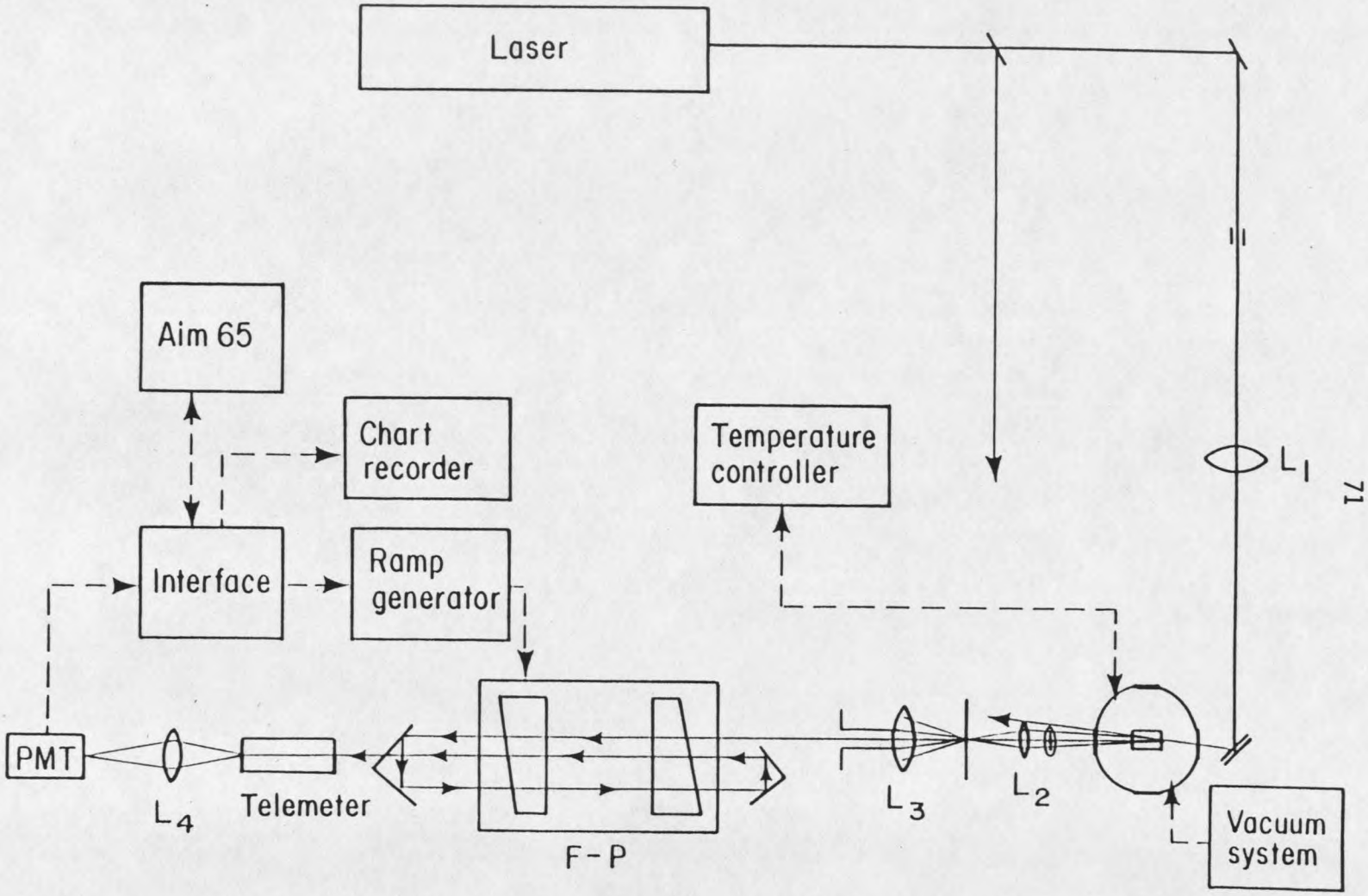

Fig. 7. Experiment diagram

illuminated volume of the sample and the temperature sensor constant, we kept the power level constant during a given run. Single-mode operation of the laser was achieved by a prism wavelength selector. The laser line broadening due to the jittering was claimed by the manufacturer to be about 10 MHz full width at half maximum (FWHM). The laser beam was highly polarized in the vertical plane. The diameter of the laser beam is 1.3 mm. One highly reflecting mirror bent the beam into the focusing optics through an aperture (see Fig. 7), which cut out the infra-red from the laser beam. For right angle scattering lens L1 focuses the beam into the sample through the window of the cryostat. For small angle and back scattering the light beam focused by lens L1 was reflected by a mirror into the sample through the window.

The sample was placed in the cryostat which will be described in detail later (Fig. 10). The cryostat was cooled by liquid nitrogen. The temperature in the vessel was controlled within 3 mK.

The divergent scattered light from the sample was focused onto the pinhole by the lens L2. Between the sample and the lens L2 there is a polarizer whose polar axis was vertical or horizontal for measuring the longitudinal or transverse phonons respectively. The pinhole diameter is 100 micron. The light from the

pinhole is considered as a point light source. The light leaving the collimator lens is parallel. The beam goes through an aperture used to adjust the collection angle by adjusting the diameter of the aperture. We used the multipass technique in which beam goes through the corner cube and then enters the Fabry-Perot interferometer.

The Fabry-Perot interferometer is a Burleigh Instruments Model RC-140. This Fabry-Perot is designed with particular emphasis on freedom from angular and linear drift with time and temperature, to help assure maintenance of mirror parallelism over long periods of time. It uses matched sets of piezoelectric PZT transducers constructed from interferometrically matched PZT discs. This PZT material offers the best linearity and hysteresis characteristics, with better than 1% inter-order linearity and 0.5% hysteresis. The PZT discs have a low coefficient of thermal expansion which greatly improves the thermal stability of the Fabry-Perot. The discs have a high piezoelectric d constant, allowing a short PZT drive which improves thermal stability and ensures a more rigid mechanical construction. The adjustment screws used in the Fabry-Perot have very high resolution capability with greater than 10 mm adjustment range. Adjustments to 0.1 μm are easily made by the screws. The mirror spacing is continuously variable from

0.1 mm to 150 mm. The RC-140 provides up to a 50.8 mm clear aperture. A thin wafer of rigid low-thermal-expansion alumino-silicate ceramic is laminated to each end of the stack to provide electrical isolation. Aluminum shields prevent accidental touching of the PZT stacks, which have up to 1000 V applied.

The RC-42 Ramp Generator drives the Fabry-Perot Interferometer, Tunable Etalons, and PZT Aligner/Translators. These instruments use three independent piezoelectric elements. The Ramp Generator controls these elements to provide two basic functions, scanning and alignment, with two independent circuits.

The scattered light leaving the Fabry-Perot interferometer goes through a telemeter lens. The parallel light beam is focused on the pinhole at the end. Another lens focuses the light from that pinhole onto the pinhole in the photomultipler housing. Just in front of the photomultiplier tube there is a color filter that will absorb stray light that enters the photomultiplier. There is a partial shutter between the lens and the pinhole at the end. The shutter is closed in the Rayleigh spectrum range and greatly attenuates the Rayleigh scattered light but it is open in the Brillouin spectrum range.

The scattered light finally goes into the photomultiplier tube. A Model R464 end-on photomultiplier

tube was used in a Model 3470 photomultiplier housing. A home-made high voltage power supply provided high voltage for the cathode of the photomultiplier tube. The output current from the anode of the photomultiplier tube is the input of a pulse amplifier. A Pacific Precision Instruments Model 33 power supply/temperature controller was connected to the photomultiplier housing, but the R464 tube does not need a cooling system, so we did not use it. The analog output of the amplifier was fed into a home-made counter and the digital number was stored in a AIM-65 computer and then the signal was displayed on an oscilloscope or chart recorder.

The AIM-65 computer and its interface control the ramp generator which in turn aligns and scans the Fabry-Perot interferometer.

1. Light gathering and focusing optics

Lens L1 focused the light beam onto the sample. In order to reduce collection angle broadening, the angle of the incident light cone should be as small as possible. In Fig. 8 we see that this angle has the same effect on linewidth as the collection angle, that is, the angle of the scattered light cone. In this sense, the focal length of lens L1 should be as larger as possible. On the other hand, if the focal length is too long it will be difficult to find the focal point and it sometime increases the

angle of incident light cone. So we have to make a compromise.

When the light is going through the sample, it produces two very bright spots A and B on the surfaces where it enters and exits. To obtain the best Brillouin scattering signal we must reduce the Rayleigh scattering. Hence, we must adjust lens L2 in such a way that the pinhole image appears in the sample between bright spots A and B (see the Fig. 8). First, with the telescope we can see the crystal center very clearly and we adjust lens L2 until we can see the pinhole very clearly. We then adjust the incident beam position until the the pinhole image appears between spots A and B. A small piece of plastic is put on top of the crystal just above the pinhole image. This piece of plastic should appear clearly in the telescope. When the telescope is shaken slightly, the pinhole image and the plastic piece should move together (parallax). If they do the pinhole image is located at the right position and the adjustment of lens L2 is correct. The alignment of lens L3 is described in B. 2.

If the aperture diameter is d_{PP}, we can calculate the collection angle $\delta\theta$ by the following formula

$$\delta\theta_2 = 2\tan^{-1}[d_{PP} \cdot L_2/(2L_1L_2)] \quad \text{---------} \quad (III-1)$$

In our case, L_1=350mm, L_2=80mm, L_3=220mm.

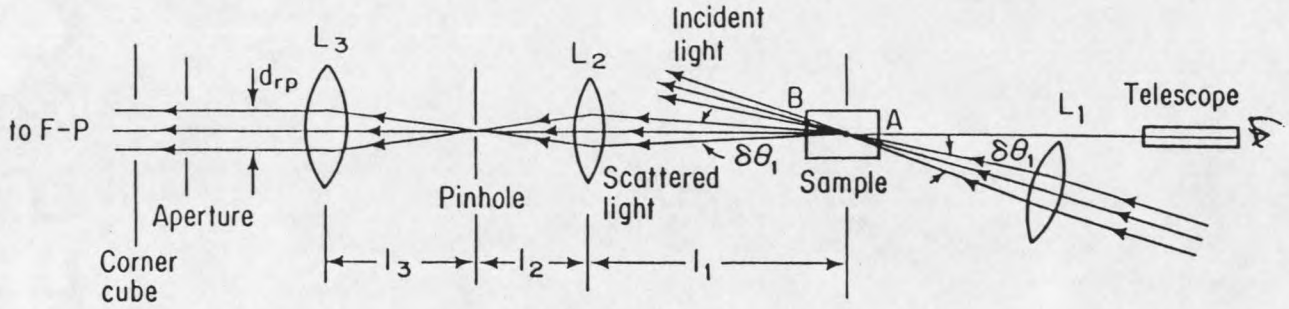

Fig. 8. Light gathering

All the lenses used in our experiment are doublet or triplet and coated.

2. Characteristics and alignment of the Fabry-Perot

(1) Characteristics of the Fabry-Perot

The condition for constructive interference for a transmitted wavefront is

$$2nd\cos\theta = m\lambda \qquad \text{(III-2)}$$

where n is the refractive index of the medium between the two reflecting surfaces,

d is the mirror spacing,

θ is inclination of the normal of the mirrors to the wavefront direction, in our case $\theta=0^{\circ}$,

m is the order of interference,

λ is the wavelength.

From Equation (III-2), we get

$$nd = m\lambda/2$$

Let d change by $\lambda/2$. The wave with the same wavelength is still able to pass this interferometer but the order of the interference lowers by one. There will be another wave with different wavelength which may pass this interferometer but with the mth order of interference. Hence we have

$$nd=(m-1)\lambda_1/2$$

$$=m\lambda_2/2$$

Then

$$m(\lambda_1-\lambda_2)/2=\lambda_1/2$$

and

$$\delta\lambda=\lambda_1/m$$

$$=\lambda_1^2/(2dn) \quad \text{----------} \quad (III-3)$$

where $\delta\lambda$ is called the Free Spectral Range (FSR),

λ_1 is the wavelength of the light.

Assuming the spacing between the two mirror changes by $\lambda_1/(2\mu)$, where μ is not an integer, the wave front of wavelength λ_3 is allowed to pass this interferometer, if the following formula is satisfied.

$$nd-\lambda_2/(2\mu)=(m-i)\lambda_3/2$$

where m, i are integers.

$$\lambda_3=2(nd-\lambda_1/(2\mu))/(m-i)$$

$$=2[nd-\lambda_1/(2\mu)]/(m-i)$$

$$=2[nd-\lambda_1/(2\mu)]/(2nd/\lambda_1-i)$$

$$\lambda_1-\lambda_3=2[nd-\lambda_1/(2\mu)]/(2nd/\lambda_1-i)-\lambda_1$$

$$=(2nd\lambda_1-\lambda_1^2/\mu)/(2nd-\lambda_1 i)-\lambda_1$$

$$=(2nd\lambda_1-\lambda_1^2/\mu-2nd\lambda_1+i\lambda_1^2)/(2nd-i\lambda_1)$$

$$=(i-1/\mu)\lambda_1^2/[2nd(1-i\lambda_1/(2nd))]$$

$$\approx[(i-1/\mu)\lambda_1^2/(2dn)](1+i\lambda_1/2dn)$$

If m>>i, then

$$\lambda_1-\lambda_3\approx(i-1/\mu)\lambda_1^2/(2nd)$$

$$\delta\lambda=(i-1/\mu)\cdot FSR \quad \text{----------} \quad (III-4)$$

where $\delta\lambda$ is the frequency shift from the original wave (Rayleigh), and i is the shift order which is different from the order of interference.

The Finesse is the key measure of the interferometer's ability to resolve closely spaced lines. The finesse can be thought of as the effective number of interfering beams involved in forming the FP (Fabry-Perot) multiple-beam interference fringes and is proportional to the time constant or decay time of the FP interferometer. The major factors which limit the net finesse are (1) mirror reflectivity of less than unity; (2) lack of parallelism and planeness of the mirrors; and (3) diffraction losses arising from the finite aperture of the interferometer. The net finesse is found by treating the component finesses as if they were parallel impedances.

The reflective finesse (F_R) is

$$F_R = \pi\sqrt{R/(1-R)},$$

where R is the reflectivity.

The flatness or figure finesse is

$$F_F = M/2 \quad \text{for a } \lambda/M \text{ plate}$$

where M is the fractional wavelength deviation from planeness across the mirror aperture.

The diffractive finesse (F_D) is

$$F_D = 2D^2/(\lambda nd),$$

where D is the diameter of the limiting aperture.

The pinhole finesse (F_P) is

$$F_P = 4\lambda L^2/(D^2 d),$$

where D is the diameter of the pinhole at the end, and L is the focal length of the collimator lens.

The net finesse (instrument finesse) is

$$F_I^2 = \sum_i F_i^2$$

For multiple pass the instrument finesse is

$$F_{IP} = F_I/(2^{1/P}-1)^{1/2},$$

where P is the number of passes.

The contrast (C_I) is

$$C_I = 4F_I^2/\pi^2.$$

The transmission due to absorption and reflection for single pass (t_I) is

$$t_I = (1 - A/(1-R))^2,$$

where A is the loss from absorption in coatings, and R is the reflectivity.

The transmission due to absorption and reflection for P passes (t_P) is

$$t_P = t_I^P.$$

By passing a beam through a FP P times, the contrast is greatly increased, from C for a single pass, to C^P for P passes.

(2) Alignment

There are two requirements for aligning a Fabry-Perot interferometer. First, the FP must be aligned relative to the incoming radiation. In our case, the FP will be normal to the input. The degree of regular alignment required is not great. Second, the FP plates must be aligned relative to each other. Initial alignment with visible or UV plates is easiest with a small laser. Reflecting a gas laser reference beam, which is coincident with the optical axis, illuminating the FP with this beam

and looking at the output on a white card, a train of dots will be observed, resulting from reflections on the mis-aligned plates. The coarse adjust mechanism should be used to collapse the dots to a single spot. In another way, we input a small parallel beam to the rear of the FP and looking at the outgoing patterns at the front of the FP by a reflective mirror, we should see a train of circles. The coarse adjustment is then used to make the circles concentric. By putting a piece of tracing paper between the pinhole and the collimator lens L_3 we can tell whether the reflecting beam coincides with the incident beam. By adjusting the screw in the front of the FP and the screw on the side we can coarsely make the two beams coincide.

The focus of the collimator lens L3 must be located just at the pinhole in the front. We reflect a laser reference beam into the pinhole by a diffuser. Then we have two ways to adjust lens L3. One way is by looking through a telescope with a prism from the side behind the lens L3 (the telescope should first be adjusted to see the far object clearly). We adjust lens L3 until we can see the pinhole clearly. Another way is by looking through a microscope with a prism from the side in front of lens L3. We can see the pinhole and the image of the pinhole (because light is reflected by the FP and through the lens

L3). We adjust the distance between lens L_3 and the pinhole until the pinhole image is the same size as the pinhole itself. By adjusting the screw in the front of the FP and the one on the side, one can make the pinhole image and the pinhole itself to overlap. That means the FP mirrors are perpendicular to the optical axis.

Now, if the FP is illuminated with a large, collimated monochromatic beam at a wavelength within the spectral range of the plates, straight lines fringes can be observed on a white card behind the FP aperture. The larger the number of lines, the more misaligned the FP is. We adjust the two knobs on the rear of the FP until the number of lines reduces to one. Then we adjust the ramp bias to the second order of the fringe, i.e. the second appearance of the fringe. (As we adjust the ramp bias, the fringe will appear and disappear successively). Finally, by adjusting the three biases, we will be able to see even transmission across the aperture. Then we check the microscope to see if the pinhole image still overlaps the pinhole itself. If not, we adjust the FP screws, and if the pattern on the white card changes, we must adjust the biases again. We do this back and forth several times until the pattern is even. For multiple pass, we insert the corner cubes and observe the pattern after the aperture of the corner cube. We adjust the biases again

until the pattern is even with maximum brightness. Now the manual alignment is done. We scan the FP and display the Rayleigh spectrum on the oscilloscope. If the finesse is not very good, the computer will optimize the bias electrically. This will be described in detail in B.3..

3. Computer control system

This system consists of the AIM-65 computer, interface osciloscope , chart recorder and software.

The AIM-65 microcomputer can provide external RAM, ROM, or I/O port. The AIM-65 monitor includes commands to allow user defined functions to interface with user provided peripherals, such as the Ramp Generator and photomultipier, etc. The monitor language, assembly language, editor language and basic language can be used for programming.

The diagram for interfacing the computer to the ramp generator is shown in Fig.9.

The Fabry-Perot interferometer is scanned by applying a high voltage ramp to three piezoelectric stacks. This voltage ramp is controlled either by the front control panel knobs on the Burleigh RC-42 ramp generator or alternatively by the computer.

Acquisition of spectra is accomplished under computer control thereby allowing the computer to make multiple scans of the spectrum and by adding these scans together,

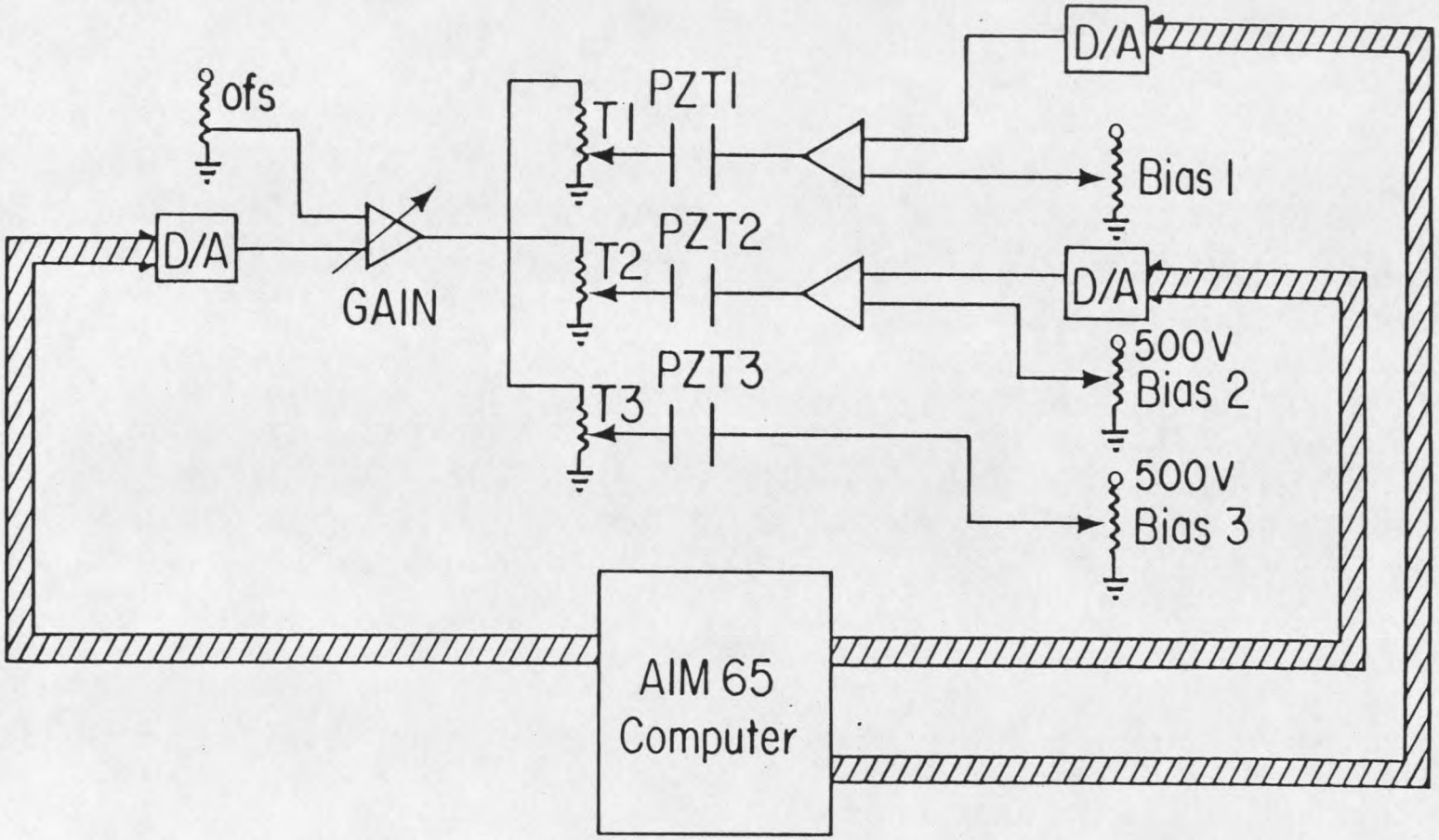

Fig. 9. Computer operating FP

provide necessary signal averaging while eliminating the effects of spectrometer drift during the course of measurement.

Each scan should be roughly 1.25 free spectral ranges in width and provide two elastic peaks in each scan. The computer also provides a signal to toggle a relay on and off which can operate a shutter or move a neutral density filter into and out of the collection optics before and after the scan through each elastic peak. The shutter will greatly attenuate the intensity of the elastic peaks without decreasing the Brillouin peaks which we want. Provision is also made for changing the scan rate through the elastic peaks from that of the remainder of the scan.

Within each scan of 256 channels the computer looks for the channel containing the maximum number of counts in the first 128 channels of the scan. This channel is assumed to be the elastic peak location and is used to generate the offset necessary to align the new scan data with the accumulated scan data before adding it into the accumulated data. In this manner drift in the offset of the Fabry-Perot is compensated for. This same offset is used to calculated a new ramp "start" position to keep the channel number of the first elastic peak in each scan constant. If this offset was found to be more than four channels then the scan is ignored and the computer assumes

that a "glitch" was observed in the first 128 channels of the scan.

The computer control is implemented by setting the RC-42 "Ramp Duration" switch in the "off" position, since we can use the computer to control the ramp rate. The "external input" connector on the rear of the RC-42 must be connected to the computer interface output. The 10 V maximum external input for the ramp generator will produce 1000 V maximum output.

The ramp generator should remain "off" until the operator, via the computer, has initialized the ramp and bias voltage of the Fabry-Perot. This is to avoid sending to the Fabry-Perot too high a voltage step which might damage the piezoelectric stacks.

The Fabry-Perot controller program is written in BASIC and accesses machine language via the BASIC USR function. The whole program has several functions such as initializing the ramp generator, ramping up or ramping down the voltage for the pieroelectric stacks, optimizing the Fabry-Perot, scan and accumulating data, display, recording data on chart recorder, transfering data from one AIM-65 computer to another and recording data on disc.

4. Temperature control and measurement

(1) The optical cell has four windows and is designed for low temperature and hydrostatic pressure up to 5 kilobars.

However, this experiment was done in this cell only under atmospheric pressure.

The cell body and various window and sample-holder parts were made of Beryllium-Copper, because of its ease of machining and heat treating and its good thermal conductivity.

The cell and the tail section of the cryostat are illustrated in Fig. 10. The dimensions of the cell present a compromise to keep the optical path length to a minimum and still have a reasonable aperture, in this case 3.17 mm diameter. The outside dimensions are 63.5 mm diameter by 76.2 mm length. The window seats are backed up with unhardened Be-Cu o-ring seals and by hardened Be-Cu threaded plugs which have a 12° tapered aperture hole to reduce shadowing. The structure of the sample holder, ring seal and support plug are similar to those of the window. The cell is connected to pressure tubing of 6.35 mm o.d. by 1.59 mm i.d. with a standard gland unit (in this experiment the tubing is only used for putting in the index matching liquid). The cell is surrounded by a copper radiation shield can and copper outer can which is connected to the liquid nitrogen tank, which acts as a constant-temperature heat sink. The space inside of the dewar is evacuated to 10^{-5} torr to minimize the heat losses and temperature gradient of the cell. The copper

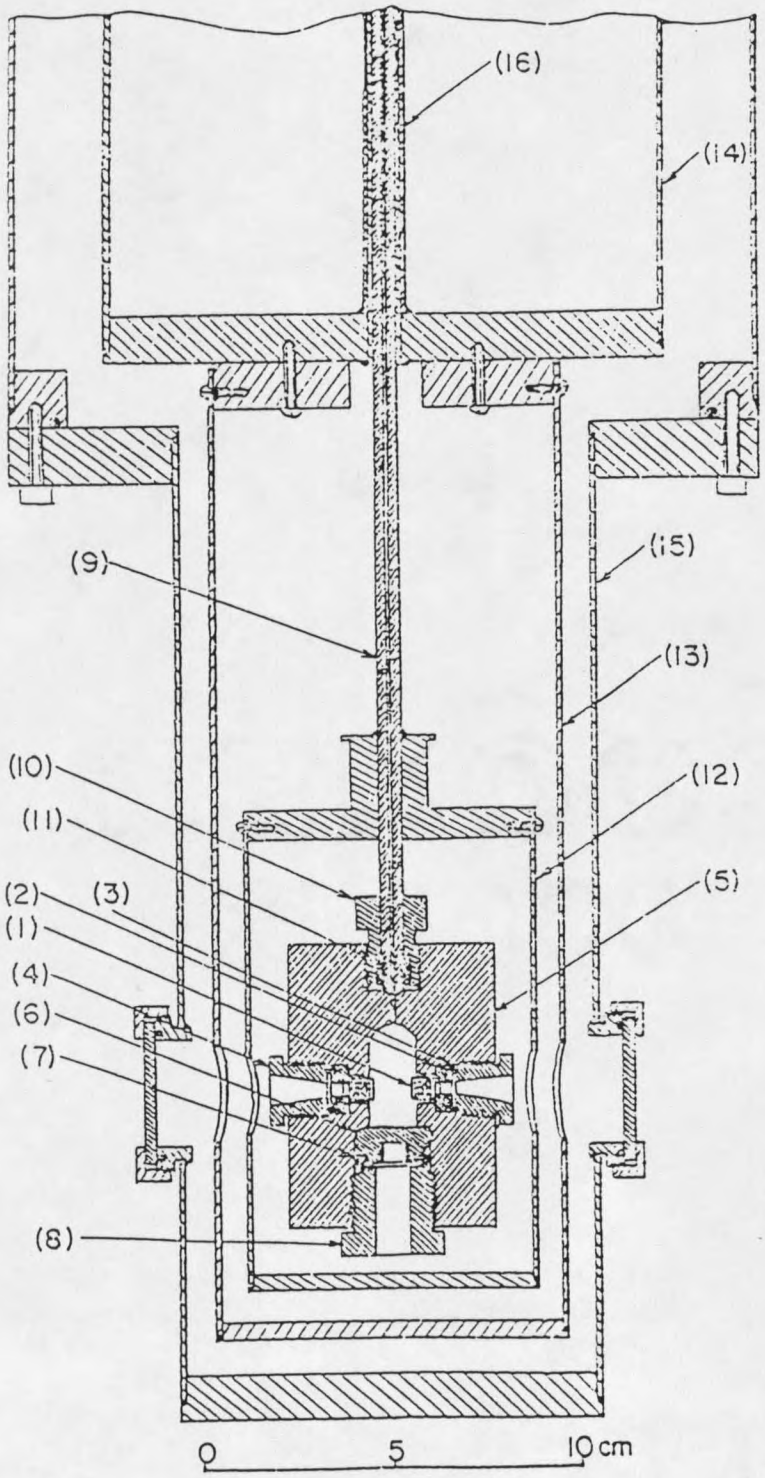

Fig. 10, Cryostat

tubing surrounding the pressure tubing inside the tank is provided to prevent changing of the temperature of the pressure tubing as the liquid nitrogen level varies. The temperatures of the cell and inner copper shield are controlled by a low-temperature capacitance controller (Lake Shore Cryotronics Inc. Model CSC400) and a Scientific Instruments, Inc. Model No. 3610 A, cryogenic temperature controller respectively. The temperature can be controlled only below about 160 K. From our experience, the temperature of the can should be about 10 K lower than the temperature of the cell to enable the capacitance controller to hold the cell temperature constant within 3 mK.

The can temperature was measured by two Copper-Constantan Type 2 thermocouples using a Keithley 177 microvolt DMM voltmeter, and the cell temperature was measured with a capacitance sensor.

5. Sample preparation

Single crystals of TSCC were grown from aqueous solutions of sarcosine and calcium chloride by slow cooling. The solution was prepared from chemical of special quality and was filtered by a 0.2 μm pore size membrane filter. The samples are carefully polished rectangular parallelepipeds. Aluminum was evaporated onto two surfaces of the sample for right angle scattering as

electrodes for measurement of the dielectric constant. This sample was annealed at 140 °C for 20 hours in an evacuated glass tube to improve the quality of the crystal.

The sample for small angle scattering and back scattering is also a carefully polished rectangular parallelepiped which is 8 mm long along the a axis by 5 mm wide along the b axis and 5 mm high along the c axis. This sample was not heat treated. In order to reduce the intensity of the Rayleigh peaks by reducing the reflection on the surfaces, we use isopentane liquid for index matching.

6. Recording Brillouin spectra

The electrical pulses coming from the photomultiplier go to a pulse amplifier and then to a homemade counter. The number of pulses per channel for up to 1024 channels is stored in the AIM-65 computer. The number are put serially into a Tektronix Model 5111 storage oscilloscope for display. Also the data is put serially into a Houston Instruments Omniscribe Mode B5127-5 chart recorder.

The data are also saved on floppy disks in case of need. There are programs to transfer the data from one AIM 65 computer to another.

CHAPTER IV

EXPERIMENTAL RESULTS

Introduction

In this chapter we present the results of our investigation of the Brillouin spectrum and the anomalies of phonon frequency, sound velocity, and attenuation of tris-sarcosine calcium chloride. We measured the Brillouin spectrum and line width from room temperature down to 110 K (the phase transition temperature is 130 K). From the Brillouin spectrum and line width we get (a) the anomalies of hypersonic sound velocities with respect to temperature, (b) the anomalies of the phonon attenuation coefficients.

Data Analysis

The sound velocities are obtained from the experimentally measured Brillouin shifts by using the Brillouin formula

$$\delta\nu/\nu_0 = v_s / c(n_i^2 + n_s^2 - 2n_i n_s \cos\theta)^{1/2} \quad --- \quad (IV-1)$$

where $\delta\nu$ is the Brillouin shift in Hz, ν_0 is the frequency of the incident light, n is the refractive index, v_s is the sound velocity, c is the velocity of light in vacuum, and θ is the scattering angle. We used small angle, right angle and back scattering. The scattering angles are different in different measurements.

We can rewrite Equation (IV-1) as

$$\delta\nu(T)/\nu_0 = v_s/c[n_i^2(T)+n_s^2(T)-2n_i(T)n_s(T)\cdot\cos\theta]^{1/2} \quad \text{----------} \quad (IV\text{-}1')$$

The refractive index is a function of both the wavelength of the light and the temperature T. We used an argon ion laser with wavelength in vacuum 5145 Å, corresponding to frequency $\nu_0 = 5.827\times10^{14}$ Hz. To obtain the sound velocities, we must have data on the temperature dependence of the refractive index at 5145 Å.

Ivanov and Arndt measured the refractive indices in a refractometer at 20°C at a wavelength of 5893 Å and found $n_a = 1.5921$, $n_b = 1.5506$, $n_c = 1.5528$.[16] This wavelength is close enough to the wavelength of 5145 Å of our laser that we assume that the discrepancy between the values of the refractive indices stated above and the values applicable to our experiment is negligible.

The temperature dependence of the refractive indices

found by Ivanov and Arndt is shown in Fig. 11, where

$$(\delta n)_3 = n_c - n_b .$$

The deviation of $(\delta n)_3$ in a range of temperature from 73 K to 300 K is less than 0.09%. We can assume that the refractive indices measured by Ivanov and Arndt at room temperature are valid for our entire temperature range.

From the calculated sound velocities we can determine the elastic constants, since

$$\rho v_s^2 = C$$

where ρ is the density and C represents a combination of one or more elastic constants that determine the sound velocity in each direction as described in Chapter II. The density of TSCC observed by Makita (1965) is ρ=1.533 g/cm^3 at room temperature,[17] while it was determined as ρ=1.530 g/cm^3 by x-ray lattice constants a=9.151±0.01, b=17.460±0.005, c=10.265±0.005 Å at room temperature.[18] TSCC undergoes a ferroelectric phase transition at temperature 130 K. Mishima, Itoh and Nakamura measured lattice constants. a=9.122(4), b=17.408(4) c=10.228(8) Å, z=4 and density ρ=1.55 g/cm^3 at 118 K.[19] The change in density from room temperature down to 118 K is about 1%. Considering other origins of error which will be shown later, we use ρ=1.533 for all our calculations.

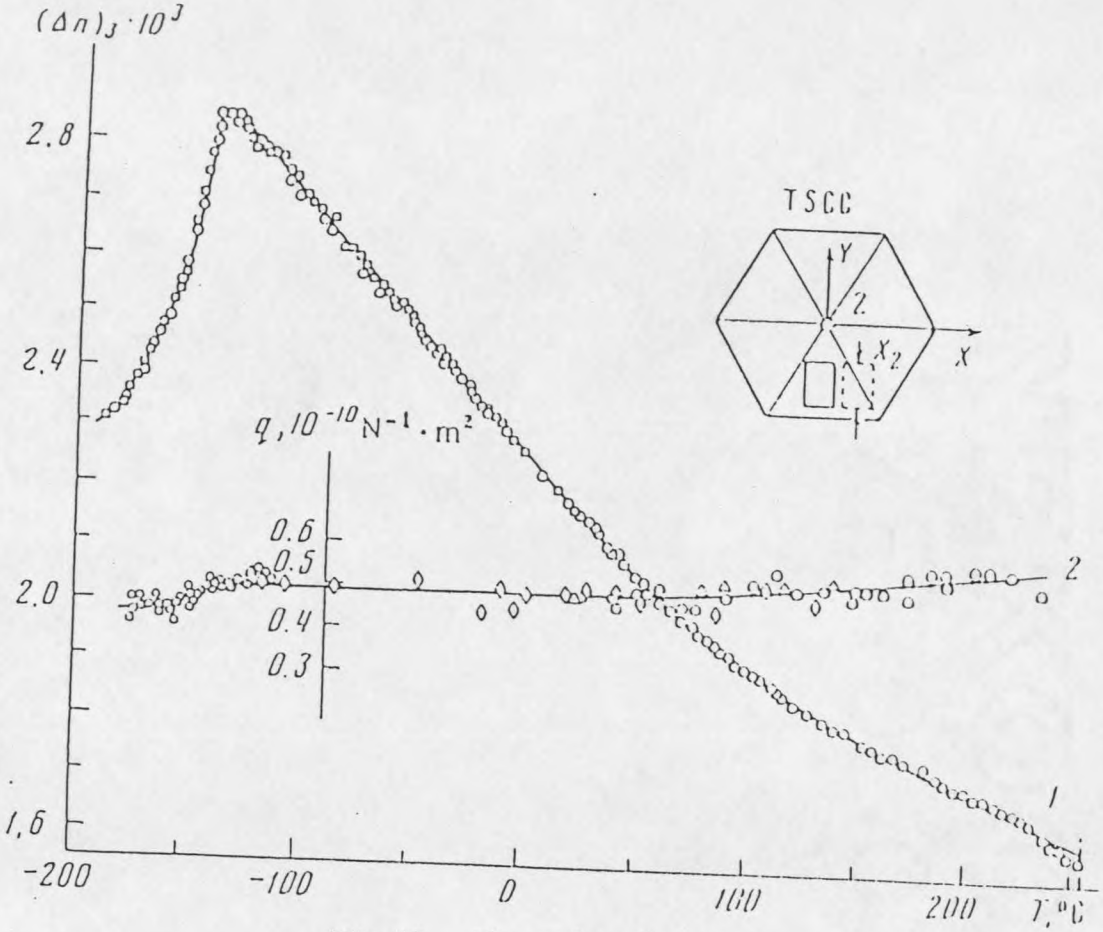

Fig.11. The refractive index

The Brillouin Spectrum

We have done Brillouin small angle, right angle and back scattering and have measured the dielectric constant simultaneously when doing the right angle scattering. The frequency range in which we were working is about 2 GHz (for small angle scattering) to 32 GHz (backscattering). The smallest angle we used is 7.48°. As far as we know it is the smallest Brillouin scattering angle ever achieved. The scattering geometry is shown in Fig. 4. The incident and scattered light are both polarized along the c axis. This scattering geometry is very convenient and simplifies the formula (IV-1), which becomes

$$\delta\nu/\nu_0 = (2n_0 v_s/c)\sin(\theta/2) \quad \text{----------} \quad (IV\text{-}1'')$$

Typical traces of the spectrum are shown in Fig. 12. The central maxima are Rayleigh peaks, whose intensity is much stronger than that of the Brillouin peaks. After thousands of scans, the spectrum has four peaks. The two at the edges of this spectrum are the Rayleigh peaks after thousand-fold attenuation by the shutter. The shutter was closed between the two troughs. The two peaks between the two Rayleigh peaks are Brillouin scattering. The original measurements are the Brillouin peak shift from the

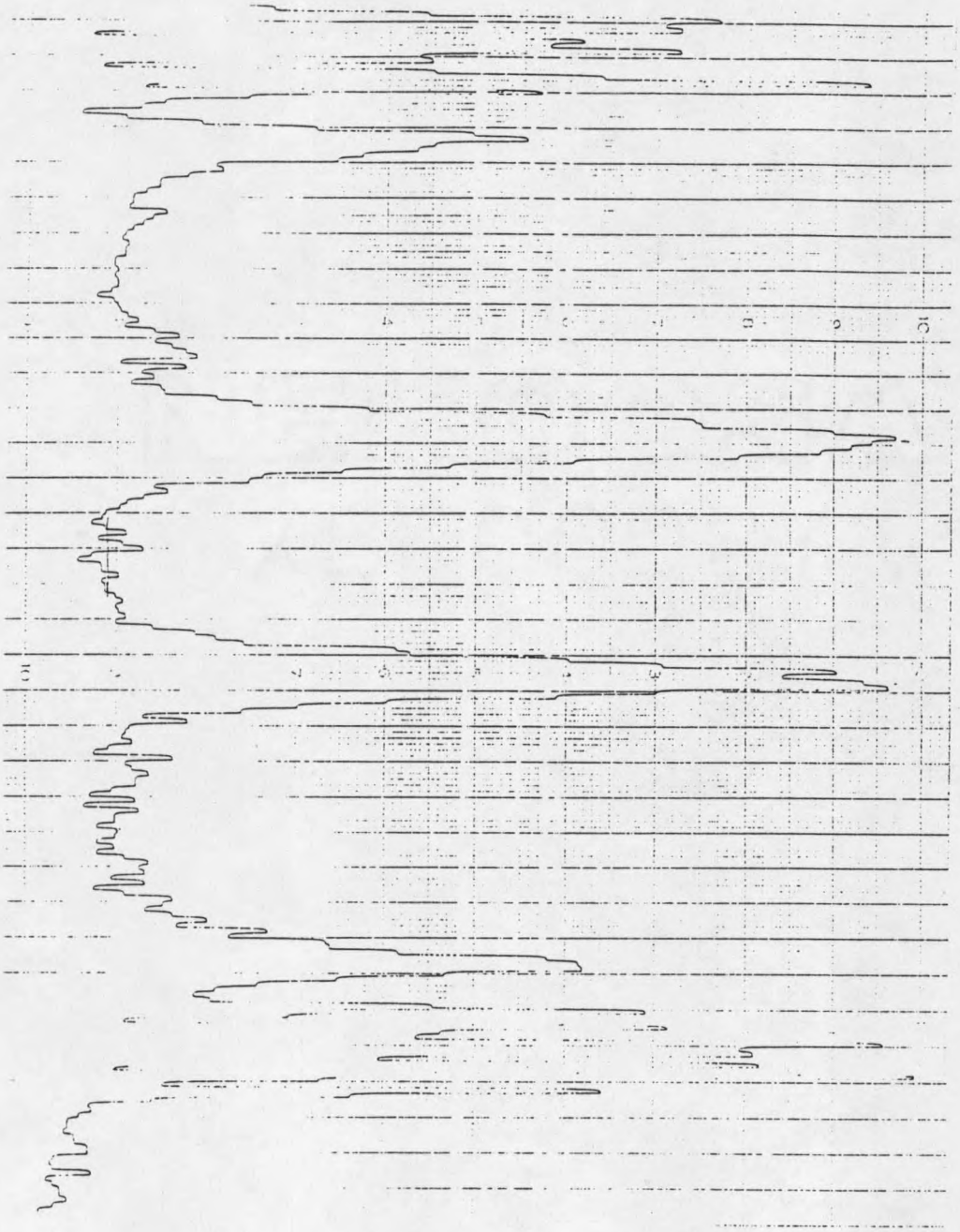

Fig. 12. Brillouin spectrum

Rayleigh peak and the line width. In order to do these measurements the peaks have to be well separated, so that the finesse of the Rayleigh peak must be about 45, The Rayleigh peak positions are shown clearly in the second set of storage channels. Before starting to take data, we estimate the frequency shift and line width by assuming the sound velocity is 4500 m/s and calculating the wavevector. Using some authors' results and the estimated results as a reference, we determine the free spectral range (FSR) and then in turn determine the mirror spacing. After obtaining the first spectrum, we had to find which Brillouin peak is Stokes and which is anti-Stokes. By changing the scattering angle a little bit, say, a little bit larger, if the two Brillouin peaks become closer, that means the right Brillouin peak is the one that shifts from the right Rayleigh peak and the left Brillouin peak is the one that shifts from the left Rayleigh peak. If the two Brillouin peaks become further apart, that means the right Brillouin peak is from the left Rayleigh peak and the left one from the right peak. In case the frequency shift decreases when the crystal undergoes the phase transition, the two Brillouin peaks will more towards each other and may overlap, which is to be avoided. We do not want the two Brillouin peaks to move into the "skirt" of the Rayleigh peaks either. After the first spectrum was

observed, we found the frequency shift approximately from

$$\delta\nu=(n+L/m)\cdot FSR \qquad (IV-2)$$

where $\delta\nu$ is the frequency shift, n is the order of interference pattern, L is the channel in which the Brillouin peak is located, and m is the total channel number change from the first to the second Rayleigh peak.

From formula (IV-2) we can choose the appropriate position of the Brillouin peaks, i.e. the number of L, by selecting a proper FSR.

Temperature Dependence of the Brillouin Shift (Phonon Frequency) and Line Width of the Longitudinal Phonons in TSCC

We measured the Brillouin shifts versus temperature for the phonons along [010] for small angle, right angle and back scattering and for phonon along [001] for small angle scattering. The results are given in Tables 1-5 and shown in the following figures.

Figs. 13-15 show the temperature dependences of the Brillouin shifts for the longitudinal phonons propagating along [010] at scattering angles 7.48°, 90° and 170° respectively. In Fig. 13, although the experimental points have a distribution due to several sources of error, the temperature dependence of the Brillouin shift appears

Table 1, q[010], $\theta=7.48^{\circ}$

T(K)	δ (GHz)	v(m/s)	W_{obs}(MHz)
153.04	1.903	4832	44.1
148.50	1.898	4820	44.1
144.91	1.909	4848	51.08
143.57	1.896	4815	43.5
140.93	1.899	4822	38.7
140.59	1.909	4848	50.3
138.08	1.891	4802	49.8
138.25	1.910	4850	51.8
137.09	1.894	4810	51.3
136.27	1.911	4853	59.5
136.02	1.891	4802	51.5
135.54	1.895	4812	49.8
135.29	1.905	4837	65.0
135.10	1.894	4810	51.1
134.49	1.900	4825	53.4
133.48	1.896	4815	57.2
132.38	1.898	4820	52.6
131.56	1.895	4812	44.1
130.6	1.892	4802	43.3
129.23	1.880	4774	51.2
129.37	1.883	4782	46.6
128.94	1.878	4769	48.9

Table 1,(cont.)

128.26	1.873	4756	45.9
127.68	1.865	4736	55.8
127.23	1.865	4736	49.7
126.77	1.855	4711	55.7
126.57	1.855	4711	52.0
126.37	1.851	4700	44.8
126.15	1.856	4713	44.1
126.15			55.1
125.93	1.854	4708	52.0
125.66	1.852	4703	55.7
125.44	1.852	4703	47.9
124.82	1.853	4705	51.2
123.40	1.856	4713	53.5
123.31	1.852	4703	45.9
123.06	1.856	4713	60.3
122.49	1.854	4708	48.2
120.67	1.851	4700	57.4
118.64	1.853	4705	44.8
116.50	1.851	4706	47.2
114.69	1.855	4711	47.9
113.16	1.854	4708	51.0
111.98	1.852	4703	50.3

Table 2, q[010], $\theta=90^{\circ}$

T(K)	δ (GHz)	v(m/s)	W_{ph}(MHz)
140.95	20.98	4913	1.25
139.95	20.98	4914	-13.0
139.75	20.97	4911	
138.84	20.97	4911	-10.1
137.74	20.96	4911	12.5
136.74	20.96	4910	8.1
135.73	20.95	4908	13.1
135.13	20.95	4906	12.7
134.72	20.94	4906	25.0
134.23	20.94	4905	1.25
133.80	20.94	4904	12.1
133.20	20.92	4901	-9.4
132.80	20.92	4900	18.75
132.52	20.92	4900	6.00
132.21	20.92	4899	0.0
131.74	20.88	4892	30.1
131.35	20.88	4892	50.0
131.14	20.86	4885	41.7
130.90	20.85	4885	68.7
130.73	20.84	4881	81.30
130.33	20.82	4876	81.2
130.05	20.75	4861	95.6

Table 2,(cont.)

130.02	20.73	4855	
129.82	20.76	4864	70.7
129.55	20.72	4853	75.1
129.62	20.68	4844	96.4
129.44	20.67	4842	88.0
129.30	20.63	4833	100.5
129.30			149.90
129.03	20.58	4820	87.0
128.75	20.58	4820	72.2
128.53	20.54	4812	100.1
128.19	20.50	4802	149.5
128.01	20.49	4799	132.2
127.81	20.44	4788	136.9
127.6	20.46	4793	153.2
127.4	20.42	4784	124.0
127.26	20.42	4784	154.3
127.03	20.40	4777	150.0
126.80	20.40	2778	213.0
126.2	20.40	2778	162.6
126.12	20.39	4776	176.1
125.98	20.38	4774	141.9
125.70	20.36	4769	176.1
125.42	20.37	4771	143.4
124.42	20.37	4771	129.8

Table 3, q[010], θ=170°

T(K)	δ (GHz)	v(m/s)	W_{ph}(MHz)
297.48	31.37	5216	102
290.25	31.38	5218	76.9
267.99	31.49	5236	117
249.08	31.56	5248	120
233.74	31.62	5258	76.9
220.38	31.69	5269	55.9
213.09	31.71	5273	99.9
202.99	31.74	5278	55.9
191.18	31.78	5284	65.9
171.34	31.86	5298	46.9
169.76	31.86	5298	55.9
163.96	31.86	5298	44.9
159.30	31.89	5303	41.9
154.36	31.90	5304	45.9
149.81	31.89	5303	47.9
146.46	31.9	5304	48.9
143.27	31.9	5304	56.9
141.41	31.88	5301	37.9
139.48	31.87	5299	51.9
137.36	31.86	5298	51.9
136.88	31.85	5296	69.9
136.35	31.84	5294	49.9

Table 3, (cont.)

135.86	31.84	5294	52.9
135.35	31.84	5294	61.9
134.96	31.83	5293	62.9
134.54	31.82	5291	60.9
133.84	31.81	5289	52.9
133.30	31.81	5289	83.9
133.02	31.80	5288	69.9
132.23	31.77	5283	73.9
131.64	31.75	5279	82.9
131.17	31.73	5276	108.9
130.69	31.71	5273	114.9
130.21	31.66	5264	170.9
129.89	31.53	5243	136.9
129.28	31.41	5223	131.9
128.74	31.23	5193	164.2
128.23	31.18	5185	154.2
127.81	31.14	5178	162.2
127.52	31.10	5171	138.2
127.26	31.07	5166	158.2
126.7	31.06	5165	167.2
126.99	31.06	5165	135.2
126.55	31.04	5161	132.2
126.23	31.03	5160	135.2
126.19	31.04	5161	131.2

Table 4, q[001], θ=7.55°

T(K)	δ (GHz)	v(m/s)	W_{obs}(MHz)
149.60	1.693	4254	
149.20	1.692	4251	47.6
149.2	1.693	4254	59.8
143.94	1.690	4246	51.0
139.13	1.698	4266	51.3
138.06	1.696	4261	53.1
137.61	1.696	4261	53.5
137.04	1.695	4258	55.6
136.37	1.694	4256	55.3
136.01	1.693	4254	52.1
135.63	1.691	4248	49.6
135.19	1.694	4256	52.9
134.68	1.692	4251	50.3
134.20	1.690	4246	47.9
133.70	1.690	4246	48.9
133.25	1.690	4246	49.6
132.73	1.690	4246	50.0
131.34	1.681	4223	50.3
130.84	1.682	4225	49.4
130.12	1.688	4241	50.8
129.32	1.651	4147	55.3
128.82	1.651	4147	57.6

Table 4, (cont.)

128.36	1.651	4147	47.2
128.02	1.652	4150	53.2
127.54	1.659	4168	53.2
127.19	1.654	4155	47.5
127.14	1.655	4158	50.6
126.65	1.659	4168	50.7
125.88	1.656	4160	48.6
125.50	1.654	4156	45.3
124.48	1.660	4170	47.3
1234.22	1.661	4173	47.6
122.46	1.660	4170	50.3
120.53	1.661	4173	55.4
120.49	1.660	4170	57.4
116.55	1.666	4186	55.4
114.25	1.663	4178	49.7
111.97	1.665	4183	45.6
129.55	1.657	4163	53.7
129.64	1.662	4176	59.1
129.95	1.682	4226	61.1
129.88	1.666	4186	70.8
129.93	1.677	4213	75.8
130.00	1.685	4233	47.6
141.49	1.694	4267	49.4

Table 5, q[001], θ=90°

T(K)	δ (GHz)	v(m/s)	W_{Ph}(MHz)
149.39	21.63	4943	15.2
143.50	21.65	4947	52.2
138.48	21.66	4950	18.3
136.61	21.66	4950	51.0
134.55	21.65	4947	25.1
132.78	21.64	4945	0.00
131.73	21.63	4943	24.5
130.90	21.62	4941	48.5
130.00	21.59	4934	75.0
129.49	21.48	4909	126.8
129.35	21.39	4888	482.4
129.21	21.34	4877	437.5
128.88	21.30	4868	348.1
128.45	21.23	4852	286.3
128.16	21.22	4849	180.6
127.33	21.24	4854	162.9
125.99	21.26	4858	150.0
124.66	21.29	4865	87.5
123.50	21.30	4868	
121.01	21.34	4877	48.4
118.77	21.37	4884	40.2
115.52	21.40	4890	10.3
112.60	21.43	4897	2.10

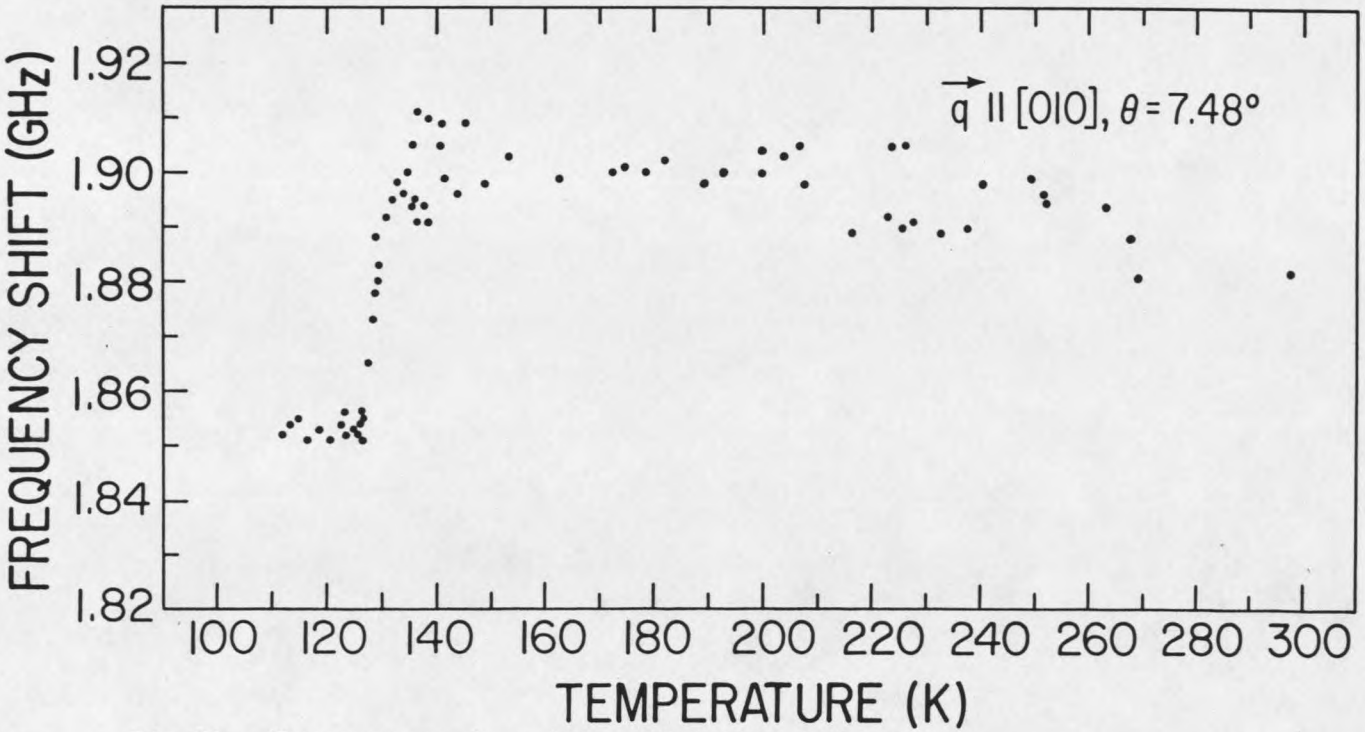

Fig.13. Temperature dependence of Brillouin shift of longitudinal (010) phonon for small angle scattering

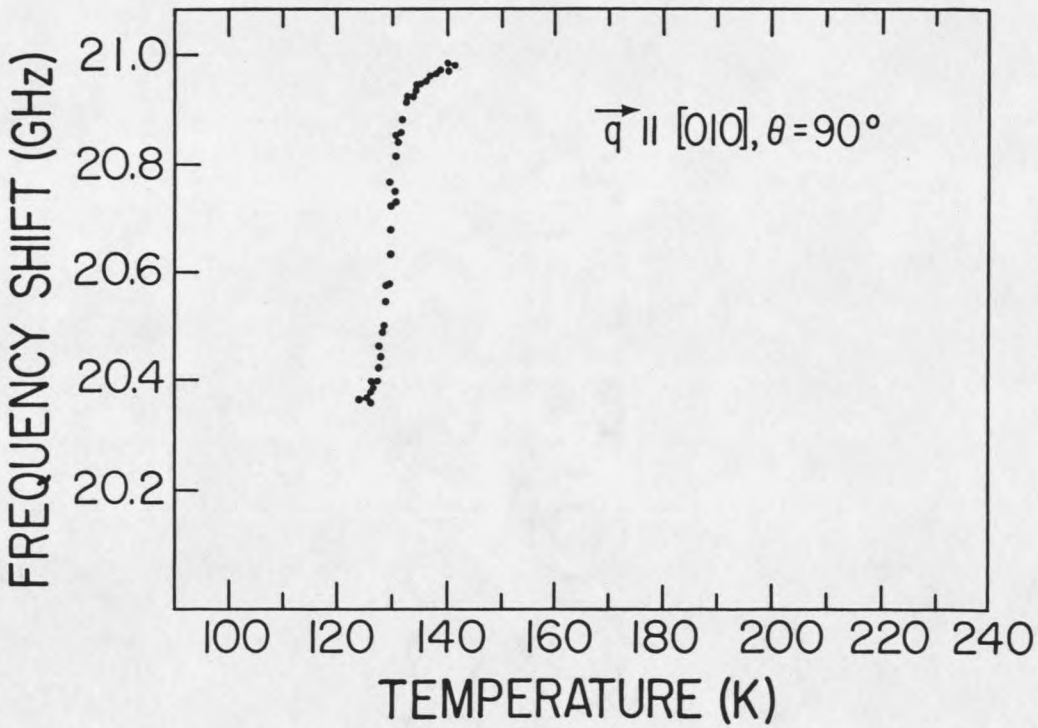

Fig. 14. Temperature dependence of Brillouin shift of longitudinal (010) phonon for right angle scattering

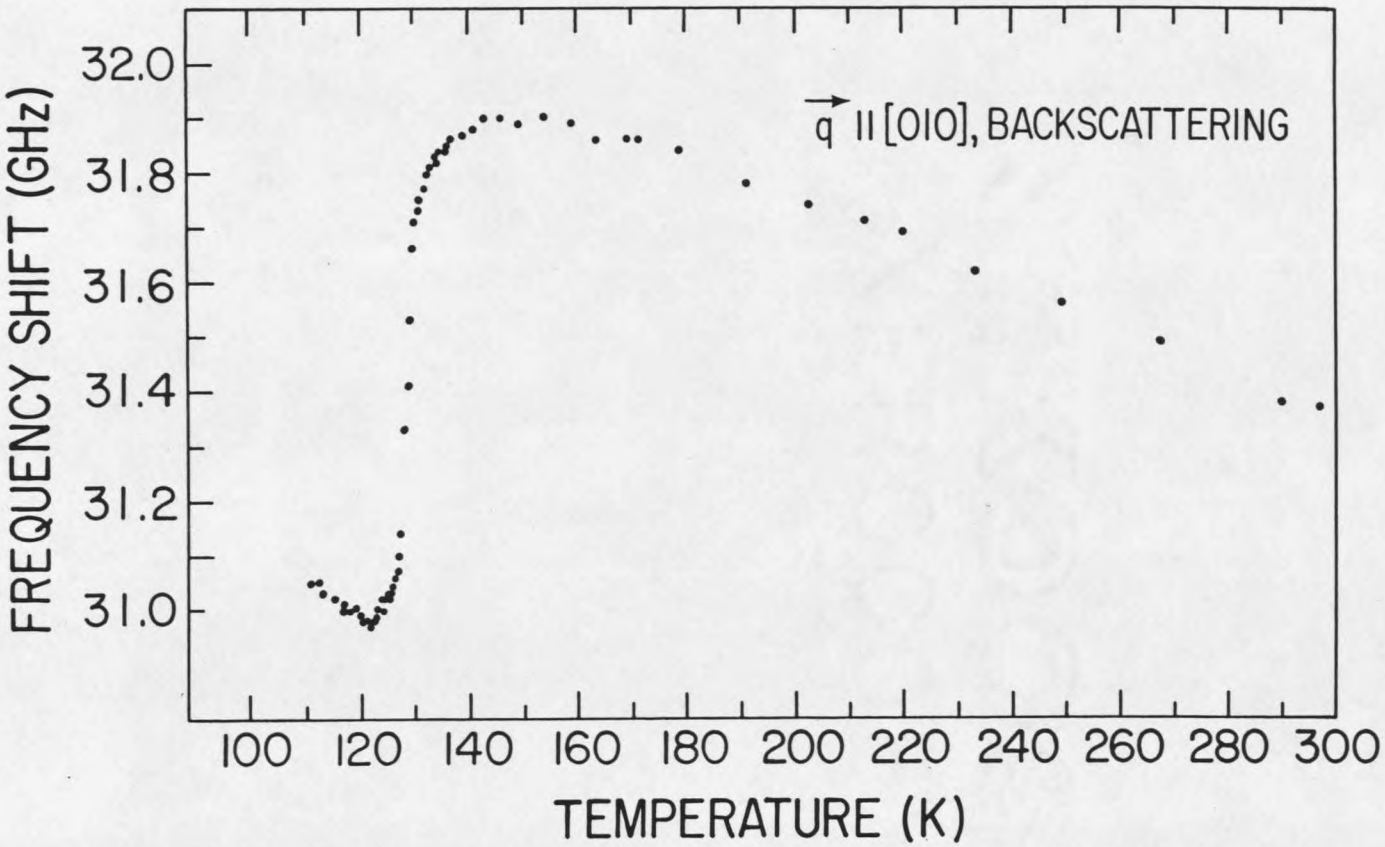

Fig. 15. Temperature dependence of Brillouin shift of longitudinal (010) phonon for backscattering

quite clearly. First, it shows the anomaly around T_c=130 K. Nevertheless, it barely shows temperature dependence in the PE phase well above T_c. Approaching T_c, the Brillouin shift first shows a slow rounding and then a quick decrease with decreasing temperature. The temperature at which the slope of the curve is maximum is defined as the transition temperature. When the temperature reaches about 125 K, the Brillouin shift shows almost no temperature dependence.

Fig. 14 clearly shows the anomaly of the temperature dependence. Unfortunately we only got data around the transition temperature. We see that the Brillouin shift shows a slow rounding down with the decreasing temperature. The fastest drop occurs at the critical point T_c, and again near 125 K the shift seems to stop decreasing. We will see more detail in Figure 3(b). This result has been shown previously.[20]

Fig. 15 shows very strong temperature dependence of the Brillouin shift in a wide range of temperature from room temperature down to about 110 K. Down to about 145 K the Brillouin shift is increasing monotonically. The shift at room temperature is about 31.35 GHz. However, at the maximum point the shift is 31.9 GHz. Below 145 K, but above T_c=130 K, the Brillouin shift shows a slow rounding down until the critical point T_c where the shift quickly

decreases. The Brillouin shift reaches the lowest value of about 30.98 GHz near 122 K. From 122 K down to 110 K, the Brillouin shift increases sharply.

Fig.16 shows the temperature dependence of the Brillouin shift for phonons propagating along [001] in the wide range from room temperature down to about 110 K at the small angle 7.55°. Above about 142 K up to room temperature, the Brillouin shift varies quite strongly with temperature. The Brillouin shift at room temperature is about 1.64 GHz. The maximum Brillouin shift of about 1.693 GHz occurs near 142 K. Below this point the Brillouin shift shows a slow rounding down as usual. Then a quick drop takes place in a very narrow region at the phase transition, less than one degree wide, followed by an abrupt increase of the Brillouin shift. The Brillouin shift increases with decreasing temperature down to 110 K where we ended our measurement in this trial.

Fig.17 shows the temperature dependence of the Brillouin shift for phonons propagating along direction [001] at scattering angle 90°. This results has been shown previously.[21] The Brillouin shift increases with decreasing temperature from room temperature down to about 140 K. From 140 K down to T_c=130 K there is slow rounding. At T_c the Brillouin shift suddenly drops and then the Brillouin shift increases quite quickly with

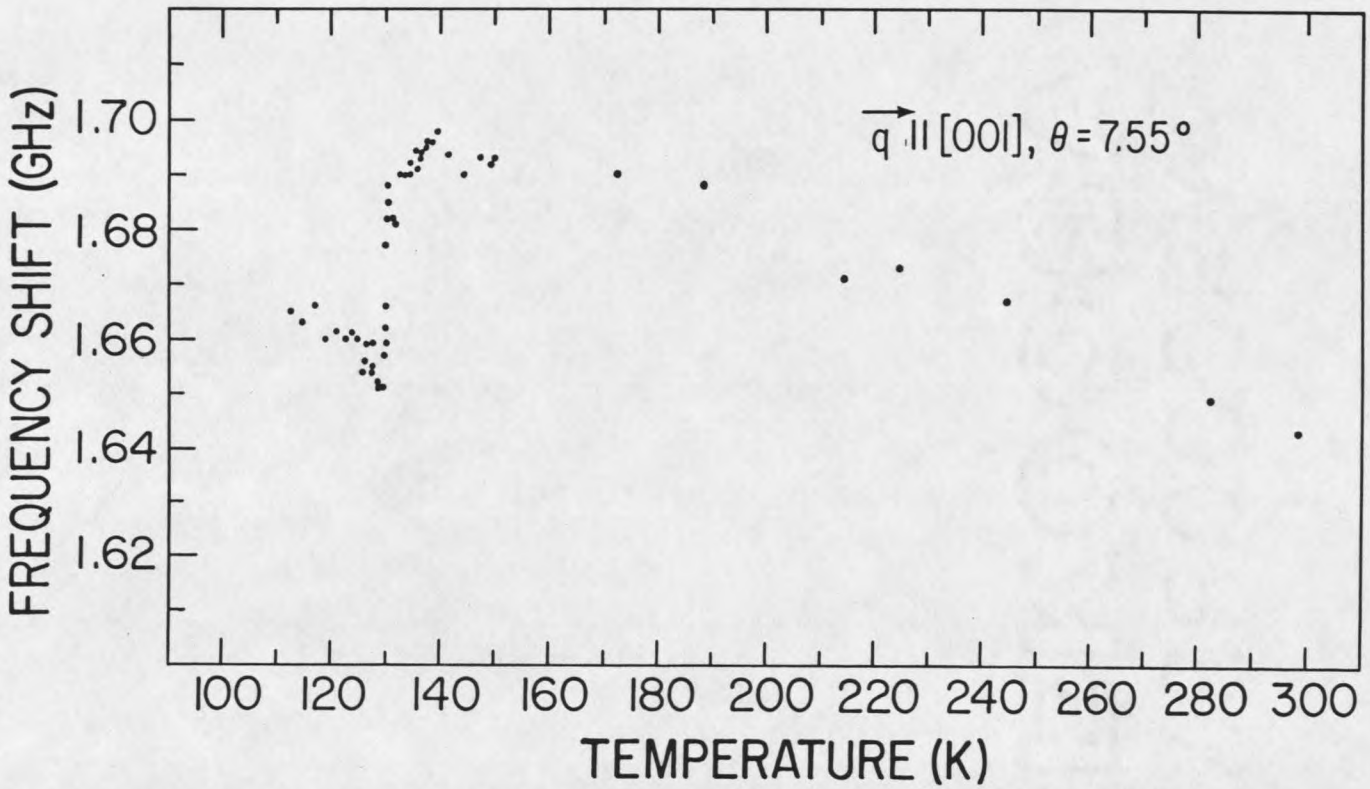

Fig.16. Temperature dependence of Brillouin shift of longitudinal (001) phonon for small angle scattering

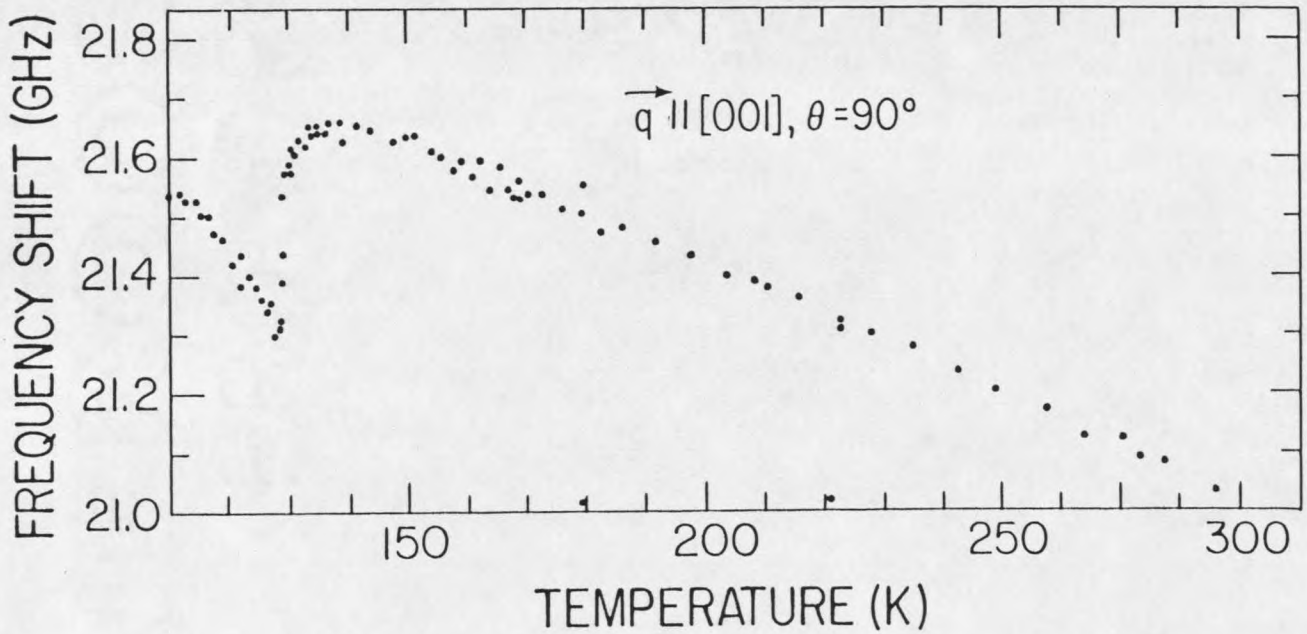

Fig. 17. Temperature dependence of Brillouin shift of longitudinal (001) phonon for right angle scattering

decreasing temperature, so there is a sharp dip around the critical region. The Brillouin shift then increase monotonically down to 110 K, where it seems to flatten out.

Fig. 18 shows the temperature dependence of the Brillouin shift for backscattering in the temperature region from 190 K down to 110 K. Above T_c the Brillouin shift shows very strong temperature dependence. Near but above T_c, there is slow rounding. At T_c the Brillouin shift drops very quickly and then just a little below T_c the Brillouin shift starts to increase slowly and increases down to 110 K. This result is from Smolensky, Siny, Tagantsov, Prokhorova and Windsch.[22]

Fig. 19 shows more detail of the temperature dependence of the Brillouin shift with a expanded temperature scale together with the observed line width W_{abs} (FWHM) for phonons propagating along [010] direction at the scattering angle 7.48°. We can see the slow rounding quite clearly near but above T_c and a rounding trough near but below T_c. It is hard to see the temperature dependence of the line width. Because the scattering angle is small, the frequency shift is small, so that the error is relatively large. The experimental line width results in this case are not very meaningful. In Fig. 19 we show the directly observed line width without

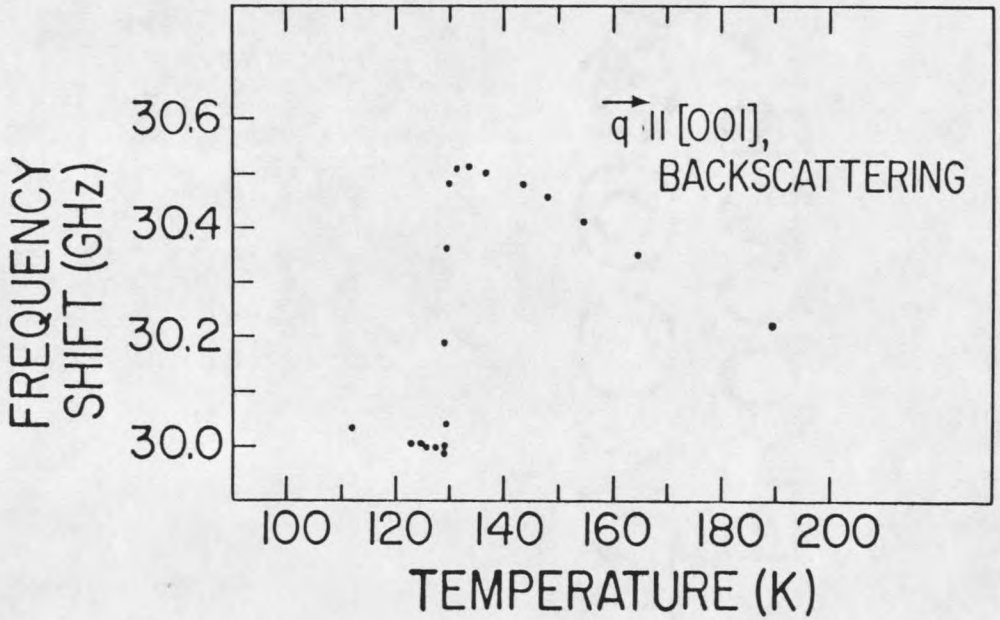

Fig. 18. Temperature dependence of Brillouin shift of longitudinal (001) phonon for backscattering

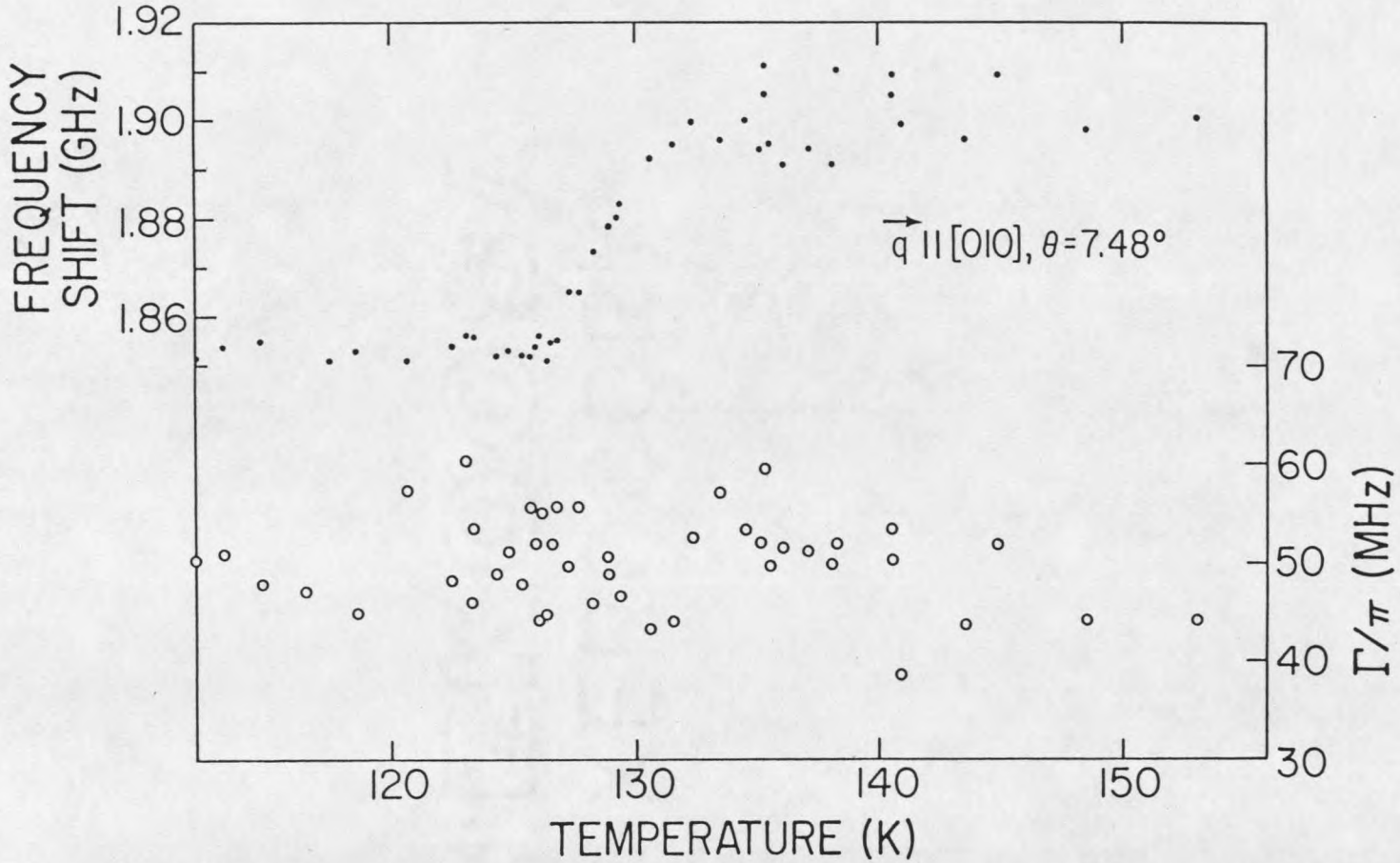

Fig. 19. Temperature dependence of Brillouin shift (.) and line width (o) of longitudinal (010) phonon for small angle scattering

considering the instrumental and collection angle broadening.

Fig. 20 shows more detail of the temperature dependence of the Brillouin shift with a expanded temperature scale together with the line width [FWHM] for phonons propagating along [010] at scattering angle 90°. We see no sudden step down in the phase transition region around T_c, but above and below T_c there is a slow rounding down and up respectively. The temperature dependence of the line width shows a round maximum around T_c. The anomalies of both the Brillouin shift and line width appear in the same temperature region and the maximum of the line width takes place at the temperature a few degrees below T_c. The line width further above T_c seems to be constant with respect to temperature. Unfortunately, we do not have many experiment points below T_c.

Fig. 21 shows the temperature dependence of the Brillouin shift and line width in more detail with a expanded temperature scale. Again, there is no sudden step around T_c. There are only slow roundings both above and below but near T_c. There is line width maximum a few degrees below T_c. Above T_c the line width is constant.

Fig. 22 shows the temperature dependence of the Brillouin shift in more detail with a expanded temperature

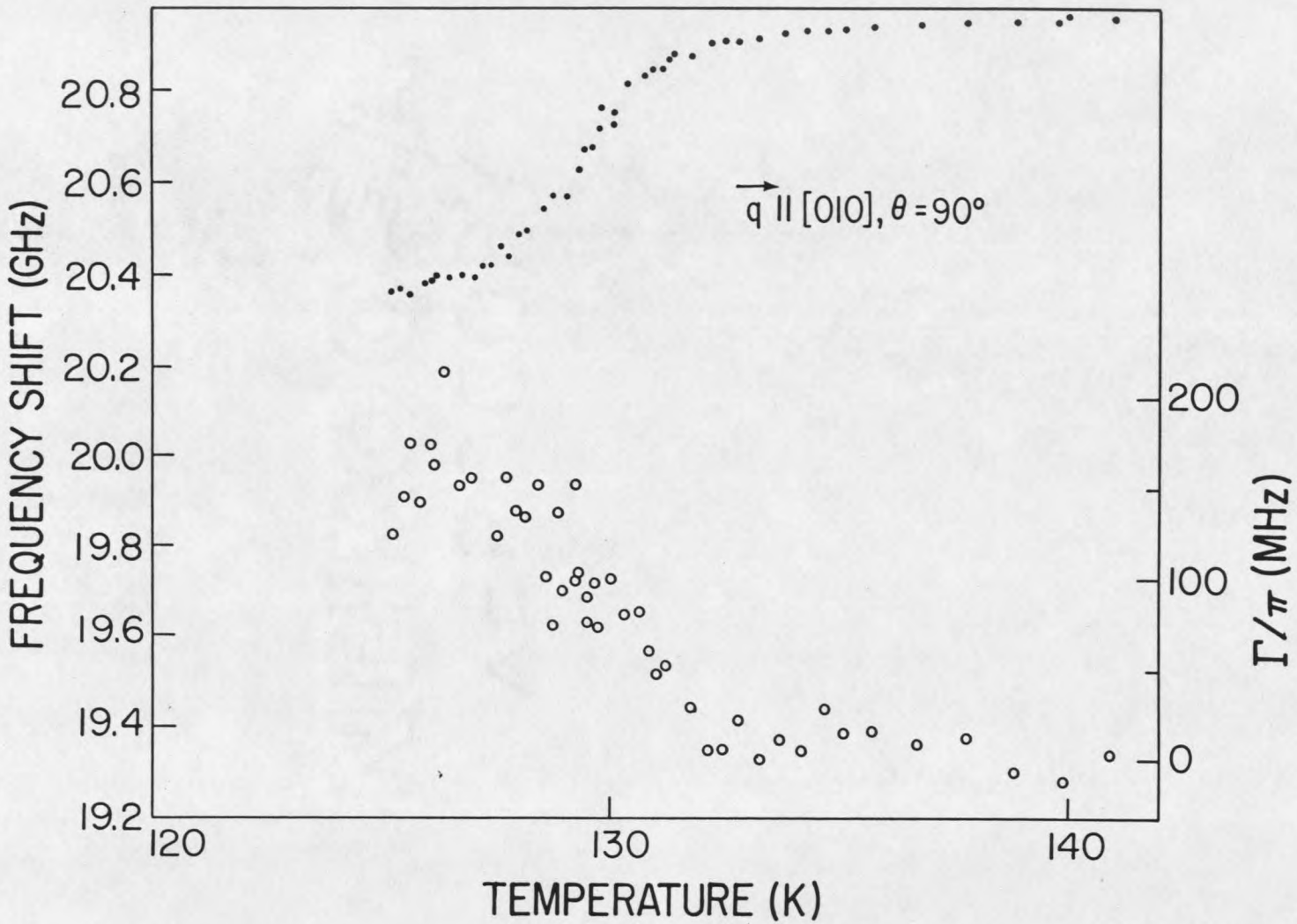

Fig. 20. Temperature dependence of Brillouin shift (.) and line width (o) of longitudinal (010) phonon for right angle scattering

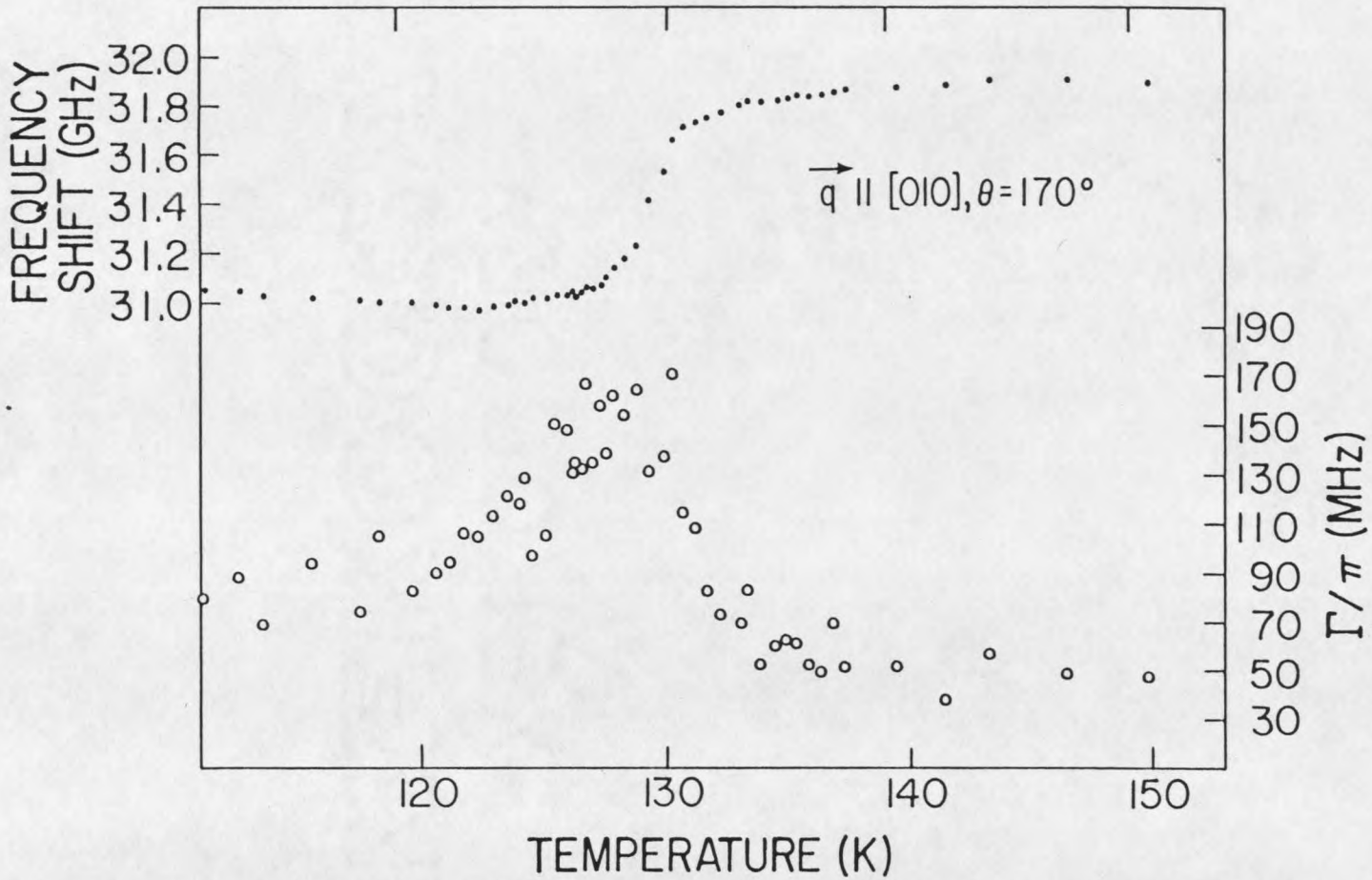

Fig. 21. Temperature dependence of Brillouin shift (.) and line width (o) of longitudinal (010) phonon for backscattering

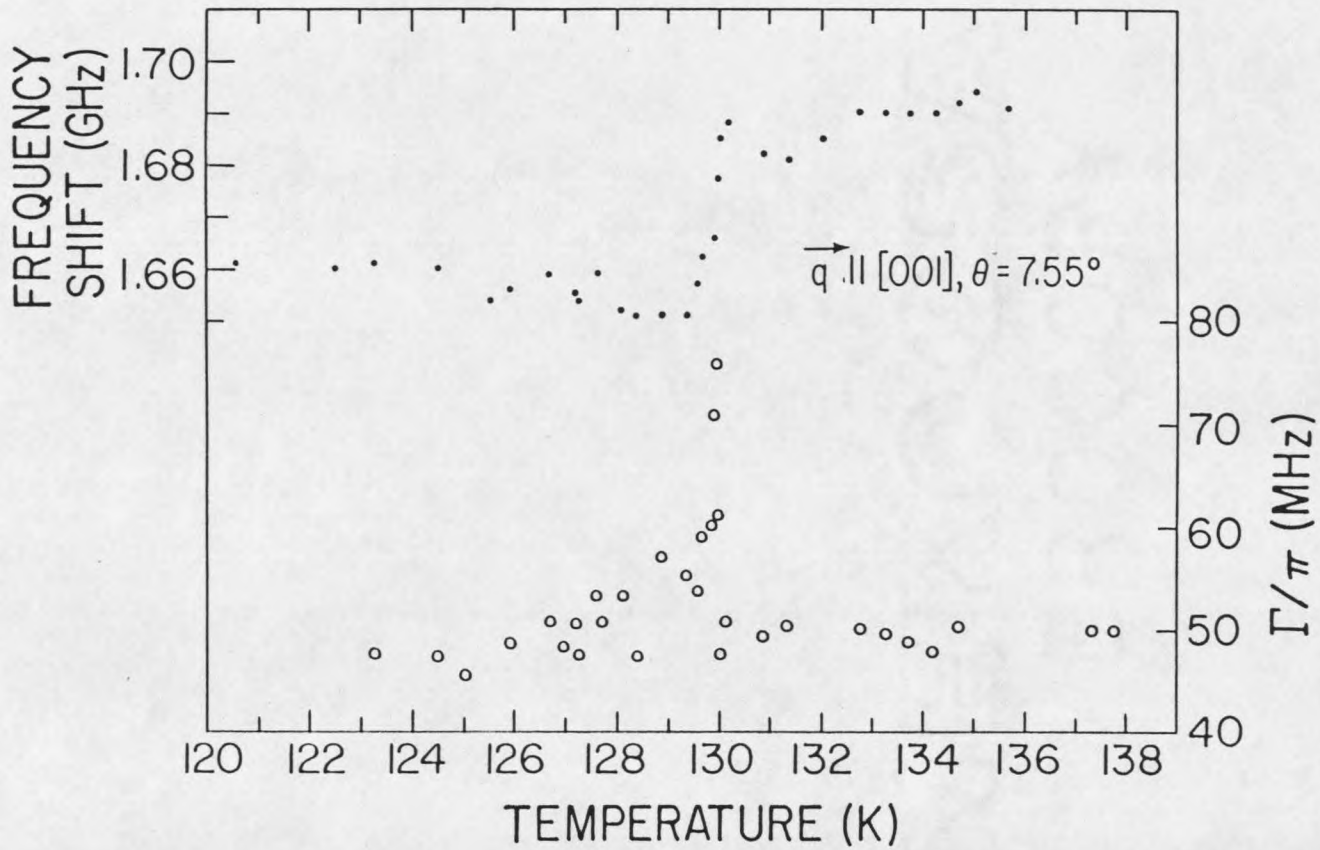

Fig. 22. Temperature dependence of Brillouin shift (.) and line width (o) of longitudinal (001) phonon for small angle scattering

scale together with the observed line width [FWHM] for phonons propagating along [001] at scattering angle 7.55°. There is a step anomaly of the Brillouin shift and a very sharp peak in the line width somewhat below T_c. Elsewhere the line width shows no temperature dependence. In Fig. 22 we show the direct observation of the line width without considering the collection angle broadening and instrumental broadening.

Fig. 23 shows the temperature dependence of the Brillouin shift in more detail with a expanded temperature scale together with the line width for phonons propagating along [001] at scattering angle 90°. It has been shown previously.[6] There is slow rounding near but above T_c. and a sharp step up near, but below T_c, with a dip below T_c. The line width has a sharp peak in the phase transition region. The maximum appears somewhat below T_c, as for small angle scattering for phonons propagating in the same direction. Above and below T_c the line width shows no temperature dependence. However, near but above T_c, the line width asymptoticaly approaches a constant value. These results have been shown previously.[20]

Fig. 24 shows in more detail the temperature dependence of the Brillouin shift with a expanded scale of temperature together with the line width for phonons propagating along [001] for back scattering. Near but

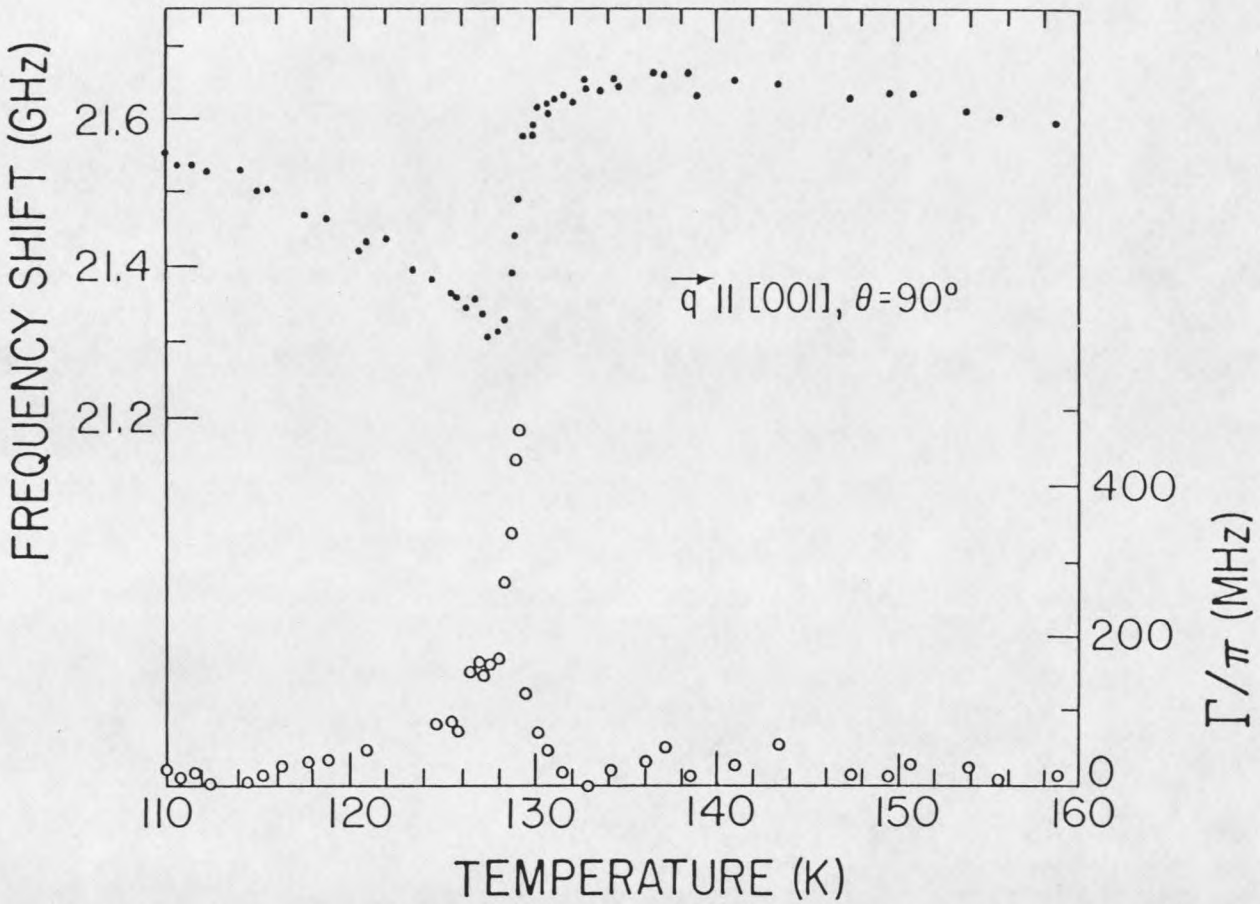

Fig. 23. Temperature dependence of Brillouin shift (.) and line width (o) of longitudinal (001) phonon for right angle scattering

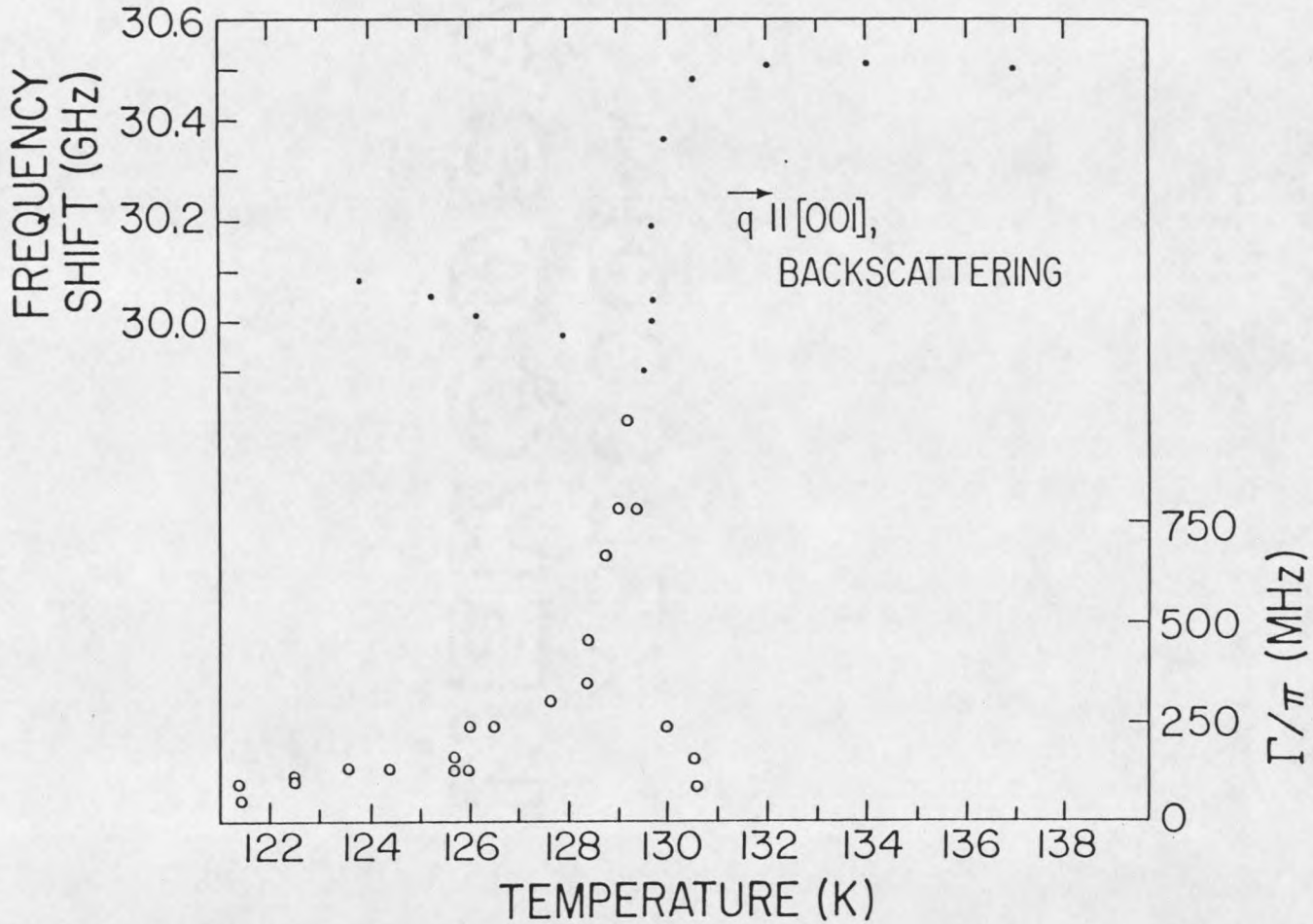

Fig. 24. Temperature dependence of Brillouin shift (.) and line width (o) of longitudinal (001) phonon for backscattering

above T_c there is slow rounding, while near but below T_c there is a discontinuity and a sharp step up. The line width again has a peak in the phase transition region, somewhat below T_c. There is no obvious temperature dependence for the line width far above or below T_c. The line width approaches a constant value faster above T_c than below T_c.

The observed line width consists of three contributions: (1) the intrinsic instrumental broadening which includes the laser line broadening due to the jittering claimed by the manufacturer to be about 10 MHz and the computer resolution and the nature of the Fabry-Perot. This is instrumental line width W_{inst}, which can be calculated by

$$W_{inst}=0.022\cdot FSR \qquad \text{(IV-3)}$$

(2) the collection angle broadening W_{ang} given by

$$W_{ang}=0.0365\cdot \delta\nu \qquad \text{(IV-4)}$$

where $\delta\nu$ is the Brillouin shift, i.e., the phonon frequency. Later we will discuss Equation (IV-4).

(3) the natural phonon line width [FWHM] W_{ph}.

For calculating natural phonon line width, the natural phonon spectrum and the instrumental function were assumed to have Lorentzian distributions, and the broadening due

to collection optics was assumed to have rectangular distribution. In this case, the natural phonon line width W_{ph} is given by

$$W_{ph}=(W_{obs}^2-W_{ang}^2)^{1/2}-W_{inst} \qquad \text{(IV-5)}$$

The Sound Velocity Anomalies

We studied light scatered by pure longitudinal modes in the [010] and [001] directions. In the [010] direction the longitudinal phonon velocity is determined by the single elastic constant C_{22} and is

$$v_L[010]=\sqrt{C_{22}/\rho} \qquad \text{(IV-6)}$$

In the [001] direction the longitudinal velocity is determined by

$$v_L[001]=\sqrt{C_{33}/\rho} \qquad \text{(IV-7)}$$

The observed Brillouin splittings and resulting sound velocities are given in Tables 1-5 The sound velocity data have been plotted in Fig. 25 for phonons propagating along [010] and in Fig. 26 for phonons propagating along [001].

In each case we have three plots for the small angle, right angle and back scattering respectively. The hypersonic sound frequencies are in the range 1.85 GHz to

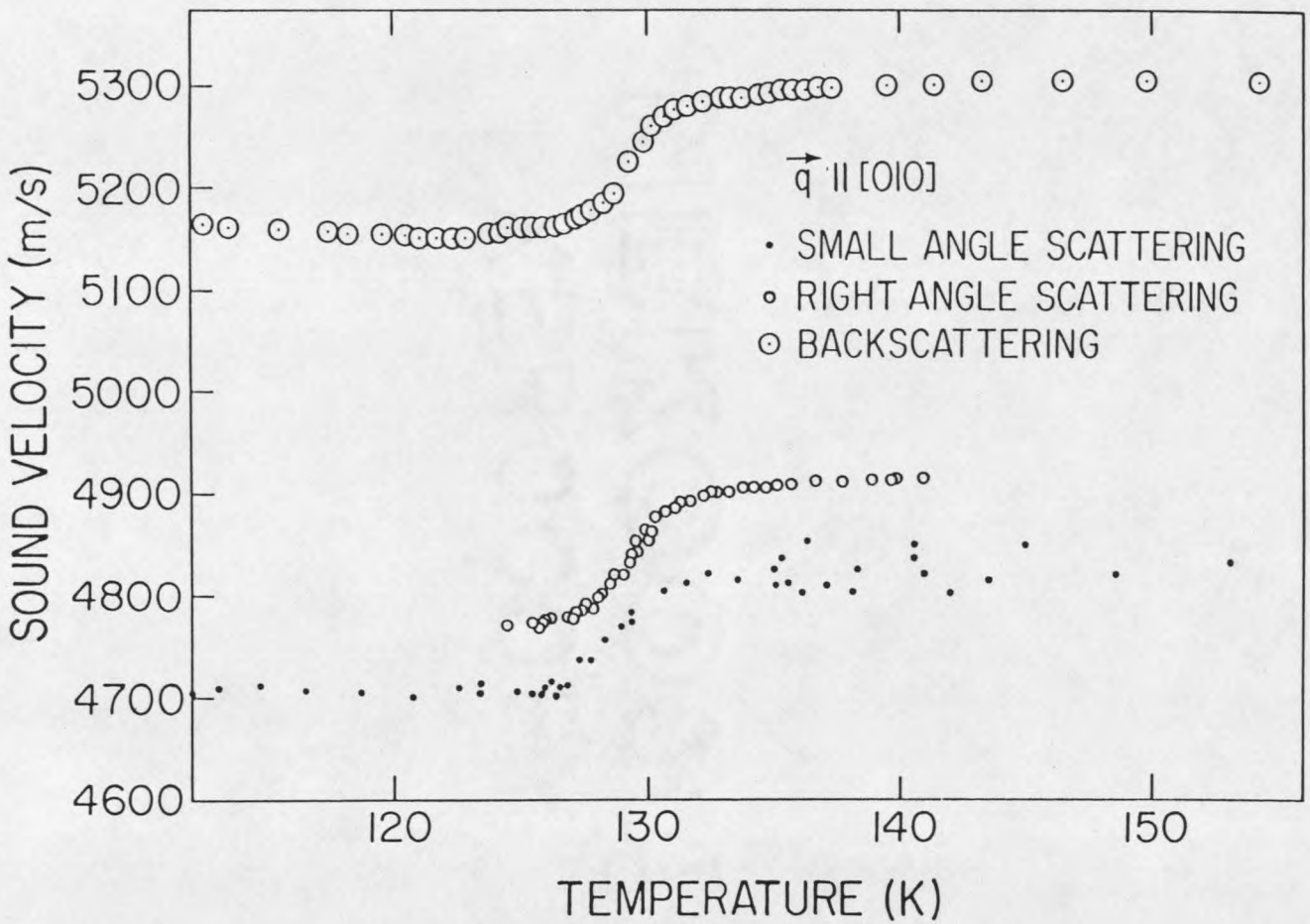

Fig. 25. Temperature dependence of sound velocities of longitudinal (010) phonons

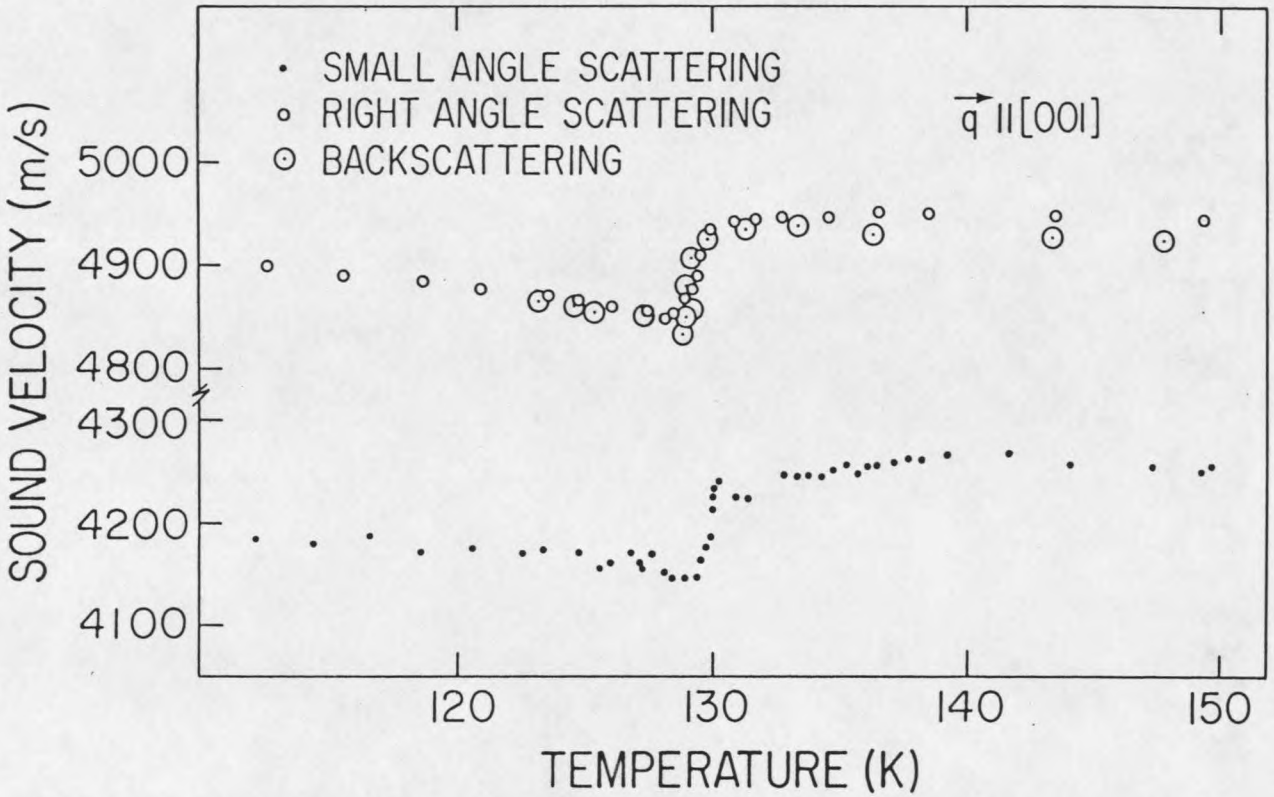

Fig. 26. Temperature dependences of sound velocities of longitudinal (001) phonons

31.90 GHz for phonons propagating along [010] and 1.65 GHz to 21.67 GHz for phonons propagating along [001].

The three plots in Fig. 25 have very similar shapes. The phase transition is marked by about the same magnitude of rounded drop in velocity with decreasing temperature in all three cases. But surprisingly, the sound velocities in these three cases at a given temperature are different and the plot for small angle scattering with $\theta=7.48^{\circ}$ shows a discontinuous dip near but below T_c. But the velocities do not vanish at T_c.

The three plots in Fig. 26 also have very similar shapes. The phase transition is marked by about the same magnitude of rounded drop. The three plots show a dip and a sharp step up from below T_c to above T_c. The sound velocities for the right angle and back scattering seem to be consistent with each other, but a deviation from small angle scattering is obvious. Later we will discuss all these phenomena.

Temperature Dependence of the Dielectric Constant of TSCC

While measuring the Brillouin shift for phonons propagating along [010] for right angle scattering, we measured the dielectric constant simultaneously to determine the phase transition temperature. The Brillouin scattering measurement involves only a small part of the

sample. The power of the laser beam is quite high, so the temperature of the illuminated volume may be higher than that measured dielectrically for the major part of the sample. There will be a discrepancy of degrees for the transition temperature. Thus dielectric constant measurement gives a more accurate determination of the phase transition temperature. The temperature dependence of the inverse of the sample capacitance is illustrated in Fig. 27. There is a dip near the transition temperature. The Brillouin shift anomaly occurs in the same region in which the dielectric constant reaches a peak. We define the temperature at which the inverse of the capacitance is minimum as the transition temperature.

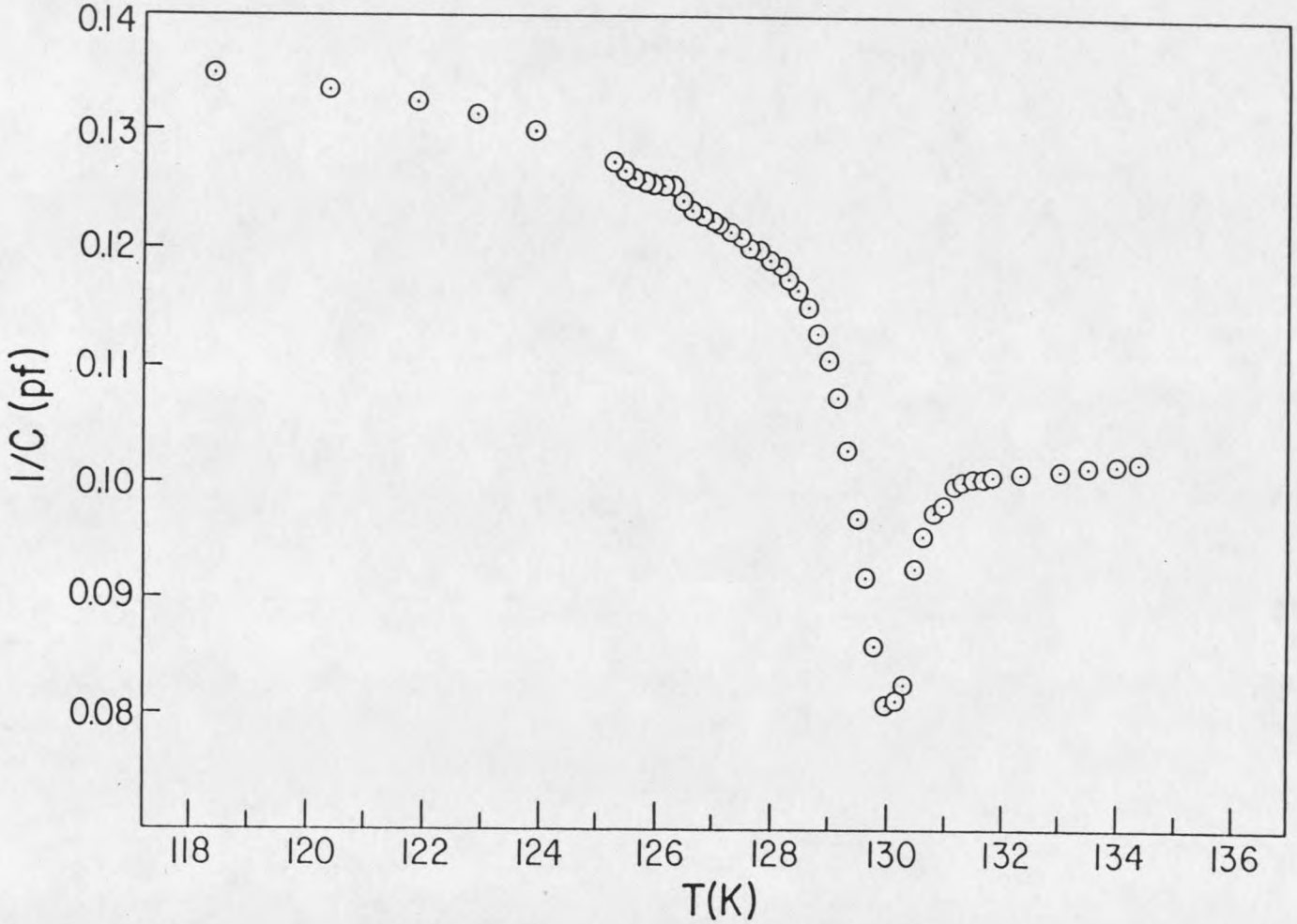

Fig. 27. Temperature dependence of dielectric constant

CHAPTER V

DISCUSSION

Introduction

In this chapter we will discuss the mechanism of the anomalies of the Brillouin shift, the sound velocity and the line width in the phase transition region.

Light scattering spectroscopy offers a direct experimental access via the fluctuation dissipation theorem to the displacement correlation function. A full derivation of these relations has been given by Landau and Lifshits (1968).[23] It seems worth emphasizing that the first theoretical works on light scattering near phase transitions[1] (Ginzburg 1955, Krivoglaz and Rybak 1957, Ginzburg and Levanyuk 1958, 1960, Levanyuk and Sobyanin 1967) have been performed in the framework of phenomenological approach. Yamada et al.(1974)[24] have studied theoretically the critical dynamical behavior of pseudo-spin-phonon coupled systems in connection with the OD (order-disorder)-SPT(structural phase transition) of molecular crystals. A type of pseudo-spin-phonon

interaction has become apparent in the spectra of TSCC, the hard-core modes. This type of mode, which is also encountered in many other ferroelectric materials of OD type, presents a temperature-dependent frequency shift on approaching T_c but remain unshifted above T_c and indicates the effectiveness of a coupling mechanism between the pseudo-spin σ and other optical phonons Q_i which is not equal to Q_s, (Q_s is soft mode), which is non-linear ($H_{in}=g\sigma Q_i^2$); (Winterfeldt and Schaack 1977, 1980).[25,26]

The FE transition is a structural phase transition. Such transitions are generally divided into two caterories, displacive and order-disorder. Particularly with TSCC, there have been strong arguments about which category the FE transition falls into. Chen and Schaack are the latest proponents of an order-disorder transition for TSCC.[27] However, a well-defined limit between these categories does not exist, and we consider that TSCC shows features of both transition types.

The Crystal Structure of TSCC

In order to understand the mechanism of the phase transition of TSCC, it will be helpful to look at its structure.

Tris-Sarcosine Calcium Chloride (TSCC), formula $(CH_3NHCH_2COOH)_3CaCl_2$, was found to exhibit a ferroelectric

(FE) phase transition at the Curie point, 130 K. (Pepinsky and Makita in 1962 claimed the Curie point for this crystal is 127 K). The crystal structure of TSCC is significant for both the dielectric and the ultrasonic velocity anomalies. The TSCC crystal is orthorhombic with lattice constants a=9.156±0.01, b=17.46±0.045, c=10.265±0.005 Å and with Z=4 formula units in the unit cell. The space group is D_{2h}^{16} (Pnma) in the paraelectric (PE) phase and C_{2h}^{9}(Pn2$_1$a) in the FE phase.[20] According to the structural analysis by Ashida et al. the crystal structure of TSCC is pseudo-hexagonal when viewed down the a axis.[28] There are 12 sarcosine zwitterion molecules in the unit cell. They belong to two types. One comprises the four molecules in the mirror plane. The other eight molecules in general position (type 2) are slightly bent. There are three kinds of N-H...Cl hydrogen bonds present in TSCC, one with a total bond length of 3.18 Å and two with 3.22 Å with different N-H distances. The structure is shown in Figs. 28-30.

Since the crystal at room temperature belongs to the orthorhombic system, it is optically biaxial. The acute bisectrix is the a axis. The optical plane is perpendicular to the c axis and the crystal is optically positive.[17]

When the crystal undergoes the PE-FE phase transition,

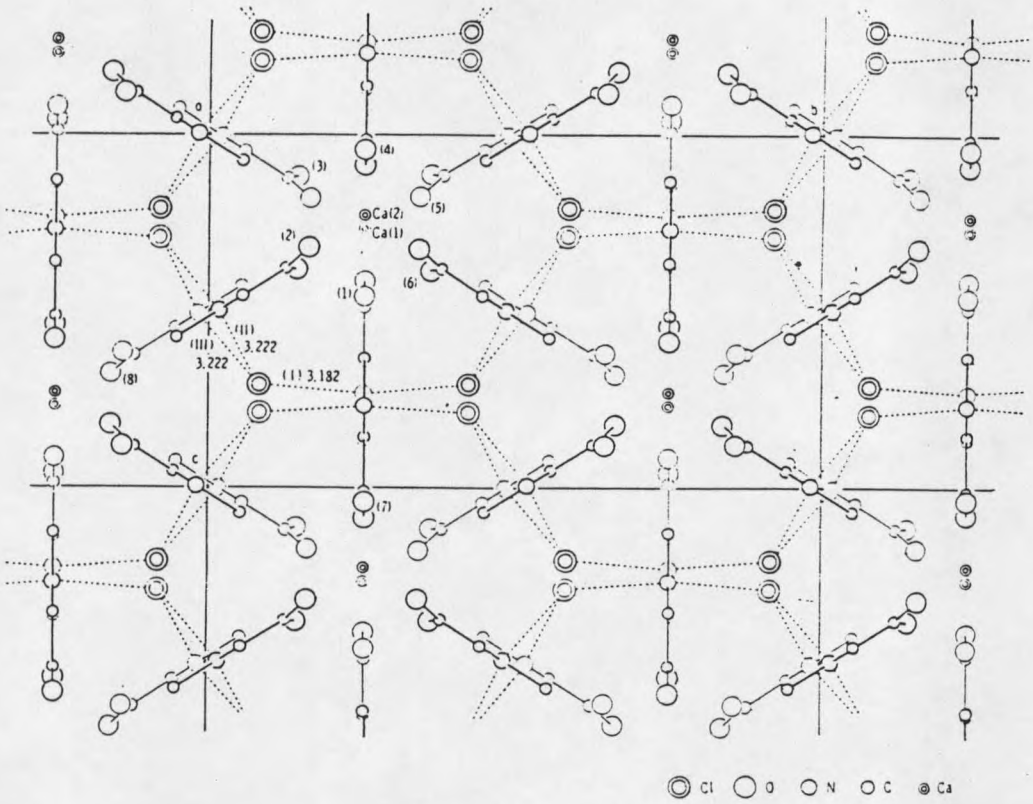

Fig. 28. The structure of TSCC viewed down its a axis

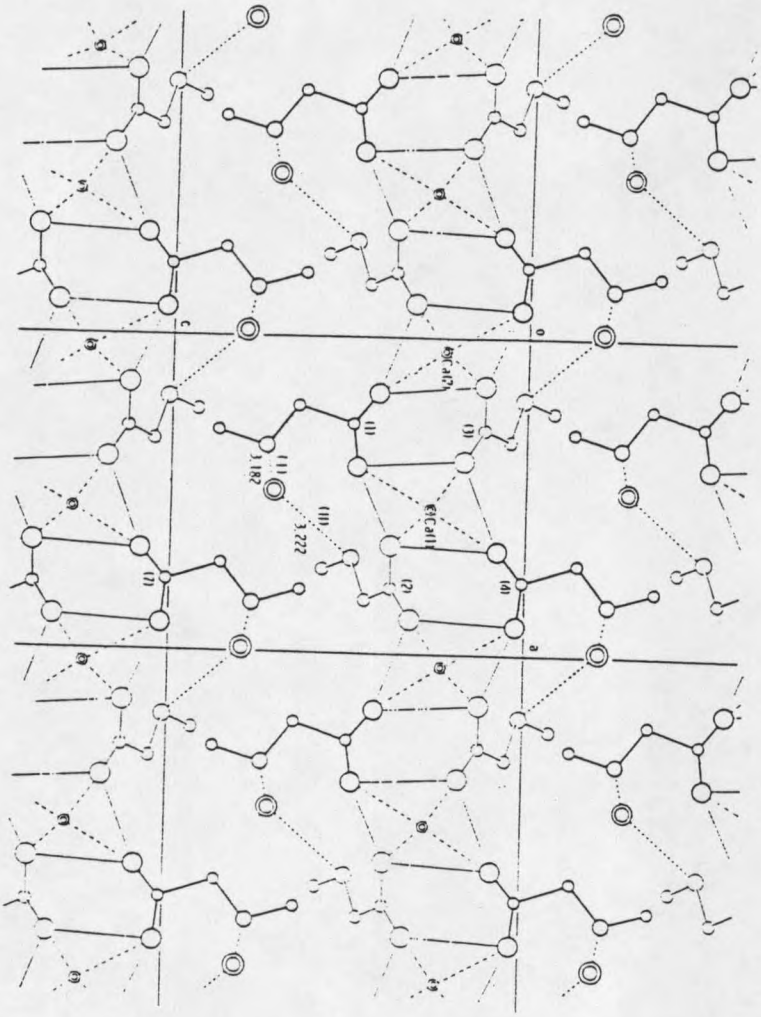

Fig. 29. Projection of half a unit cell of TSCC along its b axis

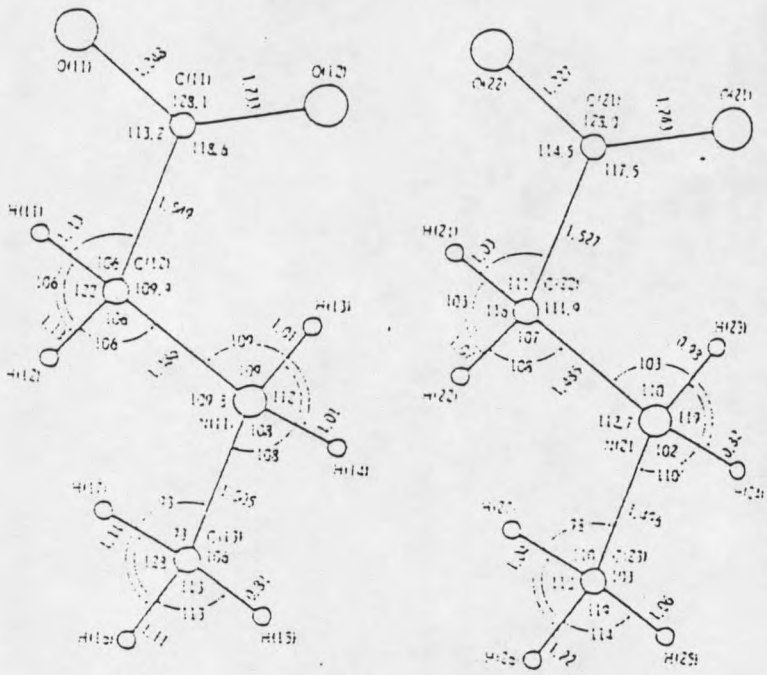

Fig.30. Bond distances and angles

the reflection planes perpendicular to the FE b axis are suppressed.

The Phase Transition Category

There are disputes concerning whether the FE transition of this crystal is of the order-disorder type or displacive type. From the structure of TSCC we can see there exist the two possible types of transition. In other words, the transition of this crystal can occur with the jumping motion of atoms, and/or with some internal displacement of atom groups such as methyl or carboxyl, because the sarcosine molecules in the TSCC crystal have the form

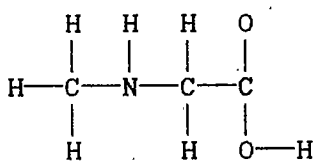

which may have permanent dipole moments formed by the NH^+ and COO^- group.

The nature of the phase transition has been unclear for many years.[29]

There is a lot of evidence for an order-disorder phase transition. Makita (1965) measured the dielectric constant and specific heat from 90 K to 160 K. His results such as the small value of the Curie-Weiss constant (58 K) observed in TSCC, and the small

spontaneous polarization Q_s obtained for a selected crystal of 0.27 $\mu C/cm^2$ suggest that the phase transition of TSCC is of the order-disorder type. A small anomaly of specific heat has observed by Makita (1965) and the difference of entropy δS=0.38 cal/mole·degree between the FE and PE phases, which is a small transition energy compared to the thermal energy, also suggest the transition is of the order-disorder type.

Lopez-Echarri and Tello (1981) claimed that low value of the transition temperature, and the confirmed existence of the zwitterion from IR spectra (Blinc et al 1970) seem to confirm the order-disorder type for this phase transition. This physical situation is somewhat similar to that in TGS.[30] The small microwave dielectric constant also suggests that the phase transition is of the order-disorder type.[28] Deguchi et al. show the dielectric dispersion in TSCC is the relaxation type in the Curie temperature region which may be indicative of an order-disorder transition, a view also presented by Windsch on the basis of Mn^{2+} EPR studies.[31]

On the other hand, there are some studies which suggest the phase transition is displacive. Recent light scattering studies[32,33] have shown softening of the optical phonon in the ferroelectric phase. The soft mode remains underdamped up to about ten degrees below T_c and

its frequency decreases with increasing temperature in the temperature range 50 K≥(T_c-T)≥20 K. It turns out, therefore, that both critical slowing-down of the polarization relaxation and softening of the optical phonon are observed in the phase transition in TSCC. They may be indicative of order-disorder and displacive transition, respectively.

Soft modes were assumed as a general feature of structural phase transitions. However, one must distinguish between oscillatory and diffusive soft modes which may be indicative of displacive and order-disorder transitions, respectively. Prokhorova et al. observed an oscillatory soft mode instead of a diffusive one which was expected beforehand.[32] The behavior of the soft A_1(LO) and A_1(TO) modes suggests that this phase transition occurs with doubling of the unit cell and therefore can be considered as an improper type transition. The Brillouin result[32] is also indicative of the improper character of the phase transition. In conclusion, Prokhorova et al. mentioned that if the phase transition in TSCC is really of the order-disorder type, at least the displacive processes play a significant role.

Some publications[33,34] indicate that the squared frequency of the soft mode Ω_{T0} varies considerable from liquid He temperature establishing a definite displacive

character to the transition.

The transition temperature of deuterated TSCC(DTSCC) was found by Fujimoto et al.[35] to be 131.3 K. This is practically the same as that of TSCC. Furthermore, it was found that the dynamic dielectric properties of DTSCC are very similar to those of TSCC, and there is no quantitative difference within the experimental accuracy. Accordingly, it seems that the claimed [31,36] jumping motion of protons within N-H...Cl bonds does not exist. The highly asymmetric nature of these bonds makes such intrabond jumping unlikely in any case.

Early nuclear quadrupole resonance (NQR) studies[37,38] showed clearly that the N-H...Cl bond length changed slowly and continuously with temperature as T_c was approached, a result clearly demonstrating displacive character, not order-disorder.

A variety of new measurements have been made, including both specific heat[39] and dielectric studies.[5] Both of these studies show the presence of logarithmic correction terms to the otherwise mean-field behavior near T_c and both indicate that the transition is second order (continuous).

Kozlov et al.[29] claimed that they have answered the primary questions about the ferroelectric transition in TSCC. They have observed the soft underdamped optical

mode in the paraelectric phase by means of millimeter wavelength spectroscopy. They have confirmed the mean-field behavior reported first by Levstik et al..[40] They have obtained an analysis of the soft TO and LO modes. Their results seem to show that the second soft mode in the ferroelectric phase reported by Chen and Schaack (at 23 cm^{-1} at 4 K) is not confirmed,[33] and also show that the suggestion[41] that TSCC has two closely spaced transitions is not verified and that the suggestion that its transition is improper is also not substantiated.

The observation by Sandvold and Courtens of logarithmic behavior of dielectric susceptibility and spontaneous polarization over a temperature range as wide as 50 K indicates that there are dipole-dipole interactions in TSCC in agreement with the report on the specific heat. It might thus turn out that TSCC is the best current example of uniaxial dipolar behavior in a ferroelectric. Another interesting property of this crystal is that the TO and LO phonons soften at the same temperature,[29] which indicates that the short-range force and Coulomb force participate in the phase transition almost equally.[34]

There is an important type of SPT in which both "spin" type variables and phonon type variables are present, and due to strong coupling between them, the condensation of phonons is "triggered by the ordering of the spins", or

vice versa. We may classify this case as a pseudospin - phonon coupled system. There are various kinds of pseudospin systems which are linearly coupled to the phonon system. From the discussion above we might conclude that the phase transition in TSCC belongs to pseudospin-phonon coupled system. The appearance of these soft modes in TSCC is in fact unique and different in several respects from the usual appearance of a soft optical phonon mode triggering a displacive SPT.

Chen and Schaack[6] present some calculations based on a model of an OD-SPT, where the order parameter (pseudospin) couples to optical phonons.

The starting point in the Chen and Schaack argument is the assumption that the deformations of the sarcosine molecules due to the soft phonon and due to the relaxational reorientation process are essentially the same. The soft mode performs a small quasi-harmonic modulation of the normal coordinate Q_s around one of the two stable values $Q_{s,0}$ (shown in Fig. 31) of the double-well potential-perhaps a twisting motion of the molecule with a maximum amplitude at the NH_2 group or a bending or librational motion of the whole molecule, while the reorientational motion may be interpreted as a stochastic switching of this group between the mirror-like positions $\pm Q_{s,0}$ (pseudo-spin $\sigma=\pm 1$) deforming the molecule according

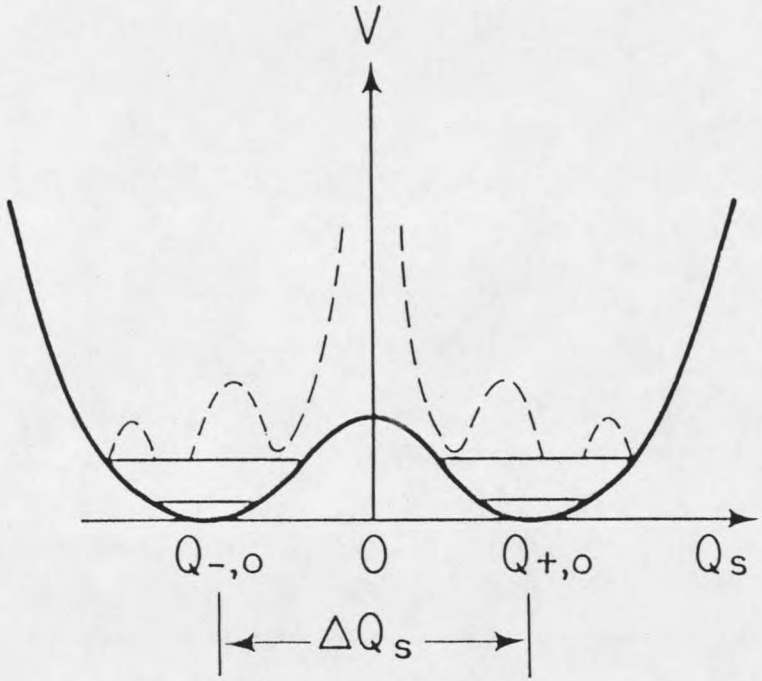

Fig. 31. Psuedo-spin-phonon-coupling model

to the same eigenvector but on a microscopic scale. In this case there is a strong interaction between the Q_s and the pseudo-spin σ. The interaction energy will enter the Hamiltonian of the system in the most simple approximation in bilinear form $H_{int}=g\sigma Q_s$.[33]

Yamada et al.[24] assumed that the TSCC crystal contains a molecular group which can take on two orientations in the local anisotropic potential. It commonly happens that the orientational ordering of the molecular group is accompanied by small atomic displacement. One can introduce an Ising variable to specify the possible configurations of the molecular groups. Therefore this case also belongs to the category of pseudo-spin-phonon coupled systems. Yamada et al. are not only concerned with the displacement-displacement correlation function, but also with spin-spin and spin-displacement correlation function. The temperature dependence of the spectra was obtained.

Chen and Schaack use this model, i.e. the pseudo-spin-phonon coupled system, to interprete the soft modes in TSCC. That seems to clear up the dispute concerning whether the FE transition of this crystal is OD type or displacive type.

Interpretation of Anomalies of Sound Velocity and Attenuation

1. The Relation Between the Sound Velocity and the Stiffness Constants

In the Brillouin scattering experiment, we study the sound velocity and attenuation by measuring the phonon frequency and use the formula

$$\delta\nu = (n v_s \nu / c) \sin(\theta/2)$$

$$= v_s k, \qquad \text{(V-1)}$$

where k is the sound wavevector and v_s is the sound velocity.

From the equations of motion, we obtain

$$v_s = \sqrt{C_s/\rho}, \qquad \text{(V-2)}$$

where v_s is the sound velocity of that mode and C_s is the stiffness constant of that mode.

If we take damping into account, the relation (V-2) will still be valid, except v_s and C_s will be complex numbers.

We rewrite (V-2) as

$$1/v_s^* = \sqrt{\rho/C_s^*} \qquad \text{(V-2')}$$

where v_s^* is complex sound velocity and C_s^* is complex

stiffness constant.

We have the plane wave

$$x = x_0 e^{i(\Omega_s t - kx)}$$

$$= x_0 e^{i\Omega(t - x/v_s + i\alpha_s x/\Omega_s)}$$

$$= x_0 e^{i\Omega[t - x(1/v_s - i\alpha_s/\Omega_s)]} \quad \text{------} \quad (V\text{-}3)$$

Then

$$1/v^* = 1/v_s - i\alpha_s/\Omega_s \quad \text{----------} \quad (V\text{-}4)$$

Substituting (V-4) into (V-2'), we obtain

$$1/v_s - i\alpha_s/\Omega_s = \sqrt{\rho/(C_s + C_{si})} \quad \text{---------} \quad (V\text{-}2'')$$

Where

$$C_s = \mathrm{Re}C^*,$$

$$C_{si} = \mathrm{Im}C^*$$

In the limit of low attenuation ($\mathrm{Im}C^* \ll \mathrm{Re}C^*$) we get the approximate expression:

$$v_s = (\mathrm{Re}C^*/\rho)^{1/2} \quad \text{----------} \quad (V\text{-}5)$$

$$\alpha_s = \Omega^2/(2\ v_s^3)\,\mathrm{Im}C^* \quad \text{----------} \quad (V\text{-}6)$$

2. Coupling Between Strain and Order Parameter

The order parameter characterizes the amount of change taking place during the transition. Normally it is

defined on an atomic scale, although in many cases macroscopic quantities are measurable that are directly proportional to the microscopic order parameter.[42]

The phenomenological Landau-Devonshire theory of phase transitions starts from an expansion of the free-energy density in powers of the order parameter components Q^i, their spatial gradient, and the components ϵ_k of the strain tensor

$$F(Q_I, \epsilon_k, T) = F_0(T) + (1/2)a_2(T)f_2(Q_i) + (1/4)a_4 f_4(Q_i)$$
$$+ (1/6)a_6 f_6(Q_i) + \cdots\cdots + (1/2)b(\delta Q)^2$$
$$+ \cdots\cdots + F_m(\epsilon_k) + F_c(Q_i, \epsilon_k) \qquad (V\text{-}7)$$

In this equation the f_n denote the nth-order invariants of the components of the order parameter, that are homogeneous functions of degree n in the components Q_i, which remain unchanged under all possible symmetric operations. The purely elastic contribution is denoted by F_m. All the coefficients are considered as weakly temperature dependent with the exception of a_2 which goes through zero like $[\alpha(T-T_c)]$ at the temperature T. For a continous phase transition a_4 must be positive and the sixth order term is usually omitted. If a_4 is negative, a discontinous phase transition takes place and a positive sixth-order term must be included.

The coupling term F_c describes the interaction between the strain and the order parameter.[7,43] This term is responsible for the spontaneous strain appearing in connection with the ordering process, and it also describes the effect of an external strain upon the order parameter.

The elastic constants $C_{mn}=d^2F/d\epsilon_m d\epsilon_n$ are usually measured under the condition that the order parameter can change freely under the influence of strain, i.e. that its conjugate force $Z_k=dF/dQ_k$ remains zero even when Q_k is not 0. These elastic constants are denoted by $C_{mn}{}^k$.

The equation $dF/dQ_k=0$ determines the spontaneous polarization. The elastic constant for the purely elastic free energy F_m are those determined under the condition $Q_k=0$ (in paraelectric phase). These elastic constant are denoted by $C_{mn}{}^Q$.

The difference $C_{mn}{}^z-C_{mn}{}^Q$ is due to the change of the order parameter, driven by the strain, and its reacting stress. We have the equation

$$\delta C_{mn}=C_{mn}{}^Q-C_{mn}{}^z=\Sigma(d^2F_c/d\epsilon_m dQ_k)\,x_{KL}{}^\epsilon\, d^2F_c/d\epsilon_n dQ_l \qquad \text{(V-8)}$$

where

$$x_{kl}{}^\epsilon=(d^2F/dQ_k dQ_l)^{-1}. \qquad \text{(V-9)}$$

We are certainly more interested in the free coupling

energy density which is usually written in terms of increasing power of ϵ_i and Q_k

$$F_c(\epsilon_i, Q_k) = \beta_{ij} Q_i \epsilon_j + \Gamma_{ijk} Q_i Q_j \epsilon_k + \delta_{ijk} Q_i \epsilon_j \epsilon_k + \cdots\cdots$$

Which of the coefficients β, Γ, δ are different from zero is determined by the symmetry of the crystal. A coefficient in the expansion of F_c can exist only if the corresponding symmetric powers of Q_i and ϵ belong to the same irreducible representation. For example, Γ_{ijk} is not zero only when the symmetric square $[Q]^2$ and ϵ have an irreducible representation in common. Under this condition their product is invariant against all possible symmetry transformations, and the term can exist.

As usual, the lowest-order term is dominant. There are three simple cases which can explain the anomalies of the elastic constants and attenuations.

Case (a) Linear coupling $F_c = \beta Q \epsilon$ and a continuous transition ($a_4 > 0$, $a_6 = 0$)

$$\delta C_{mn} = (d^2 F_c / d\epsilon dQ)(d^2 F / dQ^2)^{-1} d^2 F_c / d\epsilon dQ$$

$$= \beta^2 x^{\epsilon} \quad \text{----------} \quad (V\text{-}10)$$

where

$$x^{\epsilon} = (d^2 F / dQ^2)^{-1}$$

(1) For static effect

$$x^{\epsilon}=1/[\alpha(T-T_c)] \qquad \text{(V-11)}$$

then

$$\delta C=\beta^2/[\alpha(T-T_c)] \qquad \text{for } T>T_c$$

$$=\beta^2/[\alpha(T_c-T)] \qquad \text{for } T<T_c \qquad \text{(V-12)}$$

This is the Curie-Weiss law shown in Fig. 32.

(2) For dynamic effect

In a simple way we can take the dynamic effect into account by using a frequency dependent susceptibility in Eq. (V-10). The imaginary part of the resulting complex elastic modulus indicates the attenuation. The order parameter has relaxational behavior, and we obtained the following formula:

$$x_{k1}^{\epsilon}(\Omega_s)=x_{k1}^{\epsilon}(0) \qquad \text{(V-13)}$$

and then

$$v_s^2(\Omega_s)=\mathrm{Re}C^*(Q)=C_s^Q-(C_s^Q-C_s^z)/[1+(\Omega_s\tau_\epsilon)^2] \qquad \text{(V-14)}$$

$$\alpha_s=\Omega_s\tau_\epsilon/(2\ v_s^3)\cdot(C_s^Q-C_s^z)/[1+(\Omega_s\tau_\epsilon)^2]$$

$$=\Omega_s\tau_\epsilon/2v_s^3\cdot[v_s^2(\infty)-v_s^2(0)]/[1+(\Omega_s\tau_\epsilon)^2] \qquad \text{(V-15)}$$

where

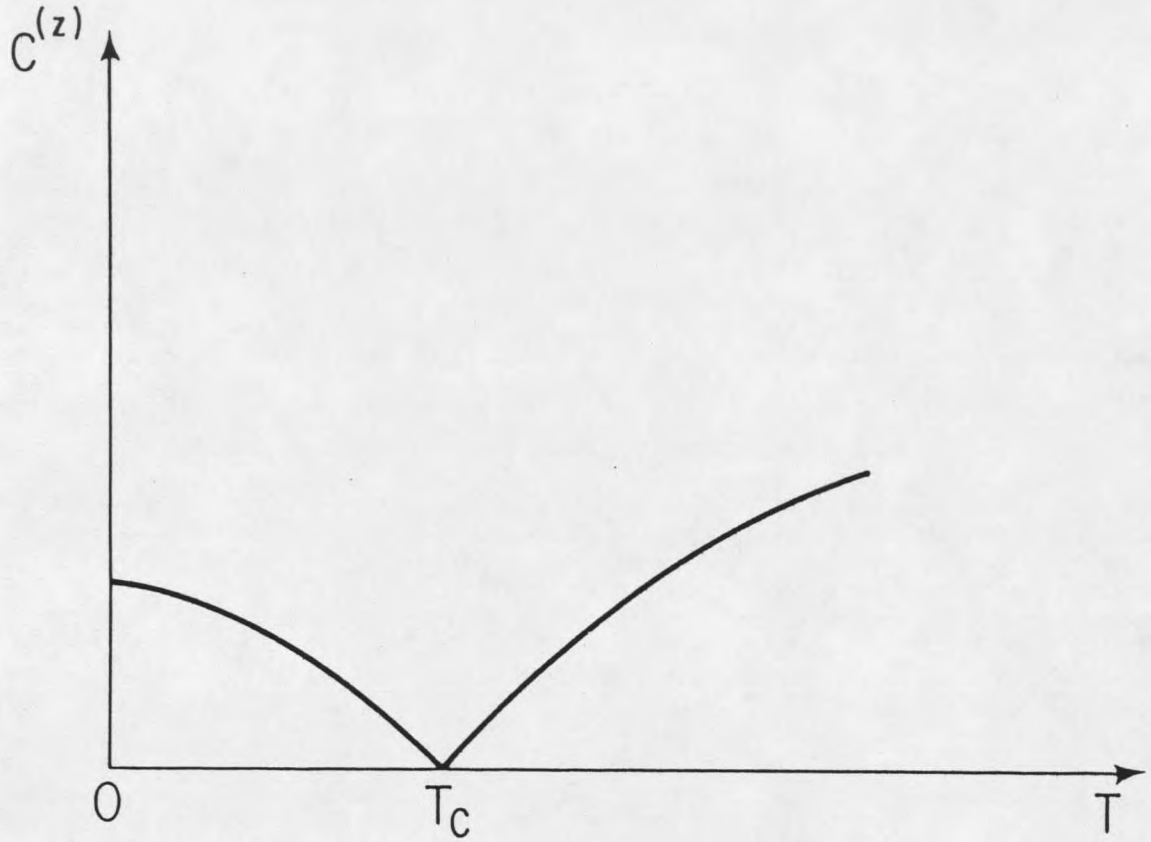

Fig.32. Temperature dependence of elastic constant for linear coupling and continuous transition

$$v_s^2(\infty)=C_s^Q$$

$$v_s^2(0)=C_s^z$$

Equation (V-14) shows that the elastic moduli C_s^Q and C_s^z are obtained in the limits $\Omega_s\tau_\epsilon \gg 1$ and $\Omega_s\tau^\epsilon \ll 1$. The relaxation time τ_ϵ is the characteristic time for the response of the order parameter to a sudden strain. It is connected to the static susceptibility through the kinetic coefficient L.[44]

$$\tau_\epsilon = x^\epsilon(0)/L \qquad \text{----------(V-16)}$$

The kinetic coefficient is assumed to be only weakly temperature dependent, so that the divergence of x^ϵ at the critical point includes a similar divergence of the relaxation time, the so-called critical slowing down.

(3) The dynamic-fluctuation damping effect

A different type of attenuation mechanism, well-known as the fluctuation interaction, comes into play, based on the classical fluctuation-dissipation theorem.

$$\mathrm{Im}C_{mn}(\Omega_s)=(\Omega_s V/2kT)\int \exp(i\Omega_s t)\langle\delta\sigma(t)\sigma_m^*(0)\rangle dt \qquad \text{----------(V-17)}$$

The imaginary part of the elastic modulus, i.e. the dissipative part of the elastic modulus, relates to the Fourier transform of the time-correlation function of

internal stress fluctuations $\delta\sigma$ in a volume V. By a Kramers-Kronig transformation we obtained for the variation of the real part of the elastic stiffness a static correlation function

$$\delta C_{mn}(\Omega_s) = C_{mn}(\infty) - C_{mn}(0) = [(2/\pi)\int \mathrm{Im}C_{mn}(\Omega_s)/\Omega_s]\,d\Omega_s$$

$$= (V/kT)\langle \delta\sigma_m \delta\sigma^*_n \rangle \quad \text{----------} \quad (V\text{-}18)$$

The stress fluctuation $\delta\sigma_m$ comprises a random force, induced by the internal parameters of the system. Mori and Tani[45,46] and Kawasaki[47] have given a rigorous derivation of equation (V-17) in terms of currents and projection operators.

In the case of a linear coupling we simply get

$$\delta\sigma_m = \beta_{im}\delta Q_i \quad \text{----------} \quad (V\text{-}19)$$

and

$$\mathrm{Im}C_{mn}(\Omega_s) = (\Omega_s V/2kT)\Sigma\beta_{im}\beta_{jn}\int \exp(i\Omega_s t)\langle \delta Q_i(t)\delta Q_j^*(0)\rangle dt$$

$$\text{----------} \quad (V\text{-}20)$$

We know that

$$\mathrm{Im}x_{ij}(\Omega_s) = (\Omega_s V/2kT)\int \exp(i\Omega_s t)\langle \delta Q_i(t)\Omega Q_j^*(0)\rangle dt$$

$$\text{----------} \quad (V\text{-}21)$$

so equation (V-20) can be written as

$$\mathrm{Im}C_{mn}(\Omega_s)=\Sigma\beta_{im}\beta_{jn}\mathrm{Im}x_{ij}(\Omega_s) \quad ---- \quad (V\text{-}22)$$

This is in fact an extension of equation (V-8) to imaginary values of C_{mn}.

Case (b) Coupling linear in the strain but quadratic in the order parameter and a continuous transition.

$$F_c=\Gamma Q^2\epsilon$$

Substituting $F_c=\Gamma Q\epsilon$ into Eq.(V-8) we obtained

$$\delta C=\Gamma^2 x^\epsilon \langle Q\rangle^2 \quad ---------- \quad (V\text{-}23)$$

(1) For static effect, at the temperature $T<T_c$ the static value of the order parameter

$$\langle Q\rangle^2 \propto (T_c-T) \quad ---------- \quad (V\text{-}24)$$

and the susceptibility

$$x^\epsilon \propto 1/(T_c-T) \quad ---------- \quad (V\text{-}25)$$

In the range of validity of the Landau theory the temperature variations of x^ϵ cancel those of $\langle Q\rangle^2$ and the elastic modulus shows a stop-like decrease by an amount

$$\delta C=\Gamma^2/2a_4 \quad ---------- \quad (V\text{-}26)$$

shown in Fig. 33.

In this type of interaction the elastic coefficients show a much weaker temperature dependence than Q and x.

(2) Fluctuation damping

In the case of a coupling quadratic in order parameter the stress fluctuations involve in general also the static order parameter

$$\delta\sigma_m = \Sigma\Gamma_{ijm}(\langle Q_i\rangle\delta Q_j + \langle Q_j\rangle\delta Q_i + \delta Q_i\delta Q_j) \qquad \text{(V-27)}$$

Substituting this into Eq.(V-17) we obtain

$$\begin{aligned} \mathrm{Im}C_{mn}(\Omega_s) = (\Omega_s V/2kT)\Sigma\Gamma_{ijm}\Gamma_{kln}[\,4\langle Q_i\rangle\langle Q_k\rangle \\ \cdot\int \exp(i\Omega_s t)\langle\delta Q_j(t)\delta Q_l^*(0)\rangle dt \\ +\int \exp(i\Omega_s t)\langle\delta Q_i(t)\delta Q_j(t)\delta Q_k^*(0)\delta Q_l^*(0)\,dt] \end{aligned}$$

---------- (V-28)

The first term of Eq.(V-28) is the Landau-Khalatnikov contribution, i.e. the piezoelectric coupling and the second term is a fourpoint correlation function describing the fluctuation interaction, i.e. the electrostrictive coupling.

One can expect two large anomalies in a Brillouin scattering study. First, we can expect large anomalies in the velocity and attenuation of longitudinal phonons propagating along directions perpendicular to the polar

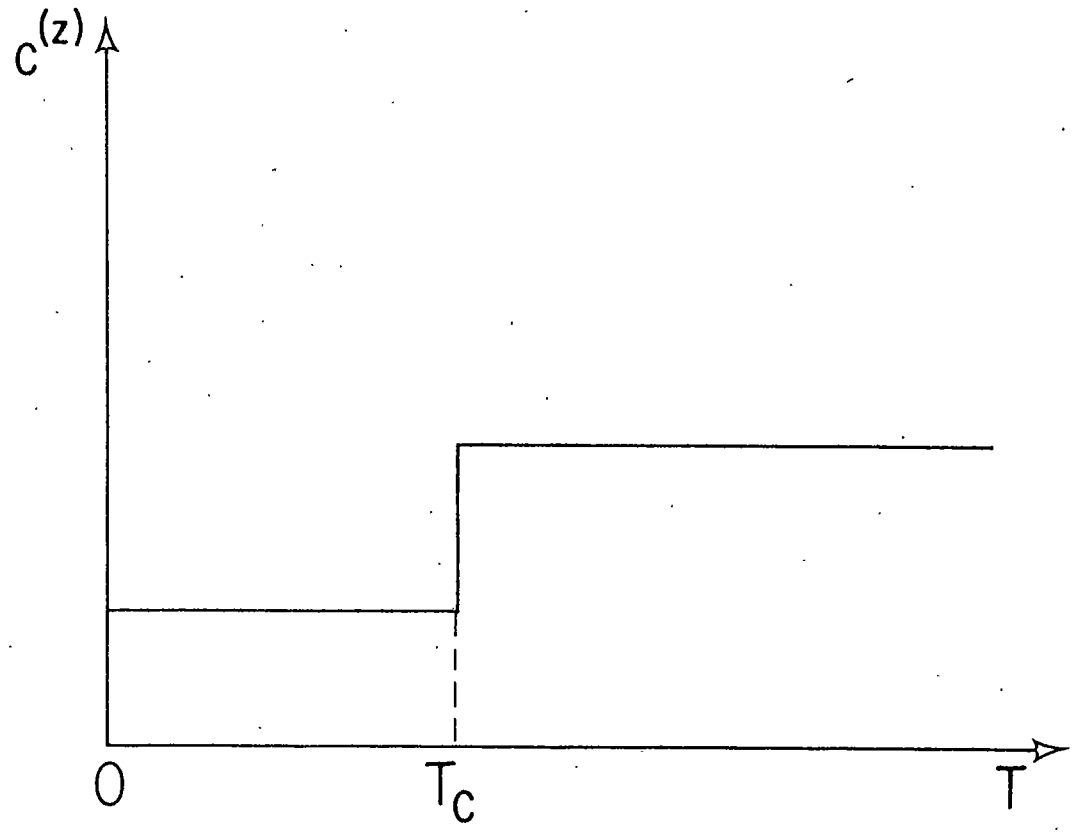

Fig. 33. Temperature dependence of elastic constant for coupling linear in the strain but quadratic in order parameter

axis.[48] These anomalies are caused by piezoelectric coupling in the FE phase, as we can see from Eq. (V-28). This coupling exists only if $\langle Q \rangle$ is not zero. Because TSCC in the PE phase is centrosymmetric and hence not piezoelectric, this coupling is not intrinsic but rather is induced by the spontaneous polarization. Second, Sorge and Straube observed that at 20 MHz the longitudinal ultrasonic wave propagating along the polar axis b also shows large anomalies of attenuation and velocity near T_c. Because of the depolarization effect in a system with electric dipole-dipole interactions such as the dipole-dipole interaction along the b axis in TSCC, these anomalies are expected to occur not from piezoelectric coupling but from electrostrictive coupling.

Phenomenologically we can write the free energy F as

$$F=(1/2)(x^{s}_{22})^{-1}Q_2^{2}+(1/4)a_4Q_2^{4}+(1/2)g_{322}\epsilon_3Q_2^{2}$$

$$+(1/2)C_{33}^{Q}\epsilon_3^{2} \quad \text{----------} \quad (V\text{-}29)$$

for phonons propagating along a direction perpendicular to the polar axis b in the paraelectric phase. Here x_{22}^{s}, C_{33}^{Q} and g_{32} are the dielectric susceptibility at constant strain, the elastic stiffness constant at constant polarization and the electrostrictive constant respectively, and a_4 is the coefficient of the fourth

order term in the Landau expansion. The acoustic wave propagating within the medium changes the distance between the dipoles which in turn induces internal energy fluctuations.[49,50] The anomalies of v and α are attributed to static and dynamic behavior of energy fluctuations.

In the ferroelectric phase, static spontaneous polarization appears and the fluctuation polarization induced by the sound wave is the deviation δQ_2 from Q_0, i.e.

$$Q_2 = Q_0 + \delta Q_2 \qquad \text{(V-30)}$$

and the oscillating strain is also the deviation from the spontaneous strain, i.e.

$$\epsilon_3 = \epsilon_{30} + \delta\epsilon_3 \qquad \text{(V-31)}$$

Substituting (V-30),(V-31), into (V-29) we obtain

$$F = (1/2)(x_{22}^{s})^{-1}(Q_0+\delta Q_2)^2 + (1/4)a_4(Q_0+\delta Q_{20}{}^4$$
$$+(1/2)g_{322}(\epsilon_0+\delta\epsilon_3)(Q_0+\delta Q_2)^2$$
$$+(1/2)C_{33}{}^{Q}(\epsilon_0+\delta\epsilon_3)^2 \qquad \text{(V-32)}$$

and

$$\delta F = [(1/2)(x_2{}^{s})^{-1} + a_4 Q_0{}^2]\delta Q_2{}^2 + (1/2)C_{33}{}^{Q}\delta\epsilon_3{}^2$$
$$+(1/2)g_{322}\delta\epsilon_3\delta Q_2{}^2 + g_{322}Q_0\delta\epsilon_3\delta Q_2 \qquad \text{(V-33)}$$

The terms $(1/2)g_{322}\delta\epsilon_3\delta Q_2^2$ and $g_{322}Q_0\delta\epsilon_3\delta Q_2$ are coupling terms in the energy fluctuation. The crystal has an electrostrictive intrinsic coupling term in the free energy F. There is also an intrinsic electrostrictive coupling term $(1/2)g_{322}\delta\epsilon_3\delta Q_2^2$ in the energy fluctuation. But there is additionally an induced piezoelectric coupling term which is not intrinsic in the energy fluctuation. Obviously, if $Q_0=0$ the piezoelectric coupling term does not exist. If there is an external electrical field, the energy fluctuation (V-33) becomes

$$\delta F=[(1/2)(x_{22}^{s})^{-1}+a_4Q_0^2]\delta Q_2^2+(1/4)a_4\delta Q_2^4$$

$$+(1/2)C_{33}^{Q}\delta\epsilon_3^2+(1/2)g_{322}\delta\epsilon_3\delta Q_2^2$$

$$+(1/2)g_{322}Q_0\delta\epsilon_3\delta Q_2-E\cdot\delta Q_2 \quad \text{----------} \quad (V\text{-}33')$$

From Eq.(V-29) we can see that there are two variables Q_0 and ϵ_{30} in the expression of the free energy. In an equilibrium system free energy should be minimum, so that

$$dF/dQ_0=0 \quad \text{----------} \quad (V\text{-}34)$$

$$dF/d\epsilon_{30}=0 \quad \text{----------} \quad (V\text{-}35)$$

Solving these equations, we obtain

$$Q_0^2=(a_4x_{22}^{s})^{-1}(B_{33}/C_{33}^{Q}-1)^{-1}$$

where

$$B_{33}=g_{322}^2/2a_4$$

Substituting Eq.(V-36) into Eq.(V-33) we have

$$\delta F=(1/2)(x_{22}^{fs})^{-1}\delta Q_2^2+(1/4)a_4\delta Q_2^4+(1/2)C_{33}^{Q}\epsilon_3^2+$$

$$+(1/2)g_{322}\delta\epsilon_3\delta Q_2^2+g_{322}Q_0\delta\epsilon_3\delta Q_2-E\cdot\delta Q_2 \qquad (V-37)$$

where x_{22}^{fs} is the static dielectric susceptibility for the fluctuation. It has the relation

$$x_{22}^{fs}=x_{22}^{s}(B_{33}/C_{33}^{Q}-1)/(B_{33}/C_{33}^{Q}+1) \quad - \quad (V-38)$$

From (V-37) we find that when the electric field E is set equal to zero, the sound wave $\delta\epsilon_3$ acts as an oscillating electric field $-a_{23}\delta\epsilon_3$, where $a_{23}=Q_0 g_{322}$.

Without considering the sound wavevector dependence, the retarded reponse of δQ_2 is described by a complex dielectric susceptibility $x_{22}^*(\Omega)$ when an oscillating electric field is applied. The induced retarded polarization acts as the retarded stress - $x_{22}^*(\Omega)a_{23}^2\delta\epsilon_3(K,\Omega)$. The complex elastic stiffness has the form

$$C_{33}^*(\Omega)=C_{33}^{Q}-a_{23}^2x_{22}^*(\Omega) \quad --------- \quad (V-39)$$

The complex susceptibility has the relation

$$x_{22}^*(\Omega)=x_{22}^{fs}(1+i\Omega\tau^*)^{-1} \quad ---------- \quad (V-40)$$

with the static susceptibility, where τ^*, the polarization relaxation time given in terms of a noninteracting susceptibility $x_0/N=\mu^2/k_BT$ and the relaxation time τ_0 of a noninteracting dipole, is

$$\tau^*=\tau_0(x_{22}^{fs}/x_0) \quad \text{----------} \quad (V\text{-}41)$$

Assuming a Curie-Weiss law for x_{22}^s, the critical slowing down is expressed in terms of the reduced temperature defined by $t=(T_c-T)/T_c$ as

$$\tau^*=\tau_0(1-B_{33}/C_{33}^Q)/2t(1+B_{33}/C_{33}^Q) \quad (V\text{-}42)$$

Owing to the piezoelectric coupling, it is convenient in the following to define the relaxation time of a non-interacting dipole below T_c as

$$\tau_0^f=\tau_0(1-B_{33}/C_{33}^Q)/(1+B_{33}/C_{33}^Q) \quad \text{----} \quad (V\text{-}43)$$

Then finally we get the complex elastic stiffness

$$C_{33}^*(\Omega)=C_{33}^Q-B_{33}\cdot(1+i\Omega\tau_0^f t^{-1}/2)^{-1} \quad \text{--} \quad (V\text{-}44)$$

where $B_{33}=2B_{33}/(1+B_{33}/C_{33}^Q)$.

Thus

$$C_{33}^*(\Omega)=C_{33}^Q-B_{33}/[1+(\Omega\tau_0^f/2)^2t^{-2}$$

$$+iB_{33}\Omega\tau_0^f t^{-1}/[2(1+(\Omega\tau_0^f/2)^2t^{-2})]$$

$$\text{----------} \quad (V\text{-}45)$$

and

$$\rho v_s^2 = \mathrm{Re}C^* = C_{33}^Q - B_{33}/[1+(\Omega\tau_0^f/2)^2 t^{-2}] \quad --- \quad (V\text{-}46)$$

$$\alpha/\Omega = B_{33}/(\rho v_s^3)\cdot\tau_0^f t^{-1}\Omega/[1+(\Omega\tau_0^f/2)^2 t^{-2}]$$

$$---------- \quad (V\text{-}47)$$

or

$$v_s^2 = v_\infty^2 - (v_\infty^2 - v_0^2)/[1+(\Omega\tau_0^f/2)^2 t^{-2}] \quad -- \quad (V\text{-}48)$$

$$\alpha/\Omega = [(v_\infty^2 - v_0^2)/v_s^3]\cdot\tau_0^f t^{-1}\Omega/[1+(\Omega\tau_0^f/2)^2 t^{-2}]$$

$$---------- \quad (V\text{-}49)$$

where $v_\infty = (C_{33}^Q/\rho)^{1/2}$ is the sound velocity of an infinite frequency sound wave, and $v_0 = (C_{33}^Q/\rho - B_{33}/\rho)^{1/2}$ is the sound velocity of a zero frequency sound wave.

As we have mentioned, equations (V-48) and (V-49) result from the piezoelectric coupling term which exists only when Q_0 is not zero, so that these equations are only valid below the transition temperature T_c. Equations (V-48) and (V-49) can interpret the anomalies of sound velocity and attenuation for the phonons propagating along the direction perpendicular to the polar axis in TSCC.

(1) Suppose there exists only the piezoelectric coupling term and v_∞, v_0 depend weakly on temperature below T_c, whereas above T_c there is no coupling term. Then the sound velocity will have a sudden step up to the maximum v_∞ near T_c with increasing temperature, as seen in

Fig. 16. Below but near T_c the sound velocity changes rapidly, while above but near T_c there is a slow rounding. This behavior has to be explained by something else. Both above and below T_c the sound velocities still show temperature dependence which may be interpreted by temperature dependence of elastic stiffness constants. The dips just below T_c in the plots of sound velocity may be interpreted by the coupling between the modes.

(2) According to equations (V-48) and (V-49), the attenuation coefficient α is zero at T_c and becomes a maximum somewhat below T_c. A similar shift of maximum from T_c is observed in the antiferromagnets $RbMnF_3$[49] and MnF_2.[49,50,51] In ferroelectric TGS and TGSe this shift appears also.[21,52,53]

There is a relation between the phonon decay rate Γ or the phonon line width Γ/π and the attenuation coefficient α given by

$$\Gamma/\pi=\alpha v_s/\pi \qquad \text{(V-50)}$$

From Eqs. (V-48) and (V-49) along with (V-50), the temperature dependence of the line width is

$$\Gamma/\pi=(\Omega^2/2\pi)\cdot(B_{33}/2)(\tau_0{}^f t)/\{(C_{33}{}^Q-B_{33})t^2 + C_{33}{}^Q(\Omega\tau_0{}^f/2)^2\} \qquad \text{(V-51)}$$

The line width becomes maximum at

$$t_m=(T_c-T_m)/T_c=[C_{33}^{Q}/(C_{33}^{Q}-B_{33})]^{1/2}(\tau_0{}^f\Omega/2)$$

$$=(v_w/v_0)(\tau_0{}^f\Omega/2) \quad \text{----------} \quad (V\text{-}52)$$

The ratio v_w/v_0 is estimated to be nearly equal to unity. Hence, Eq.(V-52) becomes

$$t_m=\tau_0{}^f\Omega/2 \quad \text{----------} \quad (V\text{-}53)$$

From Figs.22-24 we see the shift of the maximum from T_c.

For phonons propagating along [001] observed by small angle scattering, we find

$$T_c-T_m=0.072\ K$$

and

$$\Omega=1.05*10^{10}\ sec^{-1}$$

Substituting Ω, $T_c-T_m=0.072$ K and $T_c=130$ K into Equation (V-53), we obtain

$$\tau_0{}^f/2=5.25*10^{-14}\ sec$$

This agree quite well with the result $2.7*10^{-13}$ sec obtained by Hikita et al.[21] from right angle scattering. The exact measurement of t_m is a new method to estimate the relaxation time and is the only method available to

obtain the relaxation time of the order parameter in antiferroelectric molecular crystals. The higher the frequency of the sound wave, the larger the temperature deviation. Brillouin experiments are convenient for this purpose because of their higher sound frequency. Even the different angle Brillouin scatterings show very obvious evidence of this relation stated above. The relation between the temperature shift t_m and the sound wave frequency is shown in the following table

Ω (GHz)	$T_c - T_m$ (K)
$2\pi*1.68$	0.072
$2\pi*21.48$	0.776
$2\pi*32.35$	0.786

From this table we see that t_m increases with increasing sound wave frequency as shown in Fig. 34. From small angle scattering to right angle scattering the temperature shift of t_m increases almost proportionally to the frequency.

The shift of the maximum from T_c guarantees that the anomalies of sound velocity and attenuation for the phonons propagating along [001] is caused by piezoelectric coupling induced by spontaneous polarization below T_c.

For phonons propagating along [010], the polar axis, the anomalies of the sound velocity are quite different.

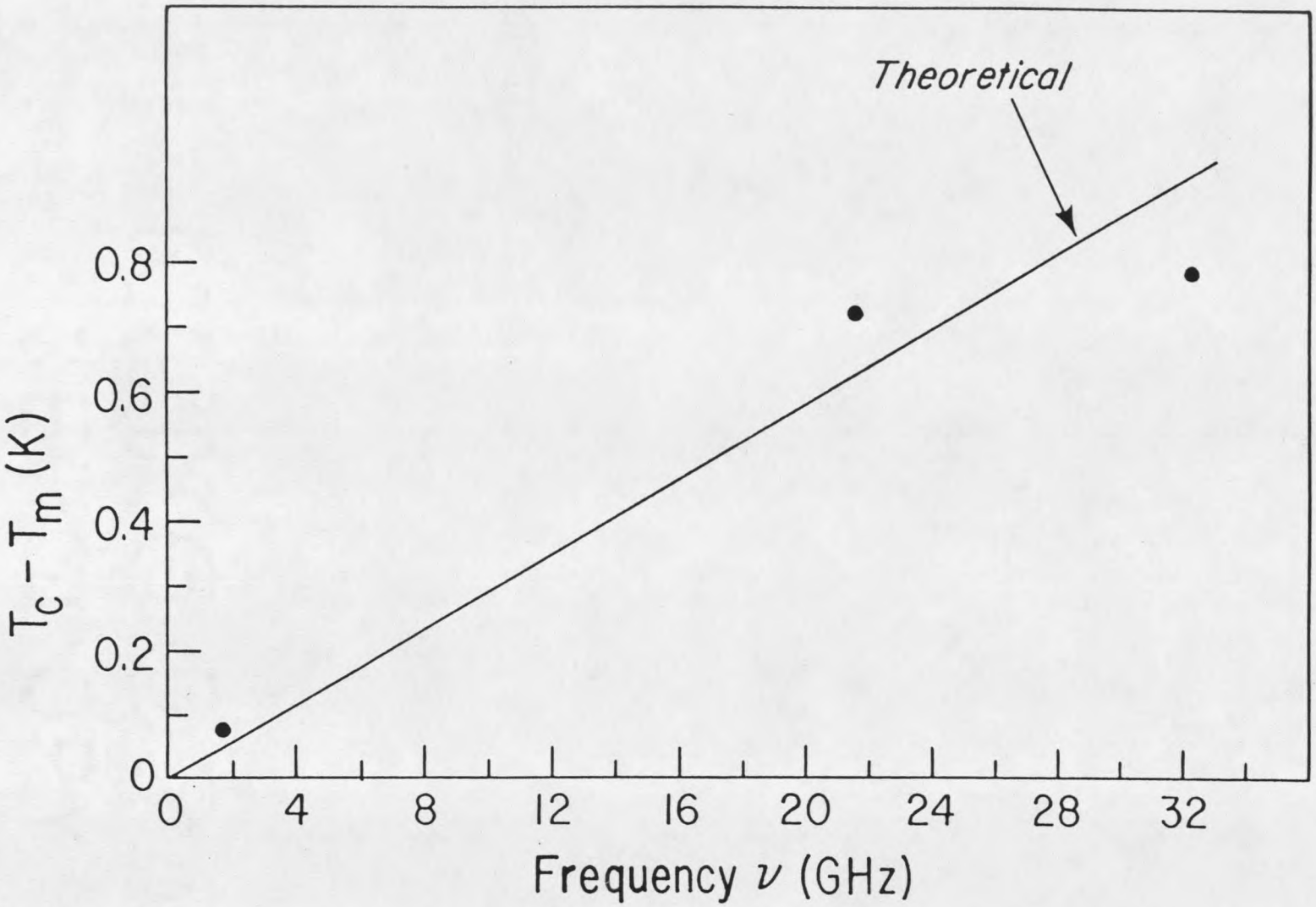

Fig.34. Relation of T_c-T_m vs. frequency for (001) phonons

These phonons induce polarization waves with the same wavevector through the piezoelectric coupling. As stated above, this K-dependent strain wave acts as an oscillating K-dependent electric field for the polarization.[54,55] When the wave vector of the polarization wave is parallel to the polar axis, a depolarization field

$$E_2 = -4\pi Q_2$$

appears. In general, this field is given by the expression

$$E_2(\bar{K}) = -L(K_2/K)^2 Q_2(\bar{K}) \qquad \text{----------} \qquad (V\text{-}53)$$

Taking this term into account in the free energy without strain, we have

$$F = (1/2)\{(x_{22}^s)^{-1} + L(K_2/K)^2\}|Q_2|^2 + (1/4)a_4|Q_2|^4 \qquad \text{----------} \qquad (V\text{-}54)$$

Namely, the K-dependent static susceptibility x_{22}^s is altered to

$$[x_{22}(\bar{K})]^{-1} = (x_{22})^{-1} + L(K_2/K)^2 \qquad \text{-------} \qquad (V\text{-}55)$$

The dielectric susceptibility is proportional to the mean square of the polarization fluctuation. Including the case of the finite $\bar{K}$ value, we can derive the generalized susceptibility for the long wavelength

fluctuation in the form

$$x_{22}(\bar{K}) = \langle |Q|^2 \rangle / k_B T$$

$$= \{ (x_{22}^s)^{-1} + L(K_2/K)^2 + \Gamma K^2 \}^{-1} \qquad \text{(V-56)}$$

where L is used to express a generalized Lorentz field from the microscopic point of view. Γ denotes the effect of the spatial fluctuation in the free energy.

The expression (V-56) is a new static susceptibility in equation (V-38). Using this expression, we can easily derive the complex dielectric susceptibility and then, the complex elastic stiffness constant.

For the transverse sound wave $\epsilon_3(K_2, \Omega)$ we can get the dependence of $x_{22}(K)$ through that of $C_{22}(K, \Omega)$ only by substituting equation (V-56) instead of x_{22}^{sf} into Eqs.(V-38)-(V-46). In our experiments, the phonons propagating along the polar direction are longitudinal and the elastic stiffness constant is given by

$$C_{22}^*(K_2, \Omega) = C_2^Q - a_{22} x_{22}^*(K_2, \Omega) \qquad \text{(V-57)}$$

and

$$x_{22}^{sf} = [(-1/2)(x_{22}^s)^{-1} - LK_2^2]^{-1}(1 - B_{22}/C_{22}^Q) \qquad \text{(V-58)}$$

$$\tau^* = \tau_0 [(-1/2)(x_{22}^s)^{-1} - LK_2^2]^{-1}(1 - B_{22}/C_{22}^Q) \qquad \text{(V-59)}$$

Substituting Eqs.(V-58, 59) into (V-40), we obtain

$$x_{22}^{*}=[(-1/2)(t+\alpha)]^{-1}(1-B_{22}/C_{22}^{Q})$$

$$\cdot\{1-i\Omega\tau_0^{f}[t+\alpha(K_2)]^{-1}\} \quad \text{---------} \quad (V\text{-}60)$$

where α is a function of K_2 and

$$\tau_0^{f}=(1/2)\tau_0(1-B_{22}/C_{22}^{Q})$$

Substituting Eq.(V-60) into (V-57), we have the following expression for the complex stiffness C_{22}^{*},

$$C_{22}^{*}(K_2,\Omega)=C_{22}^{Q}-B_{22}t/[t+\alpha(K_2)]$$

$$\cdot 1/\{1-(i\Omega\tau_0^{f}/2)[t+\alpha(K_2)]^{-1}\} \quad (V\text{-}61)$$

From (V-61) we have

$$\mathrm{Re}C_{22}^{*}(K_2,\Omega)=C_{22}^{Q}-B_{22}t/[t+\alpha(K_2)]$$

$$\cdot 1/\{1+(\Omega\tau_0^{f}/2)^2(t+\alpha)^{-2}\} \quad \text{--} \quad (V\text{-}62)$$

$$\mathrm{Im}C_{22}^{*}(K_2,\Omega)=-B_{22}t/(t+\alpha)$$

$$\cdot(\Omega\tau_0^{f}/2)(t+\alpha)^{-1}/[1+(\Omega\tau_0^{f}/2)^2(t+\alpha)^{-2}]$$

$$\text{----------} \quad (V\text{-}63)$$

and

$$\rho v_s^{2}=C_{22}^{Q}-B_{22}t/\{(t+\alpha)[1+(\Omega\tau_0^{f}/2)^2(t+\alpha)^{-2}]\}$$

$$\text{----------} \quad (V\text{-}64)$$

$$\Gamma/\pi=\alpha v_s/\pi$$

$$=-B_{22}t\Omega^2\tau_0{}^f/\{\rho v_s{}^2\pi(t+\alpha)^2[1+(\Omega\tau_{0f}/2)^2(t+\alpha)^{-2}\} \qquad \text{(V-65)}$$

From Equation (V-64) we can define $T_k=\alpha T_c$. And then when $T\to T_k$, $(t-\alpha)\to 0$, so that

$$v_s\to v_w \text{ with } [1/(t+\alpha)]\to 0$$

Comparing Equation (V-48) where

$$v_s{}^2=v_w{}^2-(v_w{}^2-v_0{}^2)/[1+(\Omega\tau_0{}^f/2)^2t^{-2}]$$

when $T\to T_c$, $t\to 0$, so that

$$v_s\to v_w \text{ with } (1/t^{-2})\to 0$$

We found that in the first case v_s approaches v_w slower than in the second case that we see in Figs. 13-18. Formulas (V-64) and (V-65) qualitatively well describe the anomalies of sound velocity and attenuation for phonons propagating along [010], if α is small. Because

$$t+\alpha=[(T_c+T_k)-T]/T_c \qquad \text{(V-66)}$$

if α is large, there is no anomaly of sound velocity and attenuation for the [010] phonon, as for TGS,[21,53] which shows no anomalies for these phonons.

We also found the maximum of the line width of these

phonons from Equations (V-64) and (V-65) at the temperature T_m which satisfies the relation

$$T_c - T_m = [C_{22}^{Q}/(C_{22}^{Q} - B_{22})]^{1/2} \propto T_c \quad ----- \quad (V\text{-}67)$$

The quantity $T_c - T_m$ has nothing to do with the frequency of the phonon. Our experimental results are shown in the following table and Fig. 35. It does agree quite well with the theoretical result stated above.[11,12,22,31]

Ω (GHz)	$T_c - T_m$ (K)
1.86	2.86
20.4	3.14
31.2	2.90

From Fig. 21 at the temperature T_m we obtained Γ/π=180 MHz, Ω=31.3 GHz, v_m=5193 m/s, v_0=4739 m/s. Substituting all those values into Equation (V-65), we get $\tau_0 = 8.24*10^{-12}$ sec. This result agrees well with the result from the ultrasonic measurement, $\tau_0 = 7.7*10^{-12}$ sec. Chen and Schaack obtained[6] $\tau_0 = 2.7*10^{-13}$ sec from their analysis of the pseudo-spin-phonon coupling of Raman and infrared spectra. This value is one order of magnitude larger than ours for the phonon propagating along the direction perpendicular to the polar axis <u>b</u>, but one order of magnitude smaller than ours for phonons propagating along <u>b</u>. Deguchi et al.[31] showed that the relaxation time

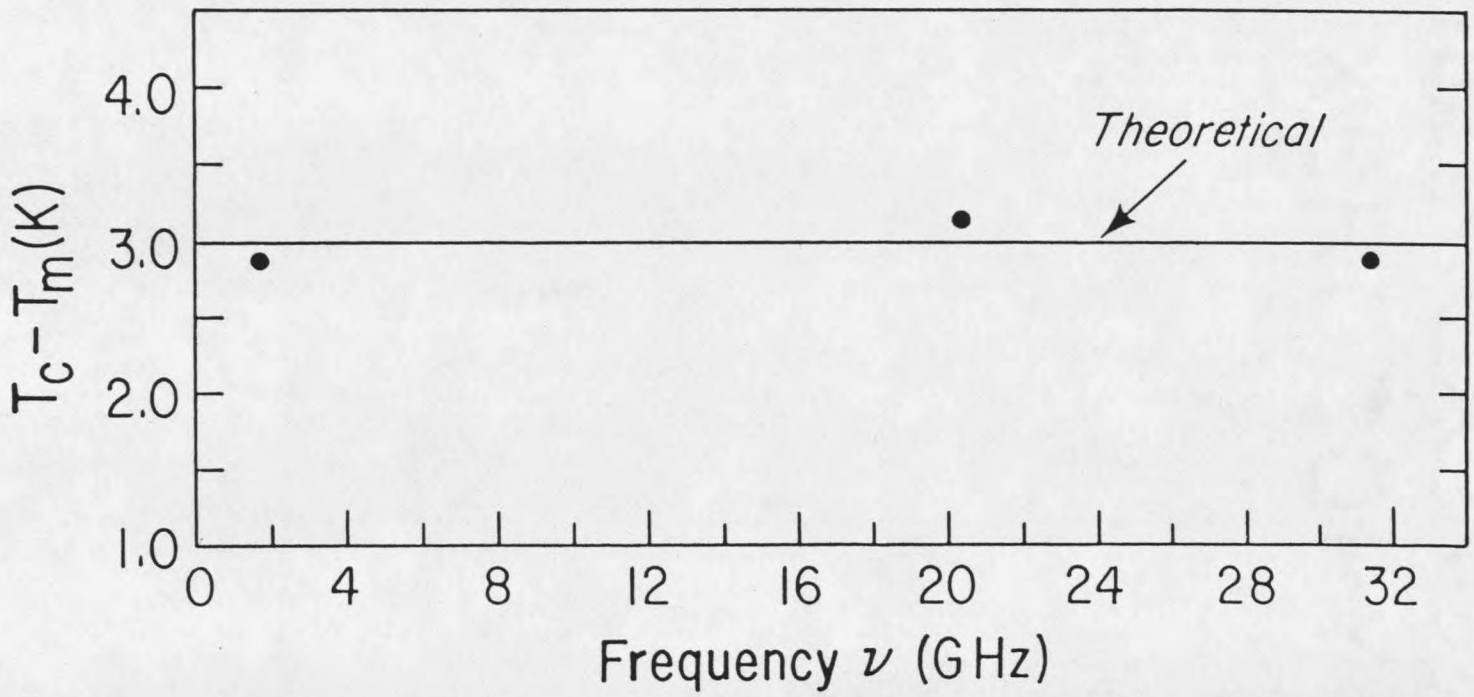

Fig.35. Relation of T_c-T_m vs. frequency for (010) phonons

in TSCC is expressed by $\tau=3.8*(\epsilon_s-\epsilon_\infty)$ sec from their dielectric dispersion measurements. If we use the values $C^+=30$ to 50 K for the Curie constant[17] and the relation $C^+/C^-=2$ we obtain the values $\tau=4.4*10^{-14}$ to $8.5*10^{-14}$ sec for the elementary relaxation time which is in relatively good agreement with our value. Though we obtain an order-parameter relaxation time from the Brillouin scattering experiment, this does not necessarily mean that TSCC undergoes an order-disorder phase transition. It is also possible to adopt the interpretation that the soft phonon mode frequency decreases and the damping constant α diverges as T_c is approached. In such an extremely damped case, the system has the same correlation function as that of the relaxational mode where the effective relaxation time is given by $\Gamma/\Omega_0{}^2$.

Finally, we note a very strange phenomena shown in Fig. 25. We find that the sound velocity of the longitudinal phonons propagating along [010] from the back Brillouin scattering is larger than those from right angle and small angle Brillouin scattering. The discrepancy of the sound velocity between the back scattering and the right angle scattering is about 8.15% and the discrepancy of the sound velocity between the small angle and the right angle scattering is about 1.64%. We considered the possibility that these deviations were caused by

experimental error, for instance, incorrect measurement of the scattering angle inside the crystal, or using the incorrect order of pattern to calculate the frequency shift. We carefully checked the pattern order and are sure it was correct. The error for the angle measurement is at most 1.0°.[56] We are sure that the differences of the sound velocities among the different scattering angles are real.

3. Experimental accuracy and effects of a finite acceptance angle

Let us briefly discuss the accuracy associated with our measurements of Brillouin splittings, sound velocity and phonon decay rate.

(1) Experimental accuracy of frequency shift

Our basic data are the observed Brillouin splittings. These splittings are influenced by the ability to take measurements off the chart recordings due to a finite signal to noise ratio, by fluctuations in the temperature that alter the Brillouin splittings via the temperature dependence of the sound velocities, by the uncertainty in the spectrograph calibration, and by shifts in the position of the Brillouin components due to the finite acceptance angle of the spectrometer. Incorrect angle measurement may cause a systematic deviation of the sound velocities.

We estimate the uncertainty due to the signal-to-noise limitation, found by examining the variation in measured splitting from one trace to another, and the uncertainty due to the accuracy of chart recorder, to be about 0.3%.

(2) Accuracy of the sound velocity

From Equation (V-69)

$$\delta\nu=(2nv\nu/c)\sin(\theta/2)$$

$$v=(\delta\nu c)/(2n\nu\sin(\theta/2))$$

$$dv/v=d(\delta\nu)_m/\delta\nu+d\nu/\nu+dn/n+\cot(\theta/2)d\theta \qquad \text{(V-68)}$$

In Equation (V-68) the first term $d(\delta\nu)_m/\delta\nu$ is due to the measurement error and temperature fluctuation, whose magnitude we have already calculated to be 0.3%. This error is random, and will not cause a systematic deviation for the sound velocities. The second and third terms are negligible. The important term is the last, $\cot(\theta/2)d\theta$, especially for small angle scattering. $\delta\theta$ may be the acceptance angle and the incorrect angle measurement. The acceptance angle which causes the line broadening of the phonon is random. It has no effect on the velocity measurement. However, incorrect angle measurement will bring a systematic deviation into the sound velocity. In our experiment the angle measurement error is estimated as 1.0^0,[57,58] so that

$\cot(\theta/2)d\theta=13.3\%$ for small angle scattering

$\cot(\theta/2)d\theta=0.08\%$ for backscattering

(3) The line width of the phonon

We again differentiate the expression

$$\delta\nu=(2nv\nu/c)\sin(\theta/2)$$

and obtain

$$d(\delta\nu)/\delta\nu=dn/n+dv/v+(d\nu)_{inst}/\nu+\cot(\theta/2)d\theta/2 \qquad \text{(V-69)}$$

In the expression above, dn/n is negligible, and dv/v is due to the velocity fluctuation induced by the temperature fluctuation. The third term $(d\nu/\nu)_{inst}$ is due to the instrument in our case,

$$(d\nu/\nu)_{inst}\approx 0.023\cdot FSR/\nu$$

because the finesse of the Fabry-Perot interferometer is about 42-46.

The instrumental effects can be measured. To do so one simply measures the line width of the elastic scattering peak. It happens that the instrument can be quite accurately described by a Gaussian profile with a half-width at half maximum of 0.023FSR. We measured the width of the central peak on each spectral trace and used this

width as the appropriate instrumental width. Most of the central intensity at room temperature is due to elastic scattering.

Thus, the observed Brillouin component profile $\bar{\Omega}(\Omega)$ is a convolution of a Gaussian instrumental function $g(w)$ of known width with a Lorentzian shaped spectrum $h(w)$ having a width determined by the phonon lifetime. The function $\bar{\Omega}(w)$ is given by[58]

$$\bar{\Omega}(\Omega)=\int_{-\infty}^{\infty} h(x)\,g(\Omega-x)\,dx \qquad \text{(V-70)}$$

where

$$g(\Omega)=g_0\exp(-\Omega^2/\beta^2)$$

and

$$h(\Omega)=h_0/[1+(\Omega/\Gamma)^2] \qquad \text{(V-71)}$$

Here $g(\Omega)$ has a full-width at half-height given by

$$W_{inst}=2\sqrt{\ln\beta}=0.023\cdot FSR \qquad \text{(V-72)}$$

and $h(\Omega)$ has a full-width at half-height given by

$$W_{ph}=\Gamma/\pi \qquad \text{(V-73)}$$

The observed Brillouin profile, $\bar{\Omega}(\Omega)$, has a full-width $W_{\bar{\Omega}}$ at half-height $\bar{\Omega}_{1/2}$. We measure $W_{\bar{\Omega}}$ and W_{inst} and want to determine Γ/π.

Fortunately, $\bar{\Omega}(\Omega)$ is a known function, the Voigt

function. It turns out that the natural line width is approximately given by

$$W_{ph}=W_{\Sigma}-W_{inst} \qquad \text{(V-74)}$$

The measured line width W_{Σ} includes the effects of a finite acceptance angle. In our case the acceptance angle $\delta\theta$ is about 0.4° and the subtended angle of the incident beam $\delta\theta'$ is about 0.4°. Because both the acceptance and the subtended angles are solid angles, the total effective acceptance angle is about $0.9(\delta\theta+\delta\theta')=0.72^{\circ}$. The line broadening due to this angle is given by

$$d(\delta\nu)/\delta\nu=(1/2)\cot(\theta/2)\,d\theta \qquad \text{(V-75)}$$

In other words, the line broadening due to this effect is

$$W_{ang}=d(\delta\nu). \qquad \text{(V-76)}$$

Assuming $\Sigma(\Omega)$ and the effects of the finite acceptance angle are Gaussian distributions, we obtain

$$W_{\Sigma}=\sqrt{W_{obs}^{2}-W_{ang}^{2}} \qquad \text{(V-77)}$$

Then finally the natural line width is

$$W_{ph}=\sqrt{W_{obs}^{2}-W_{ang}^{2}}-W_{inst}$$

Conclusions

From all the experimental analyses and theoretical calculation, some conclusions are obvious, but others are still not very clear and are topics for future work.

The clear conclusions are the following:

(1) The anomalies of the hypersonic velocities for the phonons both along the polar axis [010] and perpendicular to the polar axis for small angle, right angle and back Brillouin scattering clearly show that TSCC undergoes a phase transition at the temperature T_c=130 K.

(2) For phonons propagating perpendicular to the polar axis the phase transition is marked by a sharp step up in phonon velocity in going from the ferroelectric phase to the paraelectric phase and accordingly the decay rate has a sharp peak somewhat below T_c. These agree quite well with theoretical calculations based on induced piezoelectric coupling of the phonons to the polarization fluctuations below T_c by the intrinsic coupling quadratic in polarization and linear in strain. The theoretical results for these calculations are

the sound velocity

$$v_s^2 = v_\infty^2 - (v_\infty^2 - v_0^2)/[1+(\Omega\tau_0^f)^2 t^{-2}]$$

and attenuation coefficient

$$\alpha/\Omega=[(v_w^2-v_0^2)/(2v_s^3)]\Omega\tau_0^f t^{-1}/[1+(\Omega\tau_0^f)^2 t^{-2}]$$

(3) For phonons propagating along the polar axis, the phase transition is not marked by a sharp step up in sound velocity, but rather by a rounded increase from the ferroelectric to paraelectric phase. Accordingly, there is no sharp peak for the temperature dependence of decay rate, but only a rounded hump consistent with theoretical results based on a small depolarization effect. The sound velocity is

$$v_s^2=C_{22}^Q/\rho-(B_{22}/\rho)t/\{(t+\alpha)[1+(\Omega\tau_0^f)^2(t+\alpha)^{-2}]\}$$

and the attenuation coefficient is

$$\alpha/\Omega=-(B_{22}/\rho)\cdot t/(t+\alpha)^2\{(\Omega\tau_0^f)/[1+(\Omega\tau_0^f)^2(t+\alpha)^{-2}]\}$$

(4) The experimental data for the value T_c-T_m agree very well with the theoretical results

$T_c-T_m \propto \Omega$ for the [001] phonons

$T_c-T_m=\text{constant}$ for the [010] phonons

We are the first to obtain data to support this theoretical result.

(5) The frequency range which we covered is about 2 GHz to

32 GHz which is the largest range ever achieved. On this wide range, we found experimentally that

$$T_c - T_m \propto \Omega.$$

However, the anomalies of hypersonic velocity of these phonons are similar.

Suggestions for Future Work

(1) We have done small angle, right angle and back Brillouin scattering. Nevertheless, the angle (frequency) dependence of the sound velocity and especially, the angle dependence of the value $T_c - T_m$ is still very interesting. We suggest that a wide and continuous range of angle be employed for future Brillouin scattering experiments. There are two reasons why we suggest this.

First, we found that the sound velocity for phonons propagating along the polar axis [010] for back scattering is larger than for right angle and small angle scattering. We should measure scattering at additional angles to investigate this unusual phenomenon.

Second, the relation $T_c - T_m \propto \Omega$ also needs more experimental data to support it. These measurements play a central role in proving the validity of the phonon-polarization coupling model we proposed in the previous chapters. To do scattering at more angles we now need a

cryostat which can easily accommodate a continuous range of angle

(2) For small angle scattering, we need an accurate measurement of line width. Because smaller angle scattering corresponds to a smaller frequency region, the line width is relatively smaller. The temperature at which the decay rate is maximum is very important and very close to T_c for [001] phonons. For [010] phonons the maximum of the decay rate is relatively very small. These aspects of temperature dependence of the decay rate are very important evidence for determining the sort of phonon-polarization coupling and the caterory of the phase transition. To do this we need high spectrum contrast and high resolution. Consequently, we have to change the three pass system to a five pass system. Then the contrast will increase up to 10^{11}-10^{12}. We have to change the control program to divide the ramp for the scan voltage of the ramp generator into more steps, say from 1024 to 2048, and increase the number of accumulating channels from 256 to 1024. These changes will greatly increase the resolution of the spectrum and will allow more accurate line width measurement.

(3) The Brillouin scattering for longitudinal phonons both along the polar axis and perpendicular to it has been studied quite carefully, but transverse phonons have not

been studied very much.

It will be very interesting to study the transverse phonons and compare with the results for longitudinal phonons. These studies may lead us to understand better the category of this phase transition.

First, the transverse phonons propagating along the polar axis should not have the depolarization effect. The results for the anomalies of sound velocity and attenuation should confirm our small depolarization model.

Second, the transverse phonons propagating perpendicular to the polar axis but polarized along the polar axis are very interesting too. We should study the phonon-polarization coupling by the transverse modes.

(4) As we mentioned before, the sound velocity of longitudinal phonons propagating along the polar axis [010] for backscattering is larger than for right angle and small angle scattering. It seems that the difference of the sound velocity among the different scattering angles only relates to the frequency. That is, the effective complex elastic stiffness depends slightly on frequency of the phonons. We do not have a model to explain it yet. It does not seem to be caused by the phonon-polarization coupling. To develop a model we must first find out how the sound velocity relates to the frequency. That the basic phonon dispersion relation is

not linear seems impossible because the dispersion curves of acoustic branches, as determined by neutron scattering, invariably bend downward with increasing k which makes the sound velocity decrease rather than increase. In particular, one generally does not see such a strong nonlinearity so close to the Brillouin zone center. Some effect of this type could arise from coupling to another relaxing degree of freedom, but what is it? And also, why does it appear in the [010] data between the 90 and 180 degree data, and does not appear in the [001] data? This question requires further investigation.

(5) Brillouin scattering near the tricritical point

The paraelectric-ferroelectric phase transition temperature T_c increases quite rapidly with applied hydrostatic pressure,[59] but the paraelectric-ferroelectric phase boundary is terminated at a triple point at 5.03 kbar and 176.8 K by a first-order phase transition line with even steeper slope which bounds a third, antiferroelectric phase[60] shown in Fig. 36. Windsch found that the paraelectric-ferroelectric transition becomes first-order at a tricritical point near the triple point.[61]

Because the sound velocity anomalies are attributed to the spontaneous-polarization induced piezoelectric coupling term $g_{322}Q_0\delta\epsilon_3\delta Q_2$, the characteristics of Q_0 will

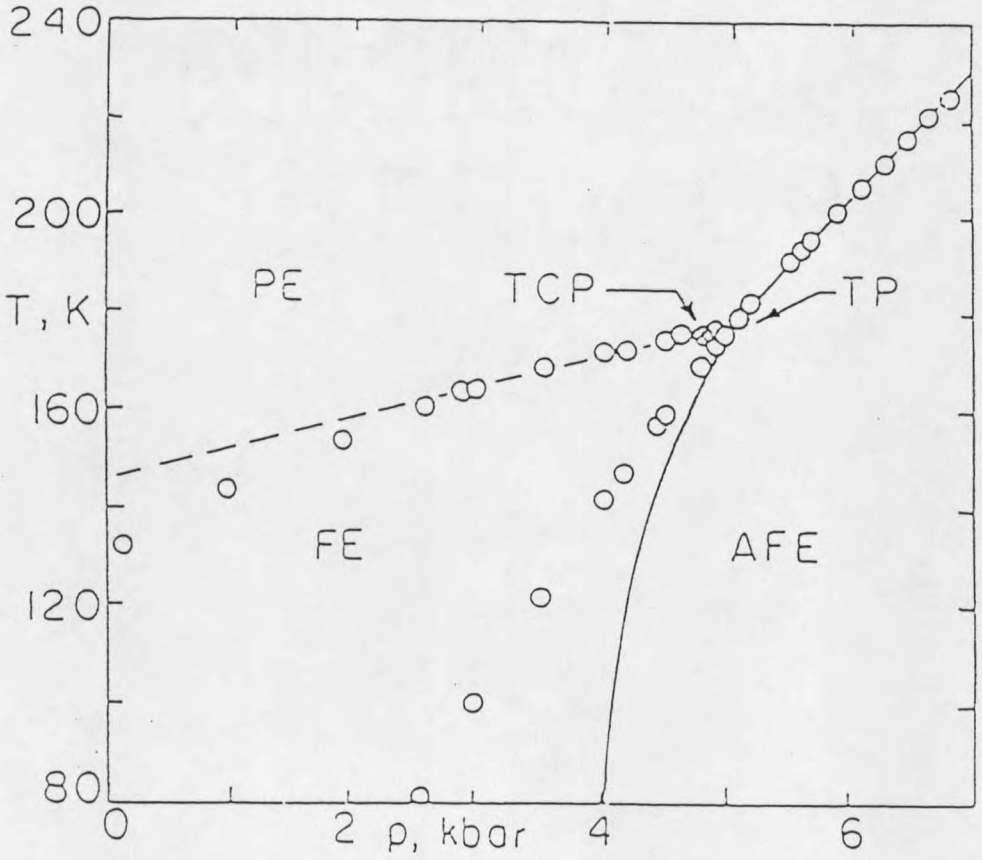

Fig. 36. Phase diagram of TSCC

strongly affect the anomalies of the sound velocity. On the other hand, if the phase transition is displacive, the features of the phase transition near the tricritical point will be very interesting. Investigation of Brillouin scattering around this region would be very helpful in understanding the mechanism of this phase transition in TSCC.

To do this involves a high hydrostatic pressure experiment. Such experiments, though difficult, allow investigation of interesting regions of the phase diagram, so it pays to do Brillouin scattering at high pressure.

REFERENCES CITED

REFERENCES CITED

1. H. Z. Cummins and A. P. Levanyuk, Introduction to Light Scattering Near Phase Transitions (Amsterdam·New·Oxford), 1983.

2. C. N. R. Rao and K. J. Rao, Phase Transitions in Solids, (W. and J. Mackay Ltd., Chatham), 1978.

3. J. F. Scott, Raman Spectroscopy of Structural Phase Transitions, (North-Holland Publishing Co.), 1983.

4. R. W .Gammon, E. Courtens and W. B. Daniels, Phys. Rev. B27, 4359 (1983).

5. E. Sandvold and E. Courtens, Phys. Rev. B27, 5660 (1983).

6. T. Chen and G. Schaack, J. Phys. C17, 3801 (1984).

7. W. Rehwald, Adv. Phys. 22, 721 (1973).

8. Fang Jun Gan and Lu Deng, Solid State Physics, (Shanghai), 1981.

9. K. A. Müller,, Proc. NATO Advanced Study Institute on "Anharmonic Lattices, Structural Transition and Melting", Ustaoset (Norway), edited by T. Riste, 1973.

10. E. F. Gross, Nature 126, 201, 400,609 (1930) and 129, 722 (1932).

11. V. L. Ginzburg, Doklady Akad, Nauk SSSR 105, 240 (1955) and Soviet Physics-Uspekhi 5, 649 (1963).

12. I. A. Yakovlev, T. S. Velichkina and L. F. Mikheeva, Kristallografiya 1, 123 (1956).

13. S. M. Shapiro and H. Z. Cummins, Phys. Rev. Lett. 21, 1578 (1968).

14. G. B. Benedek and K. Fritsch, Phys. Rev. 149, 647 (1966).

15. J. D. Jackson, Classical Electrodynamics, John Wiley and Sons, Inc. New York, 1975.

16. N.R. Ivanov and H. Arndt, Sov. Phys. Crystallogr. 24, 291 (1979).

17. Y.J. Makita, J. Phys. Soc. Jpn. 20, 2073(1965).

18. T. Ashida, S. Bando and M. Kakudo, Acta Cryst., B28, 1560(1972).

19. N. Mishima, K. Itoh and E. Nakamura, Acta Cryst. C40,

20. T. Hikita, J. T. Wang, P. T. Schnackenberg, and V. H. Schmidt, Jpn. J. Appl. Phys. 24, 494 (1985).

21. T. Hikita, P. T. Schnackenberg and V. H. Schmidt, Phys. Rev. B31, 299 (1985).

22. G. A. Smolensky, I. G. Siny, A. K. Tagantsev, S. D. Prokhorova, W. Windsch, Ferroelectrics 64, 221 (1985).

23. L. D. Landau and E. M. Lifshits, Statistical Physics (London: Pergamon).1968.

24. Y. Yamada, H. Takatera and D.L. Huber, J. Phys. Soc. Jpn. 36, 641 (1974).

25. V. Winterfeldt and G. Schaack, Ferroelectrics 15, 21,35 (1977).

26. V. Winterfeldt and G. Schaack, Z. Phys. B36, 303 (1980).

27. T. Chen and G. Schaack, J. Phys. C: Solid State Phys. 17, 3821 (1984).

28. A. Sawada, Y. Makita and Y. Takagi, J. Phys. Soc. Jpn. 42, 1918 (1977).

29. G. V. Kozlov, A. A. Volkov, J. F. Scott, G. E. Feldkamp and J. Petzelt, Phys. Rev. B28, 255 (1983).

30. A. Lopez-Echarri and M. J. Tello, J. Phys. D: Appl. Phys. 14, 71 (1981).

31. Deguchi, Aramaki, Nakamura and Tanaka, J. Phys. Soc. Jpn. 52, 1897 (1983).

32. S. D. Prokhorova, G. A. Smolensky, I. G. Siny, E. G. Kuzminov, V. D. Mikvabia, and H. Arndt, Ferroelectrics 25, 629 (1980).

33. T. Chen, G. Schack, and V. Winterfeldt, Ferroelectrics 39, 1131 (1981).

34. G. E. Feldkamp and J. F. Scott, Ferroelectrics 39, 1163 (1981).

35. S. Fujimoto, N. Yasuda, and S. Funado, J. Phys. D15, 1469 (1982).

36. R. Blinc, M. Jamsek-Vilfan, and G. Lahajhar, J. Chem. Phys. 52, 6407 (1970).

37. W. Windsch and G. Volkel, Ferroelectrics 24, 195 (1980).

38. R. Blinc, M. Jamsek-Vilfan, G. Lahajnar, and G. Hajdukovic, J. Chem. Phys. 52, 6407 (1970).

39. M. A. Perez Jubindo, A. Lopez-Echarri, and M. J. Tello, Ferroelectrics 39, 1171 (1981).

40. A. Levstik, C. Filipic, and R. Blinc, Solid State Commun. 18, 1231 (1976).

41. G. E. Feldkamp and J. F. Scott, Bull. Am. Phys. Soc. 26, 303 (1981).

42. H. Gränicher and K. A. Müller, Mat. Res. Bull. 6, 977 (1971).

43. J. C. Slonczewski and H. Thomas, Phys. Rev. B1, 3545 (1970).

44. K. K. Kobayashi, J. Phys. Soc. Jpn. 24, 497 (1968).

45. H. Mori, Prog. Theor. Phys. 33, 423 (1967).

46. K. Tani and H. Mori, Prog. Theor. Phys. 39, 876 (1968).

47. K. Kawasaki, Physics Lett. A 29, 406 (1971).

48. G. Sorge and U. Straube, Ferroelectrics 21, 533 (1978).

49. K. K. Kawasaki, Phys. Lett. 29A, 406 (1969).

50. T. J. Moran and B. Lüthi, Phys. Rev. B4, 122 (1971).

51. A. Bachellerie, J. Joffrin, and A. Levelut, Phys. Rev. Lett. 30, 617 (1973).

52. R. W. Gammon and H. Z. Cummins, Phys. Rev. Lett. 30, 617 (1973).

53. T. Yagi, M. Tokunaga, and I. Tatsuzaki, J. Phys. Soc. Jpn. 40, 1659 (1976).

54. M. A. Krivoglaz, Soviet Physics-Solid State 5, 2526 (1964).

55. J. Bornarel and V. H. Schmidt, J. Phys. C: Sol. St. Phys. 14, 2017 (1981).

56. M. Yamada and V. H. Schmidt, Rev. Sci. Instr. 49, 1226 (1978).

57. U. Straube, G. Sorge, and N. R. Ivanov, Phys. Stat. Sol.(a) 73, 467 (1982).

58. H. C. Van de Hulst and J. J. M. Reesinek, Astrophys. J. 106, 121 (1946).

59. V. H. Schmidt, Ferroelectrics, 39, 1151 (1981).

60. V. H. Schmidt, Solid State Commun. 35, 649 (1980)

61. H. Reicheit, W. Windsch, and A. Scienkiewicz F erroelectrics 34, 195 (1981).

DATE DUE
